Sand closures

A study towards the morphology under mixing layers using laboratory experiments and a numerical model

Nova Huppes

Delft University of Technology

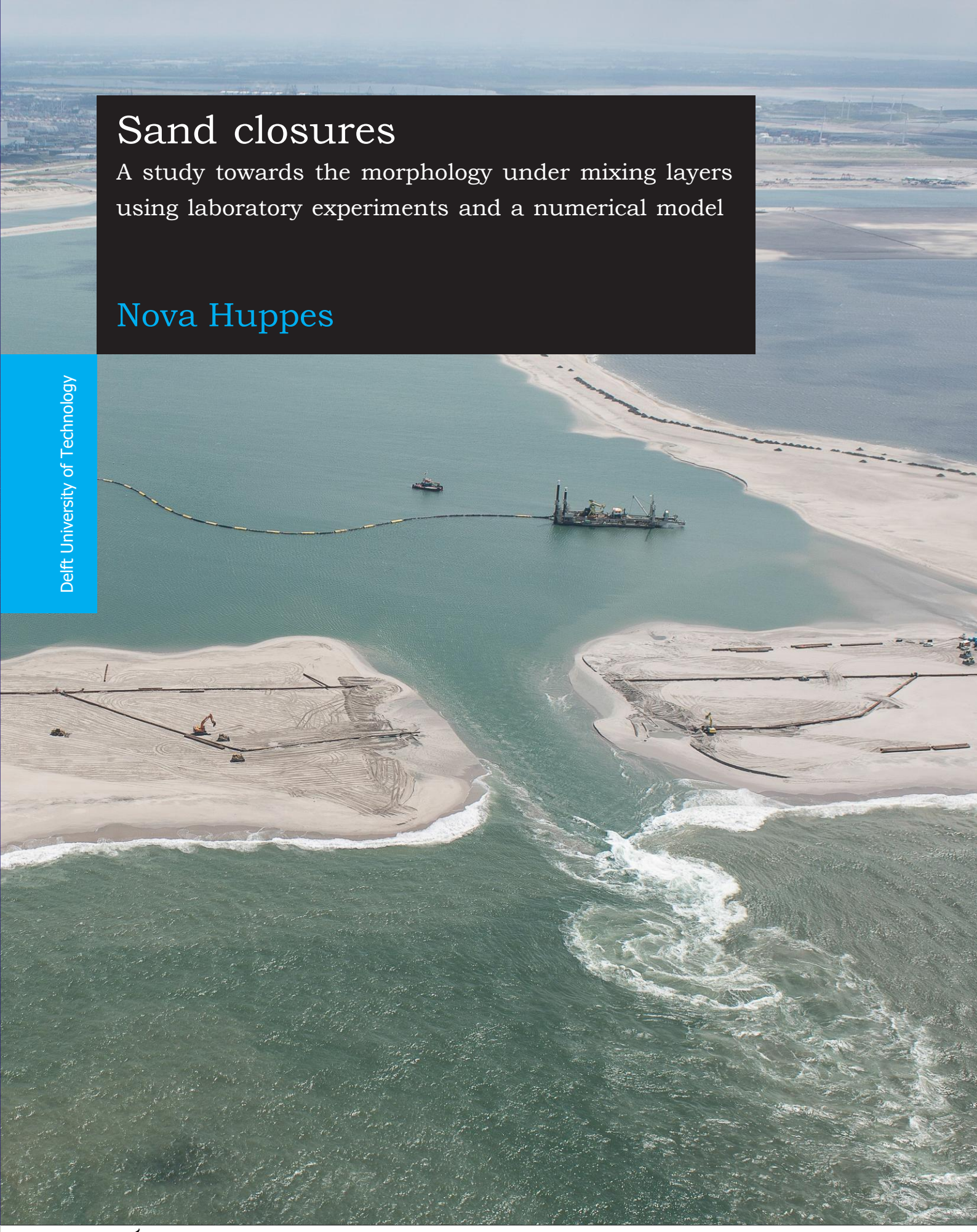

TU Delft

SVASEK HYDRAULICS
COASTAL, HARBOUR AND RIVER CONSULTANTS

Van Oord
Marine ingenuity

Sand closures

A study towards the morphology under mixing layers using laboratory experiments and a numerical model

by

Nova Huppes

to obtain the degree of Master of Science
at the Delft University of Technology,
to be defended publicly on Friday June 30, 2017 at 13.30 PM.

Student number:	4094778	
Date:	June 15, 2017	
Supervisors:	Dr. ir. R. J. Labeur,	TU Delft
	Prof. dr. ir. C. van Rhee,	TU Delft
	Dr. ir. A. M. Talmon,	TU Delft
	Ir. A. Kroon,	Svašek Hydraulics
	Ir. W. J. Ockeloen,	Van Oord Dredging and Marine Contractors BV

An electronic version of this thesis is available at http://repository.tudelft.nl/.

TU Delft Delft University of Technology

SVASEK HYDRAULICS
COASTAL, HARBOUR AND RIVER CONSULTANTS

Van Oord
Marine ingenuity

Preface

This thesis is conducted to obtain the degree of Master of Science in Civil Engineering at the Delft University of Technology. This thesis is based on the author's additional master thesis, which is a literature study on sand closures. A short recap is given to introduce the subject, but for most of the literature on sand closures, one is referred to the findings of the additional MSc thesis. The research was a collaboration between Svašek Hydraulics, Van Oord Dredging and Marine Contractors BV, and Delft University of Technology.

I would especially like to thank Svašek Hydraulics for their hospitality and openness during my stay at their company. Futhermore, I would like to thank the staff of the Dredging lab for making their resources available to me to conduct my research. I would also like to thank the Fluid Mechanics Laboratory for their expertise and measuring equipment.

I would like to thank all my supervisors for their contribution to my thesis: Cees van Rhee for his expertise and useful insights during the committee meetings; Robert Jan Labeur for his constructive criticism, especially during the writing phase of the thesis; Anna Kroon for the useful conversations about sand closures and numerical modelling; Arno Talmon for his expert view on experimental research; Wouter Ockeloen for his practical view on the construction of sand closures, providing a different angle to my research.

I want to especially thank Lynyrd de Wit for taking the time to alter his numerical model to make it possible for me to conduct my research. I want to thank him for making the numerical part of this thesis possible and his patience while explaining the features of his model.

I would also like to thank my boyfriend, Niels Kleijweg, and my study mates, Gerben Hagenaars, Melanie Schippers, and Cindy van de Vries, for their helpful comments and support during the laboratory experiments and writing of my thesis. I would like to thank my parents for supporting me through my elaborate hobby and study, continuously standing behind every decision and all my pursuits.

Nova Huppes
Delft, June 2017

Abstract

Dams are an essential part of the Dutch flood defence works to protect the hinterland from flooding by the sea. These dams can be made from several materials such as sand, and concrete. Dams do not form overnight. When one wants to close a basin off from the sea, as was done several times for the Dutch Delta Works, a dam is build up gradually. During the construction of the dam, the connection between sea and basin, through which the tide propagates in and out of the basin is called the closure gap. Sand closures are the construction of closure dams with sand as the main building material. The rising and falling tide generates a current through the closure gap, which increases in strength as the gap becomes smaller. This current is quite strong and transports a significant amount of sand from the gap to areas where the current is weaker. The sand that is transported away from the closure gap is called the sand loss. The changing tide and constantly moving sand grains result in a dynamic environment. This makes it difficult to estimate the total amount of sand that is necessary to close the dam. It is important to be able to assess the amount of sand loss accurately, because it could make the difference between needing an extra dredging vessel or not. The costs of these dredging vessels are about 1 million euro's a week; therefore, having an unnecessary vessel present due to very conservative sand loss predictions is costly.

The flow pattern during a sand closure is quite complex and three-dimensional, consisting out of a main current, two mixing layers originating at the heads of the dam under construction, and multiple recirculations. From literature, it was found that the degree of turbulence in the flow seems to have a significant influence on the amount of sediment pick-up. To predict the sand loss numerical morphodynamic models are used. Most of the inaccuracy of the present numerical models is expected to be in the sand loss prediction under the mixing layers while the degree of turbulence in these mixing layers seems to have a large contribution to the total amount of erosion. The erosion and sedimentation under a mixing layer is not known from literature; therefore, to obtain more insight into the morphology under mixing layers, both a laboratory experiment and a three-dimensional numerical morphodynamic model were set up.

The mixing layers of a sand closure partly resemble the theoretical case of a lateral expansion. Investigating the morphology for this theoretical case is the most useful first study towards describing the erosion under the mixing layers of a sand closure. A laboratory experiment was set up that contains a lateral expansion with a layer of sand on the bottom of the flume; the same layout was used to set up the numerical model TUDflow3d. For the attainability of the laboratory experiments, bedload transport was investigated, whereas the main transport mode during the last stage of a sand closure is suspended sediment transport.

For both the laboratory experiments and the numerical set-up, a streamwise bar formed behind the tip of the lateral expansion. However, it was not possible to replicate the bedforms that occurred during the laboratory experiments with the numerical model. These bedforms are deemed to be important for the morphology during bedload transport.

The numerical model was used to expand the research to suspended sediment transport by decreasing the grain size of the sediment. In the obtained morphological patterns, four areas were distinguished: a main current with high flow velocities and low turbulence intensities with a moderate amount of erosion; an area in the mixing layer with high flow velocities and high turbulence intensities with large amounts of erosion; an area inside the mixing layer with low flow velocities and high turbulence intensities where no erosion occurs but only sedimentation due to the formation of the streamwise bar; and an area in the return current with low flow velocities and low turbulence intensities where a negligible amount erosion and sedimentation is observed. It is expected that a variation of these patterns can be found during a sand closure, although these findings should be validated with a laboratory experiment or in situ measurements. Therefore, it is recommended to set up a laboratory experiment to investigate the morphology under a mixing layer for suspended sediment transport. Based on the results of the laboratory experiments and the numerical model, it is advised to look into the possibility to use the

sand deposited as a streamwise bar during a sand closure as an additional borrow pit to aid the closure process, since it would lead to less sailing time for the dredging vessels.

For the first stage of a sand closure, it is advised to use a two-dimensional model that incorporates a bedload transport formula to model the sediment transport. It is important to use a parametrization of the bedforms that occur during bedload transport. For the final stage of a sand closure, which is the most critical phase due to high flow velocities, high degree of turbulence and time restriction, it is advised to use a three-dimensional model with a pick-up equation that takes the influence of turbulence on the grains into account, such as the pick-up formula of Okayasu et al. [9].

Contents

List of Symbols

Latin Symbols

c_b	Near-bed volumetric sediment concentration	$[\%]$
C_D	Drag coefficient	$[-]$
C	Chézy coefficient	$[m^{1/2}/s]$
C_I	Inertia coefficient	$[-]$
C_L	Lift coefficient	$[-]$
C_l	Volume concentration of fraction l	$[-]$
D	Representative particle diameter	$[m]$
D_*	Dimensionless particle diameter	$[-]$
D_{50}	Median particle diameter	$[m]$
E	Sediment pick-up flux	$[kg/sm^2]$
F_D	Drag force	$[N]$
F_I	Inertia force	$[N]$
F_L	Lift force	$[N]$
g	Gravitational acceleration	$[m/s^2]$
I	Turbulence intensity	$[-]$
L	Characteristic length scale	$[m]$
n_0	Bed porosity prior to erosion	$[-]$
p	Pressure	$[Pa]$
Re_p	Particle Reynolds number	$[-]$
S	Sedimentation flux	$[kg/m^2s]$
Sc	Schmidt number	$[-]$
S_F	Shape factor	$[-]$
t	Time	$[s]$
u	Velocity	$[m/s]$
u_j'	Fluctuating part of the velocity in the indicated direction	$[m/s]$
u_*	Bed-shear velocity	$[-]$
u_{bt}	Bottom shear velocity including the turbulence component	$[m/s]$
u_i	Cartesian velocity components	$[m/s]$
u_j	Velocity in the indicated direction	$[m/s]$
$\overline{u_j}$	Time-averaged flow velocity	$[m/s]$
u_{rms}	Root-mean-square value of the velocity fluctuations	$[m/s]$
U	Characteristic velocity	$[m/s]$
v_e	Velocity of the erosion front / pick-up rate	$[m/s]$
W	Gravitational force	$[N]$
w_s	Hindered settling velocity of a particle	$[m/s]$
x_i	Cartesian coordinates	$[m]$

Greek Symbols

Δ	Relative sediment density	$[-]$
Γ	Diffusion coefficient	$[m^2/s]$
θ	Shields parameter	$[-]$
θ_{cr}	Critical Shields parameter	$[-]$

θ_t	Modified Shields parameter	$[-]$
κ	Von Kármán constant	$[-]$
μ	Dynamic viscosity	$[kg/ms]$
ν	Kinematic viscosity, $\nu = \mu/\rho$	$[m^2/s]$
ν_e	Eddy viscosity	$[m^2/s]$
ρ	Local density of water taking into account the sediment concentration	$[kg/m^3]$
ρ_s	Density of sediment	$[kg/m^3]$
ρ_w	Density of water	$[kg/m^3]$
τ_b	Bed shear stress	$[Pa]$

Acronyms

ADV	Acoustic Doppler Velocimeter
Cdam	Compartimenteringsdam
CDS2	Second-order central difference scheme
CFL	Courant Friedrichs Lewy number
CUR	Centre for Civil Engineering Research, Codes and Specifications
DNS	Direct numerical simulation
DSmag	Dynamic Smagorinsky model
HYB6	Sixth-order hybrid difference scheme
LDA	Laser Doppler Anemometry
LES	Large Eddy Simulation
MV2	Maasvlakte 2
PIV	Particle Image Velocimetry
PUMA	Projectorganisatie Uitbreiding Maasvlakte
SEM	Synthetic eddy method
SONAR	Sound Navigation And Ranging
TKE	Turbulent kinetic energy
TVD	Total variation diminishing
WALE	Wall-Adapting Local Eddy-Viscosity

List of Figures

List of Tables

1 Introduction

1.1. Background

Dams are an essential part of the Dutch defence works to protect the hinterland from the sea. These dams can be made from several materials, of which sand is by far the cheapest building material. Dams do not form overnight. When one wants to close a basin off from the sea, as was done several times for the Dutch Delta Works, a dam is build up gradually. During construction, the tide propagates in and out of the basin. The resulting flow velocities inside the gap increase as the gap becomes smaller. The increase in flow velocity is accompanied by an increasing degree of turbulence. Moreover, the changing tide and constantly moving sand grains result in a very dynamic environment. This makes it difficult to estimate the total amount of sand that is necessary to build the dam.

1.2. Problem statement

It is important to be able to assess the amount of sand loss during a sand closure accurately, because it could make the difference between needing an extra dredging vessel or not. The costs of these dredging vessels are about 1 million euro's a week; therefore, having an unnecessary vessel present due to very conservative sand loss predictions is costly.

Several attempts have been made to estimate the amount of sand that is lost during the process of closing a dam, which is called a 'sand closure'. In 1993, the Centre for Civil Engineering Research, Codes and Specifications (CUR) published a manual called the CUR Report 157 summarizing the knowledge that was gained about sand closures thus far, and hand calculations that could be used for the estimation of the sand loss.

In 2012, the next big step was made in sand loss prediction for sand closures when Maasvlakte 2 (MV2) was constructed. The new expansion of the port of Rotterdam had to be shielded from the sea by dams surrounding the basin. This basin was constructed by Projectorganisatie Uitbreiding Maasvlakte (PUMA). It was chosen to divide the basin into two compartments, each with their own dam and corresponding sand closure. These compartments were closed off from the sea sequentially. In this way, the maximum flow velocity and sand losses would be lower. Furthermore, the knowledge gained about sand loss during the first closure could be used to make a better estimation of the sand loss for the second closure. PUMA consisted out of a team of compagnies responsible for the construction of MV2, among which were Svašek Hydraulics and Van Oord Dredging and Marine Contractors BV.

In the author's additional MSc thesis it was attempted to shed light on the subject of sand closures by means of a literature study. That thesis mapped all the processes that have a relevant contribution to the amount of sand loss that occurs during a sand closure. The additional MSc thesis concluded that a three-dimensional numerical approach is necessary to obtain a reliable prediction of the amount of sand that is lost during a sand closure.

During the sand closures of MV2, large amounts of erosion were observed at the heads of the closure dam. It is expected that this erosion is a result of the attachment of the mixing layers and their high degree of turbulence. It is expected that a better estimation of the amount of sand that is picked up

underneath these mixing layers greatly improves the overall estimation of sand losses during a sand closure. The erosion of sediment under flows with a high degree of turbulence is a three-dimensional process, while the present numerical model used to predict the sand loss is two-dimensional. Modelling the sand loss under mixing layers is not straightforward, because there is no numerical model currently available that uses a pick-up formula that incorporates turbulent properties directly.

1.3. Objective

This thesis aims to improve the prediction of the sand loss during a sand closure by numerically modelling the morphological development underneath mixing layers. Most of the inaccuracy of the present prediction methods is expected to be in the sand loss under mixing layers. Once there is more knowledge obtained about the morphology underneath mixing layers, the sand loss prediction of sand closures is expected to improve as well. The main research question is therefore formulated as:

How are the morphological processes under the mixing layer of a sand closure described and how can these be modelled numerically?

The following sub-questions are formulated:

1. What are the important characteristics of the mixing layers that occur during sand closures?
2. What is the morphological development under a mixing layer in a laboratory experiment that resembles a mixing layer of a sand closure?
3. Is TUDflow3d a suitable numerical model to simulate the morphology for the mixing layers that occur during a sand closure?

To answer these questions it is chosen to use an approach that combines a laboratory experiment and a numerical model. Because there is little knowledge of the morphological changes of a sand bed under mixing layers, laboratory experiments are conducted to obtain more insight on the actual processes. This information is used to validate a numerical model for the use of predicting bed level changes in a turbulent flow.

1.4. Structure of this report

In Chapter 2, an extensive introduction is given on the relevant theory for sand closures. This chapter starts with a general introduction, of which more background information can be found in the author's additional MSc thesis. Then, the flow patterns and sediment transport are discussed in more detail, giving especial attention to mixing layers and the pick-up of sediment in turbulent conditions. Since there is little knowledge about the morphology under mixing layers, it is found necessary to execute laboratory experiments in order to validate the morphological prediction. Chapter 3 treats the experimental set-up of these laboratory experiments, after which the results are treated in Chapter 4. It was attempted to measure the flow velocities with an Acoustic Doppler Velocimeter (ADV), but the acoustic properties of the experimental set-up made the use of this measurement equipment impossible. Appendix A goes into the executed measurements with the ADV and provides insight into the usability for anyone who plans to use an ADV to measure flow patterns.

A total of eight experiments were executed, Chapter 4 treats three of these experiments in more detail, the remainder of the results can be found in Appendix B. The chapter is subdivided into a part with the results regarding the flow patterns that were found, and a second part treating the morphological changes that were measured. Chapter 5 treats the numerical model used to replicate the laboratory experiments. Again, the chapter is subdivided into a part treating the flow patterns and comparing them to the results found in Chapter 4, and a part that treats the morphological results. Only the most relevant results are presented in Chapter 5. The remainder of the numerical results regarding the flow patterns can be found in Appendix C, and a complete set of morphological results can be found in Appendix D. A discussion on the found results and main points of improvement are presented in Chapter 6. In conclusion, the formulated research questions are answered in Chapter 7.

2

Literature review

The goal of this chapter is to give an overview of the relevant theory on the erosion during sand closures and the corresponding processes. First, an introduction to sand closures is given in Section 2.1. In Section 2.2, the flow patterns occurring during a sand closure are discussed. Section 2.3 describes the relevant theory on sediment transport during sand closures. Finally, Section 2.4 provides a discussion about the intended laboratory and numerical experiments in the light of the presented literature.

2.1. Sand closures

This section gives an overview of the relevant techniques and general characteristics of a sand closure. Most of the information on sand closures can be found in the author's additional master thesis [5]; a short recap is given in this section.

Sand closures are the construction of a closure dam with sand as the main building material. These closure dams are usually constructed at the inlet of a tidal basin, of which the future dam's location is a connection to the sea. During the construction of the dam, this connection is called the closure gap. The rising and falling tide generates a current through the closure gap, which increases in strength as the gap becomes smaller. The strength of this current can be substantial with sediment transport to low-velocity areas as a consequence.

The construction of a sand dam consists out of three stages. First, the general outline of the dam is constructed by dredging vessels by means of rainbowing marine sand. Then, a sill is build up by hovering over the outline of the dam, dumping sediment directly on top of it by using dredging vessels with bottom doors. Finally, when these vessels can no longer hover over the dam anymore because of the limited water depth, pipelines are lead to the edge of the closure gap. The pipelines discharge a mixture of sand and water onto the heads of the dam. Bulldozers spread out this mixture, after which this mixture flows down the heads of the dam into the gap. In this way, the dam is slowly built up from two sides, until the gap is closed. This final stage of the construction of the sand dam is called a sand closure. The final stage of a sand closure is always around slack water, because the flow velocities through the gap are then as low as possible. It is critical to completely close the gap before the tidal forces increase the flow velocities again.

The most recent example of a sand closure is the construction of Maasvlakte 2 (MV2), for which two individual sand closures were executed. MV2 was a land reclamation project, which was part of the expansion of the Port of Rotterdam. The port was in need of new harbour area and needed the sand closures to expand towards the sea. This new harbour area had to be shielded from the sea by dams surrounding the basin. This constructed basin was divided into into two compartments, each with their own closure dam and corresponding sand closure. These compartments were closed off from the sea sequentially. In this way, the maximum flow velocity and total amount of sand loss would be lower. More information about MV2 is available in the author's additional MSc thesis [5].

Figure 2.1 shows a photograph of the final stage of the first sand closure, the Compartimenterings-dam (Cdam). The pipes that are used to transport the sand from the dredging vessels to the edge of

the closure gap are clearly visible in the photograph. It can be seen that the flow patterns are chaotic and the muddy water suggests high sediment concentrations downstream of the dam heads. These chaotic flow patterns and high sediment concentrations are associated with large amounts of erosion. It is possible that this erosion is caused by the mixture of water and sand discharged from the pipelines, but an investigation by Rijkswaterstaat [21] showed that excess erosion by this mechanism can be avoided by limiting the maximum unloading rate of the dredging vessels. Another possible mechanism that can be seen in Figure 2.1 is the turbulent character of the flow. The large eddies that can be distinguished in the photograph could cause large amounts of erosion and a mixing of the sediment in the water, preventing the sediment from settling.

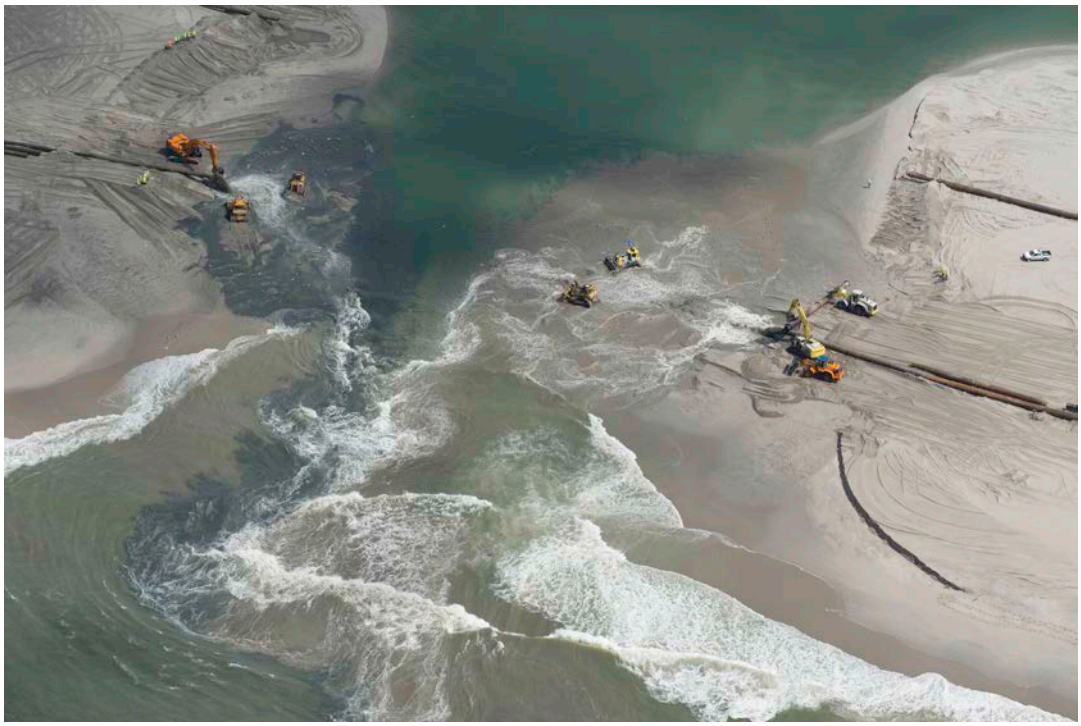

Figure 2.1: Aerial photograph of the final stage of the construction of the Cdam of MV2.

2.2. Flow patterns

During a sand closure, the flow velocities through the gap are caused by a water level difference between the sea on one side of the gap and the closed off basin on the other side. The inflow and the outflow of the tide through the closure gap generates a number of different flow patterns. These patterns are treated in the following section. The flow patterns that are deemed to be most important for the erosion of sand at the closure gap are treated in more detail, because they are especially relevant for this research.

The flow patterns of a general sand closure are depicted in Figure 2.2. Note that the water level upstream and downstream of the closure gap are depicted at the same height in the figure, but this is not necessarily the case, since the water level at sea constantly changes due to the tide. This figure depicts a main current that is, in both horizontal and vertical direction, contracted into the gap and holds the highest flow velocities. Figure 2.2c depicts the vertical contraction of the flow, with the corresponding water level drop on top of the sill. Downstream of the part of the dam that is already constructed, there are two eddies depicted which form recirculation zones. Between the main current and these recirculation zones, there is a sharp transition from high to low flow velocities. These large velocity gradients cause shear forces, resulting in two mixing layers between the main current and the recirculation zones. Looking at Figure 2.1 again, it can be observed that the mixing layers are interacting, because the dams are already build up so close together.

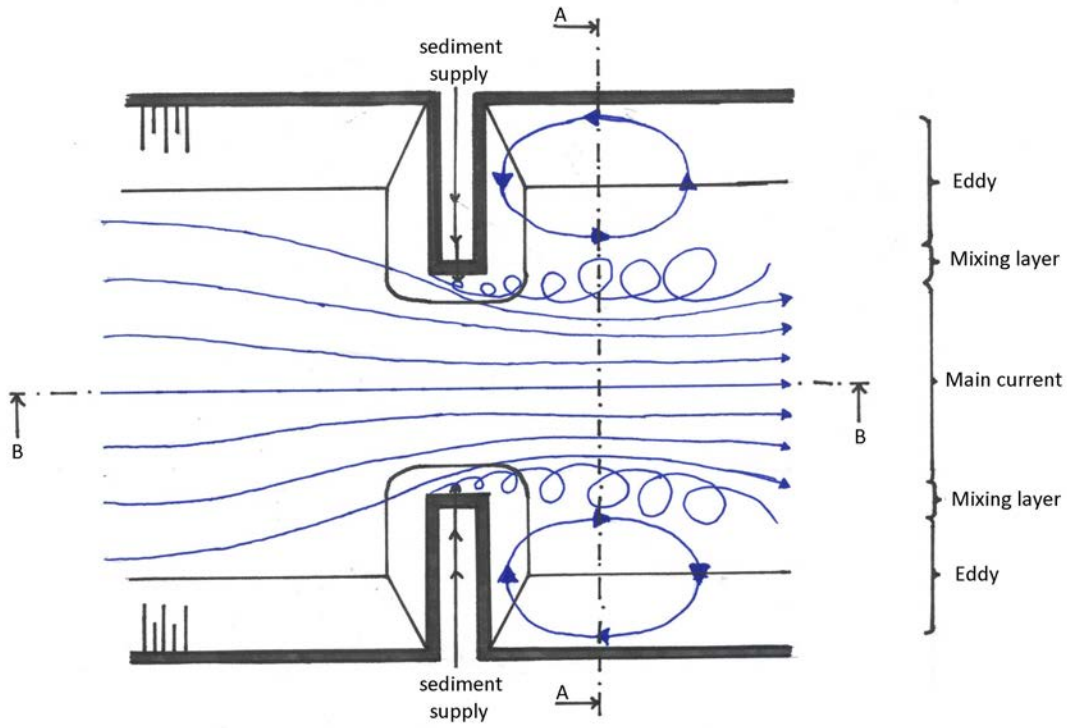

(a) Top view of the general flow pattern of a sand closure.

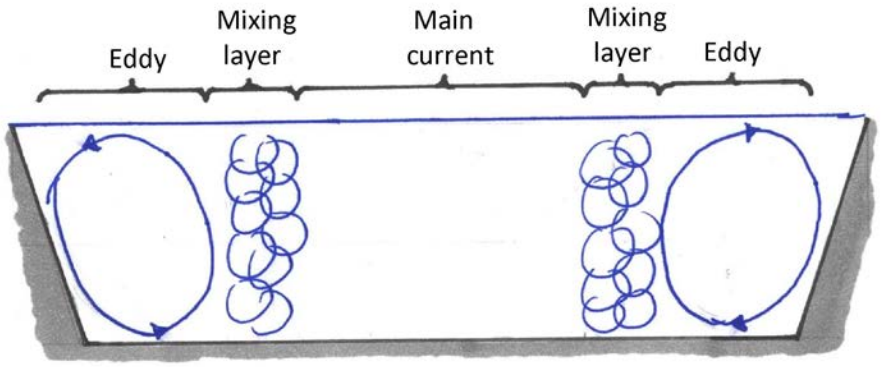

(b) Front view of the general flow pattern of a sand closure at cross section A-A' which is perpendicular to the main current.

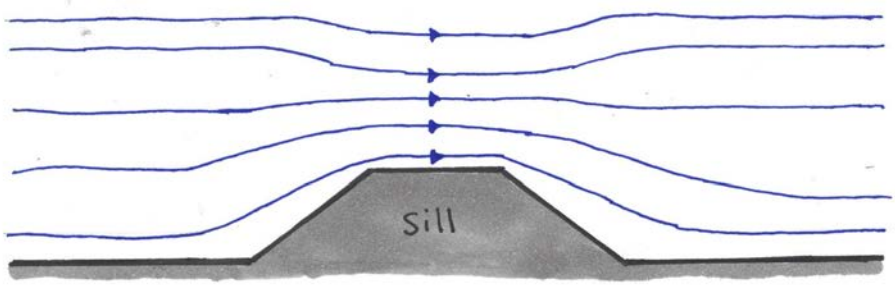

(c) Side view of the general flow pattern of a sand closure at cross section B-B' which is oriented in streamwise-direction.

Figure 2.2: Overview of the general flow pattern of a sand closure. Figures based on CUR Report 157 [13] and Rijkswaterstaat [21].

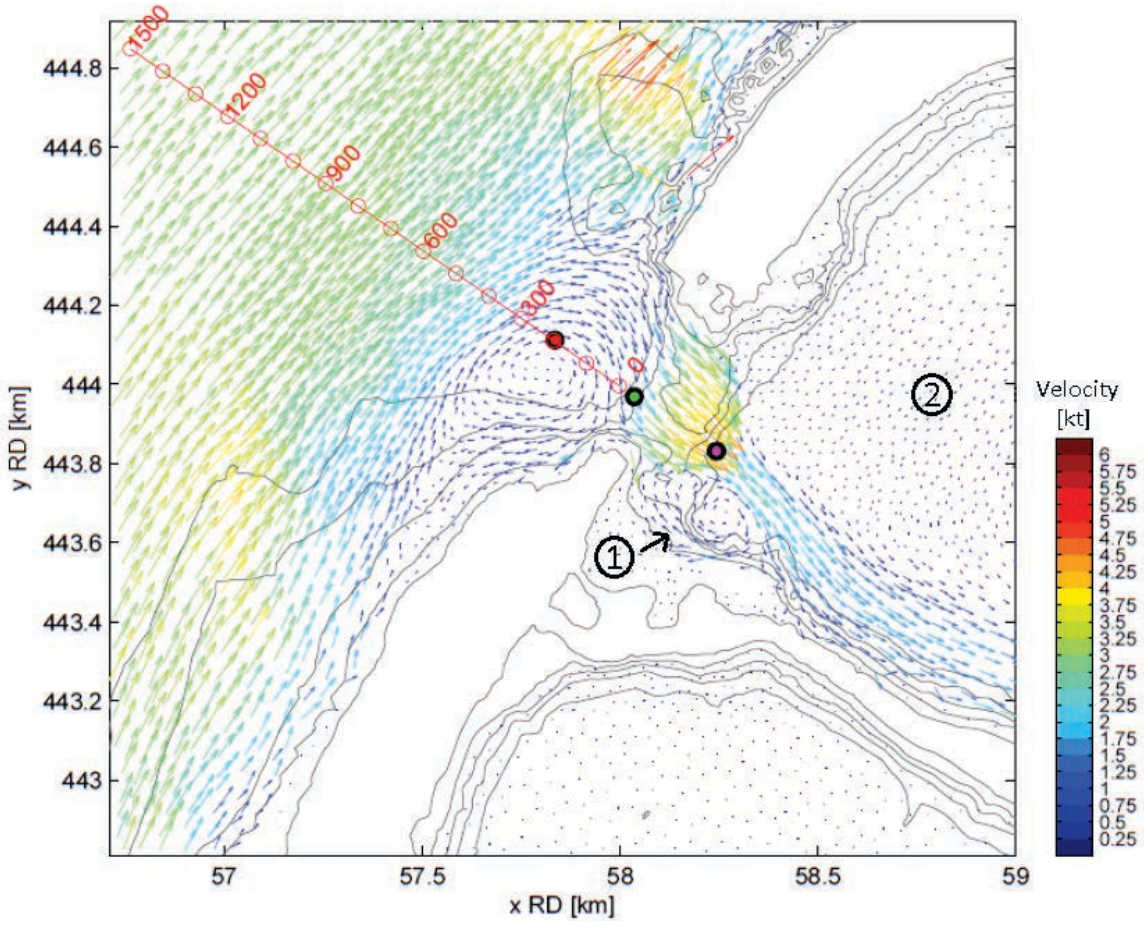

Figure 2.3: Flow velocity field for the final stage of the MV2 closure during rising tide, computed with FINEL2D.

There are two transverse circulations due to the momentum exchange from the main current towards the eddies visible in Figure 2.2b. Because the main current has a more or less logarithmic velocity profile, the flow velocities at the top of the water column are higher than at the bottom, resulting in a larger momentum exchange with the eddies at the top of the water column than with those at the bottom. As a result of mass conservation, an equal amount of momentum should flow towards the main current at the bed. The outward flow at the free surface and the inward flow at the bed therefore form a recirculation current, as depicted in Figure 2.2b. Both these eddies and the just described recirculation currents are not necessarily visible when the banks that restrict the eddies are far away.

The flow patterns depicted in Figure 2.2 are a general schematization of the actual flow patterns that occur during a sand closure. Figure 2.3 shows the result of a depth-averaged numerical simulation of the flow field that occurred during the closure of MV2 at a certain moment in time, when the flow is entering the basin. It can be seen that on the side of the gap idicated with a one, where the basin is constricted by the shore, an eddy is formed that resembles the eddies shown in Figure 2.2; however, on the other side of the closure gap, indicated with a two, no eddy is formed, because the flow is not constricted by the bathymetry there.

Another flow pattern that can be observed in Figure 2.3 is an additional contraction of the flow somewhat downstream of the closure gap. This can be explained by the concept of potential vorticity and will not be discussed in this study. A more elaborate explanation of this mechanism can be found in the author's additional MSc thesis [5].

Due to the recirculations in multiple directions and high turbulence levels in the mixing layers, it can be concluded that the flow is three-dimensional.

2.2.1. Dimensionless numbers

For a general view and description of the flow, two dimensionless numbers are considered: the Froude number and the Reynolds number. To obtain a general characterization for the flow of a sand closure, the dimensionless numbers are discussed below.

The Reynolds number is defined by

$$Re = \frac{UL}{\nu} = \frac{\text{Inertia forces}}{\text{Viscous forces}}, \tag{2.1}$$

where U is the characteristic flow velocity, L is the characteristic length scale, and ν is the kinematic viscosity. For open channel flows, the water depth is usually taken as the characteristic length scale.

For MV2, although the final stage was performed around slack water in order to keep the flow velocities as low as possible, the measured flow velocities varied between one and three metres per second. It was not possible to measure the flow velocities at all times. The maximum value of the velocity was expected to be up to five metres per second. The depth of the closure gap was 1.5 metres at the beginning of the final stage of the sand closure. This implies Reynolds numbers between $1 \cdot 10^6$ and $6 \cdot 10^6$, which indicates turbulent flow.

The second dimensionless number which is important to describe the flow patterns of a sand closure is the Froude number, which is defined by

$$Fr = \frac{U}{\sqrt{gL}} = \sqrt{\frac{\text{Inertia forces}}{\text{Gravity forces}}}, \tag{2.2}$$

where g is the gravitational acceleration. When the Froude number is smaller than one, gravity dominates and the flow is called subcritical. When it is larger than one, the flow is supercritical, and when the Froude number is exactly one, the flow is said to be critical. In the general flow pattern of a sand closure that is depicted in Figure 2.2 cross-section B-B' shows the flow pattern of the flow over a sill. The Froude number on top of the sill cannot exceed a value of 1. A more extensive description of the implications this has on a sand closure can be found in the author's additional MSc thesis [5].

Looking at the example of MV2, the Froude number has a value of about 0.25 for a flow velocity of one metre per second and a depth of the closure gap of 1.5 metre. When the flow velocities increase and the water depth decreases, the Froude number can reach a value of 1.

2.2.2. Turbulence

To obtain more insight in the turbulence that is observed during sand closures, some general information about turbulence is given in this section. In the next section, the turbulent flow of a mixing layer is discussed, which is in essence the main turbulence mechanism found during sand closures. To introduce the subject of turbulence, the definition of turbulence by Tennekes and Lumley [15] is followed. According to them, a turbulent flow is highly irregular and highly diffusive, has a high Reynolds number, large three-dimensional vorticity fluctuations and a high energy dissipation. These flow characteristics are briefly discussed below.

Irregularity

Since turbulent flows vary in both time and space, a statistical approach is needed to describe turbulent flows. One way to do this is by means of Reynolds decomposition. In a certain time frame, where the mean motion may be taken as a constant, the flow can be subdivided into a mean and a fluctuating part as follows:

$$u_j = \overline{u_j} + u_j', \tag{2.3}$$

where u_j is the momentary velocity in the indicated direction, $\overline{u_j}$ is the mean velocity averaged over a specified time frame, and u_j' is the fluctuating component of the velocity. Because the fluctuating component describes a random motion, the value cannot be described directly but is described by a statistical quantity.

Diffusivity
Diffusivity causes mixing and increased momentum transfer, which is important for the description of mixing layers, which are discussed in Section 2.2.3.

Three-dimensional vorticity fluctuations
Turbulent flows are rotational and exhibit large vorticity fluctuations. These fluctuations could not maintain themselves if the velocity fluctuations would be two-dimensional, since vorticity-maintenance is driven by the three-dimensional mechanisms called vortex stretching. The size of the velocity fluctuations relative to the mean flow velocity is called the turbulence intensity and is defined by

$$I = \frac{u_{rms}}{\overline{u_j}} , \tag{2.4}$$

where I is the turbulence intensity, and u_{rms} is the root-mean-square value of the velocity fluctuations u_j'.

Dissipation
Molecular viscosity causes energy decay in any flow. For turbulent flows, the eddies in the flow cause additional energy decay, because they increase the viscous shear stresses on the fluid. This is called eddy viscosity. For larger Reynolds numbers, the relative importance of the eddy viscosity increases.

Large Reynolds numbers
The Reynolds number is large for turbulent flows, however this is not the only demand for the flow to be turbulent.

Although these general characteristics of turbulent flow always hold, all turbulent flows are different. The relative size of the turbulent fluctuations may differ, and the shape of the turbulent eddies can be different. The flow observed from a running tap is not the same as smoke from a chimney, while both are turbulent flows. In the next section, mixing layers are discussed, because these resemble the turbulence that is observed during sand closures the most.

2.2.3. Mixing layers

Mixing layers are an important part of the flow patterns that occur during a sand closure. They are driven by the main current and in turn cause multiple large-scale circulations, like the return currents downstream of the gap. The mixing layers are also expected to cause large amounts of erosion at the heads of the dam.

In general, mixing layers are subdivided into two categories: lateral expansions and free mixing layers. Figure 2.4 shows the flow pattern and streamwise velocity that can be observed for a free mixing layer. In this case, the free mixing layer is induced by a splitter plate with flows of two different velocities flowing past it. When these two flows meet, the velocity difference between the flows causes shear stresses that result in Kelvin Helmholtz instabilities that lead to turbulence. The width of the resulting mixing layer increases linearly downstream.

Figure 2.5 shows a mixing layer as the result of a shallow lateral expansion. The flow pattern differs from the pattern of a free mixing layer, because at the expansion, there is an adverse pressure gradient giving rise to a separation point. The resulting flow pattern has a fast flowing part and a part with low flow velocities, transferring energy through turbulence. In the part with the low flow velocities, recirculations occur, as depicted in Figure 2.5. This is the result of side-wall effects. It should be noted that the smaller eddy in the bottom of Figure 2.4a only develops in certain situations and after a long time.

The location where the recirculation area ends and the flow reattaches to the side of the flume is called the reattachment point. The distance between the expansion and this point is called the reattachment length. Talstra [14] on shallow mixing layers showed that the reattachment length depends on the expansion width, the water depth and the roughness of the bed. Furthermore, an increase in discharge would lead to a slight increase in the reattachment length. Talstra also found that for rela-

tively deep flows, the reattachment length is proportional to the lateral expansion width. The largest reattachment lengths found by Talstra were between six and ten times the lateral expansion width, where the smallest reattachment lengths were found for the shallowest flows.

Mixing layers may occur in deep or in shallow water. For both situations, their characteristics are different. In deep water, a mixing layer widens according to the self-similarity principle. This means that the shape of the velocity profile does not change in downstream direction, but with the widening of the flow the largest flow velocities decrease. For shallow flows, the influence of bottom friction increases in downstream direction, which hampers the development of the width of the mixing layer. Most research on shallow mixing layers uses a depth-width ratio of about 1:20 [14,18,17]. For this research, it is assumed that if a mixing layer has a depth-width ratio of 1:20, it is a shallow mixing layer.

The mixing layers of sand closures are in essence mixing layers as the result of a lateral expansion, but do not fall into this category because they also exhibit a contraction before the flow expands. Furthermore, the sand-body that forms this contraction and expansion has slopes which alter the flow pattern even further. At the head of the closure dam, the flow pattern is that of a shallow mixing layer. Downstream of the dam, the depth increases and so does the width of the mixing layer. Further downstream, the mixing layer slowly changes from a shallow mixing layer to a regular mixing layer.

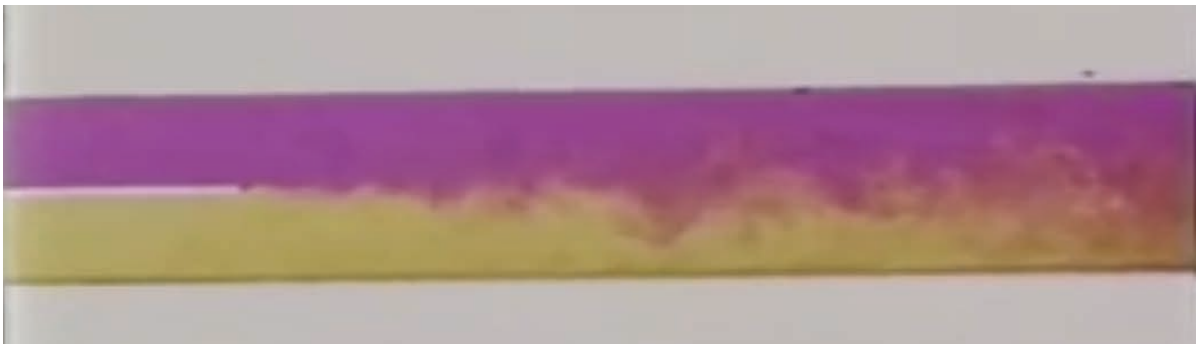

(a) A visualization of the flow pattern of a free mixing layer. Figure from video 'turbulence' by The national committee for fluid mechanics films [8]

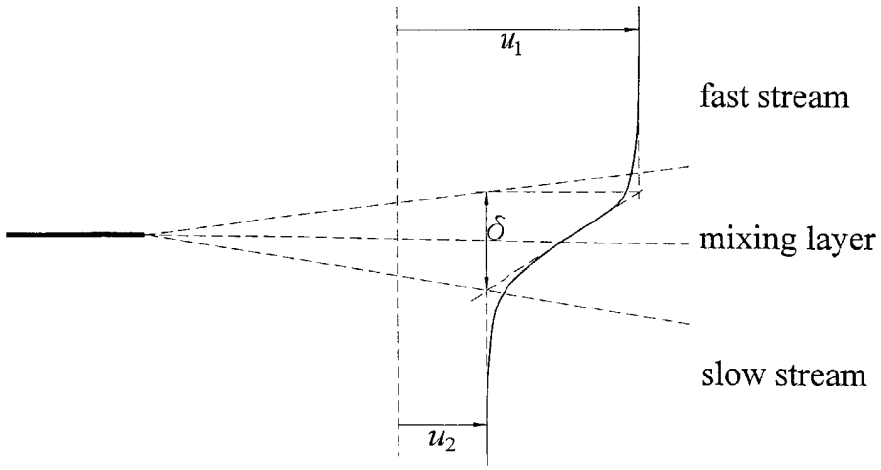

(b) A schematic of the streamwise velocity of a free mixing layer. Figure from Tukker [17].

Figure 2.4: Flow pattern of a free mixing layer.

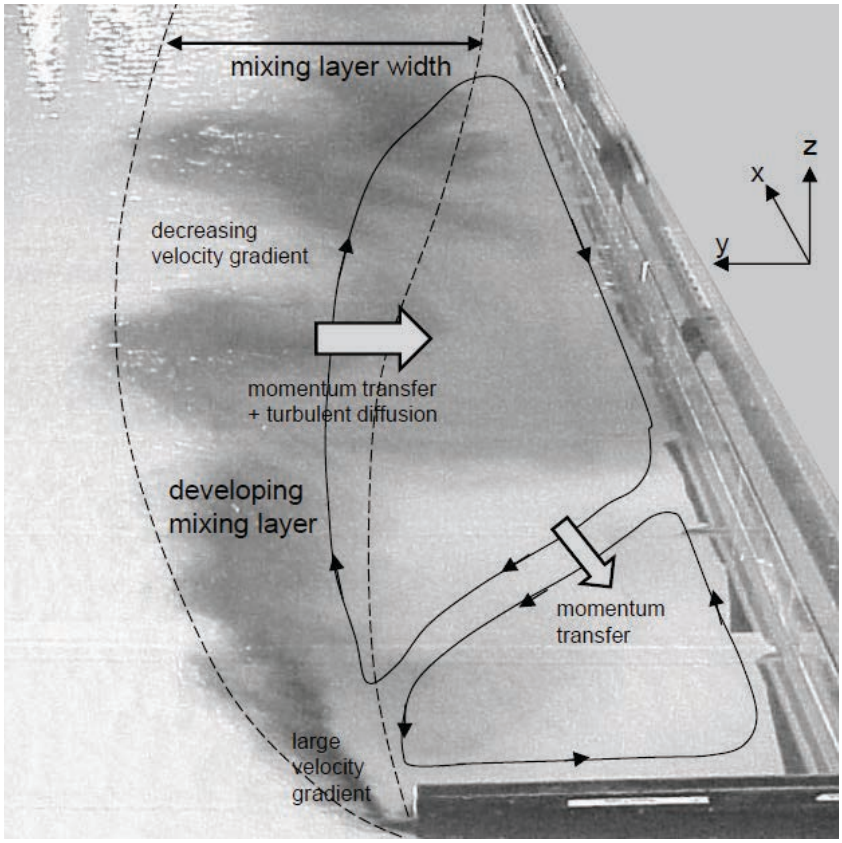

Figure 2.5: The flow pattern of a shallow mixing layer, of which the lateral expansion is located at the bottom of the figure. Figure from Talstra [14].

Figure 2.6: Damage pattern of gravel under a mixing layer caused by a lateral expansion. Figure from Zuurveld [23].

2.2.4. Erosion under mixing layers

There is little known about erosion under mixing layers. In literature, one research on the erosion of mixing layers can be found. Zuurveld [23] investigated the damage pattern of gravel under a shallow mixing layer. Gravel has a different morphological behaviour than sand, for instance, gravel does not form bedforms, while sand does. Still, the research gives insight in where most of the erosion of the sand bed can be expected. Figure 2.6 shows the damage pattern after an experiment of Zuurveld. It can be seen that most of the erosion occurs in the mixing layer where the highest flow velocities and the highest degree of turbulence occurs.

2.3. Sediment transport

The morphology prediction of sand under a mixing layer is not known from literature. To be able to estimate the amount of erosion that occurs during a sand closure, knowledge about sediment transport is crucial. This section aims to provide an overview of the relevant theory on sediment transport for sand closures. The section starts with a general description of sediment transport, and then goes into the specific case of sediment pick-up under turbulent conditions.

When looking at sediment transport in general, there are two ways in which the sediment can be transported: as suspended load and as bedload. There is a gradual transition between bedload and suspended load for which both transport modes are distinguished, depending on the flow conditions. The transport mode is defined by the Rouse number which is given by Fredsøe and Deigaard [3] as:

$$P = \frac{w_s}{\kappa u_*} , \tag{2.5}$$

where w_s is the settling velocity of a particle, κ is the Von Kármán constant, and u_* is the bed-shear velocity. Commonly used ranges for Rouse number are:

$P > 7.5$	Little movement	
$7.5 \geq P \geq 2.5$	Bedload	Sediment rolls and slides over bed; bedforms are formed
$2.5 \geq P \geq 1.2$	Incipient suspension	Bedforms increase in length and decrease in amplitude
$P < 1.2$	Suspension	Plane bed

For high Rouse numbers, there is no transport of sediment. When the Rouse number decreases, the picked-up sediment gets higher into the water column. Figure 2.7 shows the distribution of sediment over the water column for different Rouse numbers. It can be seen that for high Rouse numbers, only a layer at the bottom of the water column is filled with sediment. When the Rouse number decreases, the sediment becomes more uniformly distributed over the depth. When the Rouse number becomes even higher than the values depicted in Figure 2.7, and the transport mode becomes bedload transport, the profile reduces to a small layer of sediment rolling and sliding over the bed.

The sediment from MV2 had a diameter of about 400 micrometres and, based on the flow properties mentioned in Section 2.2, the Rouse number for the final stage of a sand closure varies between 5.5 and 1. This means that for the lower flow velocities of a sand closure bedload would be the significant transport mode; however, as the flow velocities increase, the amount of sediment in suspension increases. For the final stage of the sand closure, suspended sediment transport is definitely the most important transport mechanism, as can be seen in the photograph of the Cdam in Figure 2.1. This photograph shows very turbid water, suggesting that a large amount of sediment is in suspension. This is not entirely due to the pick-up of sediment. It is also due to the fact that a large amount of additional sediment is added to the gap in order to close it, bringing a significant amount of additional suspended sediment into the system.

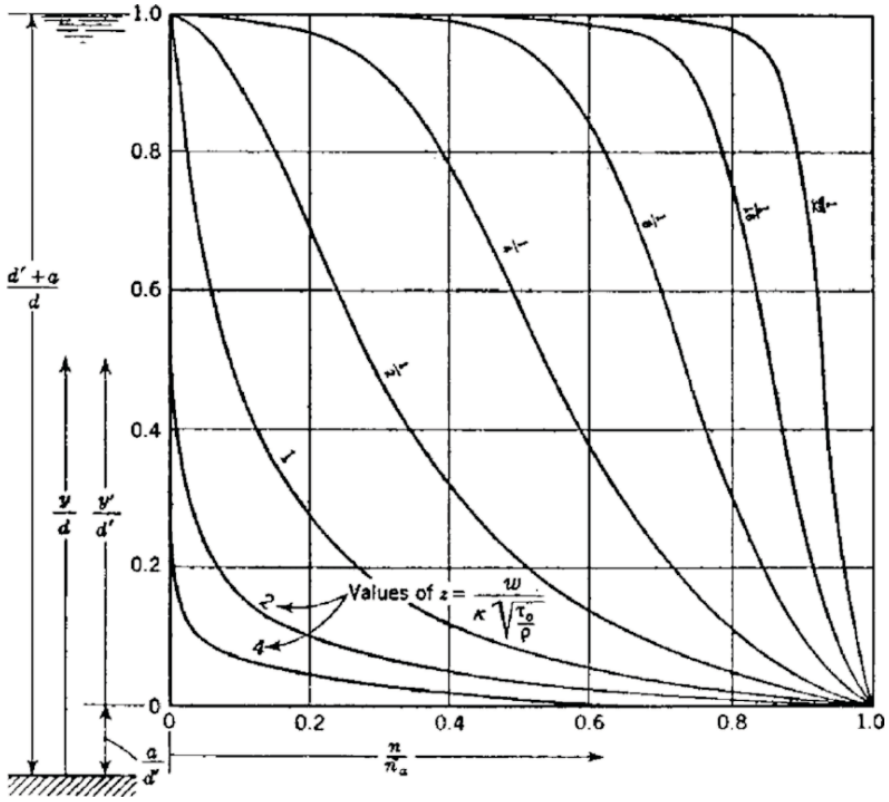

Figure 2.7: Plot of the dimensionless sediment distribution over the dimensionless depth plotted for various Rouse numbers. Figure from Rouse [12].

Generally, the transport of sediment through water is described using an advection-diffusion equation, also called the transport equation. This equation describes the transport of the volume fractions of sand, water and air in the flow, C_l, and is given by:

$$\frac{\partial C_l}{\partial t} = \frac{\partial}{\partial x_1}\left(\Gamma\frac{\partial C_l}{\partial x_1}\right) + \frac{\partial}{\partial x_2}\left(\Gamma\frac{\partial C_l}{\partial x_2}\right) + \frac{\partial}{\partial x_3}\left(\Gamma\frac{\partial C_l}{\partial x_3}\right) - \frac{\partial u_i C_l}{\partial x_i}\ , \tag{2.6}$$

where C_l is the volume fraction of sediment, water or air; t is time; x_i, x_1, x_2 and x_3 are Cartesian coordinates; u_i are the Cartesian velocity components; and Γ is the diffusion coefficient $\frac{\nu_e}{Sc}$ in which Sc is the Schmidt number. The subscript i can have a value 1, 2, or 3 to represent the Cartesian coordinates x_1, x_2 or x_3, and their corresponding velocity components u_1, u_2, u_3.

In short, this equation states that the change of the volume fraction of sediment in time depends on the advection and diffusion of the sediment particles in the flow. The second, third and forth term are the diffusion terms, and the last term is the advection term. Furthermore, the sediment fraction also depends on an interaction with the bed. When the sediment is eroded from, or deposited onto the bed, the ratio between the water fraction and the sediment fractions changes.

Numerically, the advection-diffusion equation can be solved directly when choosing the proper discretization schemes. However, determining the erosion and deposition fluxes is not straightforward and requires some additional equations. To parametrize the interaction between the transport equation and the bed, pick-up equations and sedimentation equations are used. Pick-up equations attempt to predict the upward flux of sediment from the bed into the flow, where it is transported by the transport equation. The sedimentation equation calculates the settling flux of particles onto the bed, reducing the volume fraction of sediment particles in the transport equation.

To parametrize the erosion of sediment from the bed, a distinction is made between equations that describe suspended load and equations that are used for bedload transport. Usually, bedload transport is calculated using bedload transport formulas. The erosion and deposition of suspended sediments

is mostly calculated using pick-up equations. It was established above that during the final stage of a sand closure, when most of the sand is eroded, the transport mode has the form of suspended load. For this reason, only equations that are applicable to suspended transport are discussed. These are called pick-up equations. The parametrization for sedimentation of particles is discussed in Section 2.3.2.

2.3.1. Pick-up equations

Pick-up equations are equations that calculate the entrainment of sediment by the flow. Because pick-up equations do not assume an equilibrium transport for the amount of sediment being picked-up and deposited onto the bed, they should be especially suited for mixing layers. However, almost all pick-up equations, such as the pick-up equation of Van Rijn [20], are designed for river flows, which have lower flow velocities and turbulence intensities than sand closures, and use a mean flow velocity to calculate the sediment pick-up.

When the turbulence levels in the flow are higher, the flow velocities fluctuate more around the mean velocity. This has implications on the sediment pick-up. For flows with higher turbulence intensities, the highest shear stresses are higher and show larger variations than the shear stresses for a typical river flow. This is due to flow bursts. The higher shear stresses imply increased instability of the grains.

For any flow, pick-up is stochastic. This is because not al grains are the same and thus each grain has a different value for incipient motion. Furthermore, the flow and thus the fluid forces on the particle change in time as well. These changes increase as the turbulence in the flow increases, which could have influences on the pick-up.

For a typical river flow, the thickness of the laminar sublayer is not constant in time and place due to eddies passing by in the flow. When the turbulence intensity increases, the variations in the thickness of the laminar sublayer becomes larger as well. With eddies penetrating further into the laminar sublayer and maybe even eliminate the presence of the laminar sublayer at certain times, it seems possible that locally the pick-up of sediment can increase significantly.

For the high flow velocities that occur during a sand closure, the pick-up equation of Van Rhee [19] is available, of which the details are discussed in the author's additional MSc thesis [5]. Since turbulence seems to play such an important role during sand closures, the turbulent kinetic energy (TKE) method [22] is discussed because it uses the turbulence intensity as a parameter to determine erosion. Finally, the pick-up equation of Okayasu et al. [9] is treated. This equation is similar to the formula of Van Rijn, but incorporates the effects of turbulence on sediment pick-up.

The pick-up formula of Van Rijn

The pick-up formula of Van Rijn [20] was developed to predict the pick-up of sediment for non-equilibrium transport in rivers. Van Rijn conducted experiments to verify this formula for flow velocities up to one metre per second. The dimensionless shear stress exerted on the bed is called the Shields parameter, θ, and is used as a dimensionless number to compare the fluid force that removes grains from the bed and the restoring downward force by the specific weight of the particles. The Shields parameter is defined by

$$\theta = \frac{\tau_b}{(\rho_s - \rho_w) g D_{50}} = \frac{u_*^2}{\Delta g D_{50}} , \tag{2.7}$$

where τ_b is the bed shear stress, ρ_s is the density of sediment, ρ_w is the density of water, D_{50} is the median particle diameter, Δ is the relative sediment density, and u_* is the bed-shear velocity defined by

$$u_* = u \frac{\sqrt{g}}{C} , \tag{2.8}$$

in which C is the Chézy coefficient. The relative sediment density, Δ is defined by

$$\Delta = \frac{\rho_s - \rho_w}{\rho_w} . \tag{2.9}$$

The Shields parameter is compared to a critical value for the initiation of motion of a particle, called the critical Shields parameter, θ_{cr}. The critical Shields parameter serves as a threshold of motion for the sediment particles based on a critical shear stress. The critical Shields parameter is defined by Van Rijn as:

$$\theta_{cr} = \begin{cases} \frac{0.24}{D_*} & \text{for } 1 \leq D_* \leq 4 \\ \frac{0.14}{D_*^{0.64}} & \text{for } 4 \leq D_* \leq 10 \\ \frac{0.04}{D_*^{0.1}} & \text{for } 10 \leq D_* \leq 20 \\ 0.013 D_*^{0.29} & \text{for } 20 \leq D_* \leq 150 \\ 0.055 & \text{for } D_* \geq 150 \end{cases} . \tag{2.10}$$

This critical parameter depends on the dimensionless grain diameter, D_*, which is given by

$$D_* = D_{50}\left[\frac{\Delta g}{\nu^2}\right]^{1/3} , \tag{2.11}$$

where ν is the kinematic viscosity of water. The dimensionless grain diameter depends on the properties of both the sediment and the fluid. The sediment pick-up flux, E, can now be calculated with

$$E = 0.00033\rho_s \left(\frac{\theta_t - \theta_{cr}}{\theta_{cr}}\right)^{1.5} \frac{\Delta^{0.6} g^{0.6} D^{0.8}}{\nu^{0.2}} , \tag{2.12}$$

which can be converged into the erosion velocity of the bed, v_e, as follows:

$$v_e = \frac{E}{\rho_s(1 - n_0)} , \tag{2.13}$$

where n_0 is the bed porosity prior to erosion.

TKE method

In the author's additional MSc thesis, the TKE method was introduced as a promising pick-up equation for pick-up of sediment under the turbulent flows of a sand closure. This method uses the Turbulent kinetic energy (TKE) in the flow to estimate the shear stress on the bed with the equation found by Pope et al. [10]:

$$\tau_b = C_1 TKE , \tag{2.14}$$

where TKE is the Turbulent kinetic energy in the flow, and C_1 is a constant, which was found to be 0.19 for a typical river flow by Le Courtier et al. [6] and Thompson et al. [16]. The TKE method for different turbulence intensities are shown in Figure 2.8. A turbulence intensity of 0.1 is typical for a river flow, and the TKE method depicts similar results as the formulas of Van Rijn and Van Rhee. The TKE method shows that for a turbulence intensity of 0.3, the predicted pick-up is 200 times higher than for a flow with a twice as high flow velocity and a turbulence intensity of 0.1. These are in no way trustworthy results but it is expected that turbulence plays and important role in the amount of sediment pick-up.

Pick-up equation of Okayasu et al.

The TKE method uses the amount of turbulent kinetic energy in the flow as a factor in the shear force. The equation of Okayasu et al. [9] uses a different approach to take turbulence into account in the amount of pick-up.

Okayasu et al. derived a variation on the Van Rijn's equation [20]. The equation of Okayasu et al. differs from the equation of Van Rijn by the incorporation of inertia and the root-mean-square value of the velocity fluctuations in the force balance on a grain.

The pick-up rate, E, is defined by Okayasu et al. as:

$$E = 0.00033\rho_s \left(\frac{\theta_t - \theta_{cr}}{\theta_{cr}}\right)^{1.5} \frac{(\Delta)^{0.6} g^{0.6} D^{0.8}}{\nu^{0.2}} , \tag{2.15}$$

where θ_t is the modified Shields parameter, θ_{cr} is the critical Shields parameter, Δ is the relative sediment density, and D is the particle diameter. This equation is equal to Equation (2.12), which is used

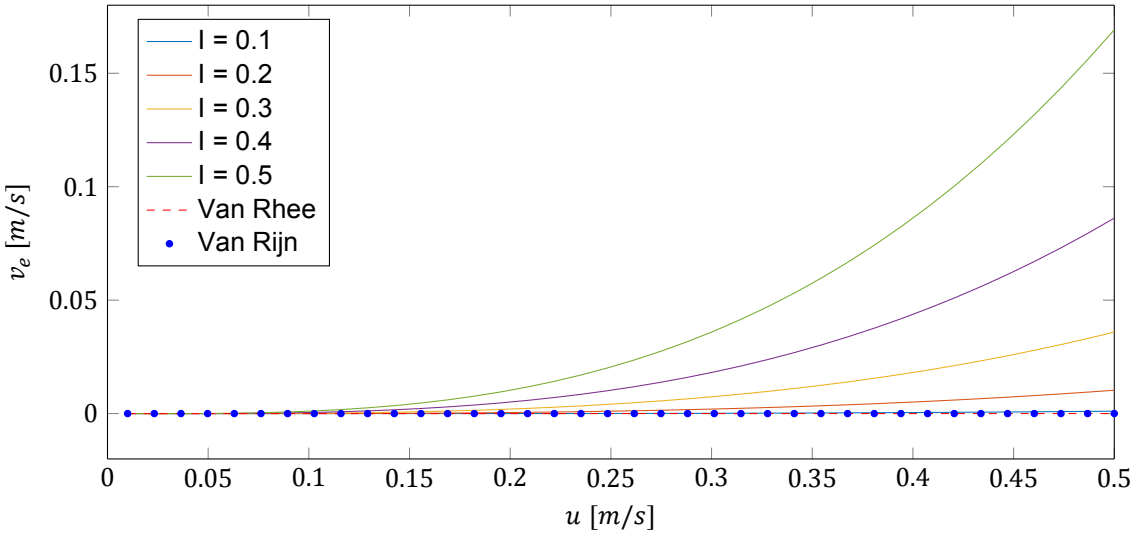

Figure 2.8: Comparison of the pick-up formula of Van Rijn [20], Van Rhee [19] and the TKE method [22]. I is the turbulence intensity in the flow.

by Van Rijn [20], except the Shields parameter is defined differently. In the formula of Van Rijn, the Shields parameter is defined by Equation (2.7), which is based on the mean flow velocity. Okayasu et al. proposed a modified Shields parameter defined as the forces acting on a grain, including the inertia force:

$$\theta_t = \frac{F_D + F_I}{W - F_L} , \tag{2.16}$$

where F_D is the drag force, F_I is the inertia force, W is the gravitational force, and F_L is the lift force. All these forces include turbulence effects. The drag force, in line with the formula of Michaelides [7], is given by

$$F_D = \frac{1}{2} C_D \rho_w \frac{\pi D^2}{4} u_{bt}^2 , \tag{2.17}$$

where C_D is the drag coefficient, and u_{bt} is the bottom shear velocity including the turbulent component. The bottom shear velocity is given by

$$u_{bt} = \frac{\kappa}{\ln\left(\frac{30.1z}{D}\right)} u , \tag{2.18}$$

where κ is the Von Kármán constant, z is the height of the velocity measuring point from the bed, and u is the instantaneous flow velocity. This formula assumes a logarithmic velocity profile to calculate the shear velocity at the bed and assumes hydraulically rough bed conditions without bedforms. In Formula (2.17), the drag coefficient is given by

$$C_D = \frac{24}{Re_p}\left(1 + 0.15 Re_p^{0.687}\right) \quad \text{for} \quad Re_p < 1000 . \tag{2.19}$$

This formula assumes spherical grains and uses the particle Reynolds number, Re_p, which is defined by

$$Re_p = \frac{\rho_w u_{bt} D}{\mu} . \tag{2.20}$$

The inertia force is defined by

$$F_I = C_I \rho_w \frac{\pi D^3}{6} \frac{\mathrm{d}u_{bt}}{\mathrm{d}t} . \tag{2.21}$$

In essence, this states Newton's second law with a factor C_I that seems to account for the fact that

sand grains are not spherical. Okayasu et al. used a value of 1.5 for the inertia coefficient, C_I.

The lift force is given by

$$F_L = \frac{1}{2} C_L \rho_w \frac{\pi D^2}{4} u_{bt}^2 \,. \tag{2.22}$$

This formula is based on the study of Einstein and El-Samni [2], who found that the lift coefficient, C_L, is 0.178. This only holds if the flow velocity is measured at a distance of 0.35 diameters from the theoretical wall. However, the experiment was conducted for half spheres with a diameter of about seven centimetres glued to a wall. The value of the lift coefficient is thus uncertain for sediment grains. Okayasu et al. used a value of 0.2 for the lift coefficient.

The gravity of a particle is defined as the submerged weight:

$$W = g\,(\rho_s - \rho_w)\,\frac{\pi D^3}{6} \,. \tag{2.23}$$

This formula is especially interesting for turbulent flows because it incorporates an inertia force that most other formulas do not take into account. This inertia force depends on the accelerations in the flow, of which the importance increases for an increasing turbulence intensity.

Discussion

The three presented pick-up equations are all parametrizations of the actual sediment pick-up, each with its own assumptions. The pick-up equation of Van Rijn uses the ratio between the shear forces of the flow and the submerged gravity of particles to determine the amount of erosion. It only uses the mean flow velocity to determine this ratio. This might be a problem during sand closures, because the flow velocities are very variable due to both the tide and the large turbulent fluctuations.

The TKE method uses the turbulent kinetic energy in the flow to estimate the bed shear stresses. It gives untrustworthy results when the turbulence intensity in the flow increases. The formula of Okayasu et al. seems to have better physical grounds than the TKE method with respect to the incorporation of turbulence on the prediction of the amount of pick-up under a turbulent flow. However, this formula presumes hydraulically rough bed conditions without bedforms. Furthermore, it is unsure if the presently used lift force is applicable to sand. The presumption of hydraulically rough bed conditions should not be a problem for sand closures as long as there is suspended sediment transport and the grain diameter is large enough. However, this is not the case for all stages of a sand closure, since it was established that for the lower flow velocities there are bedforms present.

The different formulas cannot be compared because more detailed information on the turbulent fluctuations is necessary to calculate the pick-up equation of Okayasu et al. [9].

2.3.2. Sedimentation

Besides pick-up equations, there are also lots of sedimentation equations available in literature. Only the sedimentation formula of Van Rijn [20] is discussed. This is a generally applicable formula and is suitable for grain diameters between 100 and 1000 micrometres. It calculates the settling velocity as follows:

$$w_s = 11.4 \frac{\nu}{D_{50}} \left[\sqrt{1 + \frac{0.01(\rho_s - \rho_w) g D_{50}^3}{\rho_w \nu^2}} - 1 \right] , \tag{2.24}$$

where w_s is the settling velocity of a particle, D_{50} is the median particle diameter, μ is the dynamic viscosity of water, and S_F is the shape factor of sand grains. Since natural sand grains are not spherical, a shape factor of 0.7 is used to obtain the settling velocity for sand. To transfer this settling velocity to the amount of sedimentation, the following formula is used:

$$S = \rho_s w_s c_b \,, \tag{2.25}$$

where S is the sedimentation or settling flux, and c_b is the near-bed volumetric sediment concentration.

As can be seen in the above formula, the flow characteristics do not play a role in the settling of particles in the flow. This would mean that turbulence would not have any influence on the settling velocity of a particle. Nevertheless, it is expected that when turbulence plays an important role in the pick-up of sediment, it is important for sedimentation as well.

2.4. Discussion

Based on the literature discussed in this chapter, some general conclusions are drawn about the important properties that the experiments and the numerical model should incorporate. In Section 2.2, it was found that the flow patterns of a sand closure are three dimensional and that, at certain locations, the flow is turbulent. Turbulent eddies in the flow cause the flow velocities to deviate from the mean flow velocity. The larger the eddies, the larger these deviations. To describe these characteristics of the flow accurately, a three-dimensional model is needed.

Turbulence is most important for the erosion that occurs during a sand closure. To predict the pick-up of sand a number of formulas are available. Unfortunately, most of them incorporate a mean flow velocity to predict the pick-up, while a different approach is required for a turbulent flow. Despite that the pick-up formula of Okayasu et al. [9] makes some assumptions about the properties of the turbulence, it seems to be the best choice for a pick-up equation to calculate the erosion for a sand closure. The pick-up equation of Okayasu et al. incorporates the effects of turbulence on the pick-up of sediment. Unfortunately, only laboratory experiments were executed for grid turbulence. No literature can be found that suggests that this formula has been implemented in a numerical model.

It can be concluded that the turbulence that occurs during a sand closure resembles a lateral expansion, but with an additionally a contraction of the flow before it reaches the expansion; furthermore, the heads of the dam exhibit a sloping bed. No literature is available on the pick-up of sediment for the turbulent conditions that are found during a sand closure. To gain knowledge about the pick-up of sediment under turbulent flows, laboratory experiments are set up in this thesis. A laboratory experiment that investigates the morphology for a lateral expansion is set up, because it resembles the turbulence that is found during a sand closure, but does not involve additional complicated mechanisms like a slope or contraction.

does not add too many extra sediment pick-up mechanisms. To make sure that the experiments resemble the conditions during a sand closure as much as possible, the suspended transport mode should be taken into account.

To make sure the research can be extended to predict the sand loss during a sand closure, a numerical model is required. It is chosen to combine the laboratory experiments with a numerical model for this research. The same set-up was chosen for both the numerical model and the experimental model. The layout of both is based on a lateral expansion. The experiments are used to validate the flow pattern and to compare the erosion and sedimentation predicted by the numerical model.

3

Experimental set-up

The goal of the laboratory experiments is to obtain data about the morphology under a mixing layer. As shown in Chapter 2, the flow patterns of a sand closure are complex, because of the high flow velocities, high degree of turbulence and multiple circulations in the flow.

One of the most important parts of the flow for erosion are mixing layers. Unfortunately, little is known about the morphology patterns underneath mixing layers. Therefore, it is chosen to conduct experiments on these erosion and sedimentation patterns. To make sure that the observed patterns are actually caused by a mixing layer, other complicated flow mechanisms that occur during a sand closure, such as a sloping erodible surface and contraction of the flow, are avoided as much as possible in the set-up of the experiment. It is chosen that the best way to investigate the pick-up under a mixing layer is with a flume originating from a lateral expansion.

The results from the experimental study are used to validate the numerical model and to predict the sediment pick-up under a mixing layer in Chapter 5. The goal of these experiments is to obtain quantitative data about the flow characteristics and the development of the bed level over time in order to be able to compare the data with the results of the numerical study.

Two sets of experiments are executed, one with a fixed bed and one with an erodible bed. The first set of tests is meant to provide a reference for the flow patterns of the experiments, without the interference of bed level changes. During the second set of tests, an erodible bed is placed on the bottom of the flume and the bed level changes are measured. Furthermore, it is desired to determine the influence of the changes to the bed on the flow; therefore, flow measurements should be executed for this set of experiments as well.

Some considerations that resulted in the set-up of the experiments are treated in Section 3.1. Section 3.2 discusses the set-up of the laboratory experiment. The measurement methods used during the experiments are discussed in Section 3.3. Finally, Section 3.4 gives an overview of the executed experiments.

3.1. Model considerations

To make sure that the experiments are similar to the flow and morphology conditions observed during sand closures, the relevant dimensionless numbers that need to be taken into account are discussed in Subsection 3.1.1. An elaboration on the used measuring equipment is discussed in Subsection 3.1.2. Subsection 3.1.3 describes the considerations that let to the flume dimensions. Finally, considerations regarding the sediment diameter are discussed in Subsection 3.1.4.

3.1.1. Dimensionless numbers

Four dimensionless numbers need to be taken into account when designing the laboratory experiments. These numbers have been discussed in Chapter 2, and are used in this section to see which restrictions these dimensionless numbers impose on the laboratory experiments.

There are two dimensionless numbers that make sure the flow characteristics are equal to those of a sand closure, being the Froude number and the Reynolds number. In case of a free surface flow, the Froude number should be kept the same as for a sand closure. Furthermore, the Reynolds number should be large enough to make sure the flow stays in the turbulent regime. Flow velocities between one and three metres per second were measured for MV2, and it was expected that flow velocities could be up to five metres per second locally. As discussed in Chapter 2, for MV2, the Froude number varied between 0.25 and 0.78, and could even become one for the highest flow velocities. For MV2, the Reynolds number varied between $1.15 \cdot 10^6$ and $3.45 \cdot 10^6$.

To replicate the morphology of a sand closure, two other dimensionless numbers are used, being the Shields parameter and the Rouse number. The Rouse number is a measure for the way in which sediment is transported; as suspended or as bedload transport. The Shields parameter represents the ratio between the fluid forces on a grain and its weight. For MV2 the values for the Shields parameter varied between 0.3 and 7.5. The values for the Rouse number were between 5.5 and 1, ranging between bedload and suspended load.

When designing the experiments, it should be attempted to keep the values of these four dimensionless numbers as close as possible to the values of MV2.

3.1.2. Measuring equipment

Because the flow measurements are used to validate the flow patterns of the numerical model, it is desired to perform extensive and accurate flow measurements that can measure the turbulent characteristics of the flow, in order to have a thorough validation of the numerical model.

Most measuring equipment is well suited to measure flow velocities in clear water, but for more turbid water, less options are available. Particle Image Velocimetry (PIV) or Laser Doppler Anemometry (LDA), for instance, cannot be used to measure in a flow that is too turbid. With these considerations and the availability of measurement equipment, it was chosen to execute point measurements with an Acoustic Doppler Velocimeter (ADV). The bed level changes are tracked by using laser distance meters along three streamwise defined transects.

3.1.3. Flume dimensions

The dimensions of the flume are restriced by some diverse demands caused by both the nature of the experiments and the laboratory facilities. The water depth cannot be too large because of the maximum capacity of the pump. There are also several restrictions to the width of the flume. To avoid sidewall effects, the flume should be as wide as possible. Frostick et al. [4] advises a width-to-depth ratio between three to five in order to minimize secondary circulation ($b/h > 3$) and avoid the development of non-uniform bed conditions ($b/h < 5$). Also, a flow stabilisation zone of 10 to 20 times the water depth is advised. Finally, the flume should be long enough to allow the mixing layer to reattach to the side of the flume before it reaches the end of the flume. If the mixing layer does not reattach before the end of the flume, it could lead to significantly different flow patterns. Because the maximum length that the flume could reach is seven metres, and the reattachment length depends on the expansion width, this implies that the expansion width should not exceed a value of 25 centimetres.

3.1.4. Sediment diameter

In order to keep the Rouse number in the same range as the values of MV2, the laboratory experiments need to be conducted with a fine sediment with a diameter between 70 and 170 micrometres. For these small grain diameters, more sand suspends during the experiments, which makes the water turbid. Because the lasers need clear water to be able to measure the bed, pausing the experiments for hours would be required to obtain accurate measurements. Therefore, a sediment with a median grain diameter of 330 micrometres is used to conduct the experiments.

3.2. Experimental set-up

In this section the experimental set-up is presented, taking the restictions discussed in the previous section into consideration. This layout of the laboratory experiments is depicted in Figure 3.4. The layout consists out of a flume with a flow direction from left to right in the figure. A flow straightener, as

depicted in Figure 3.2, is placed at the beginning of the flume to make sure that the turbulence present at the inflow is broken up before it enters the test section. The flow straightener consist out of tubes with one-centimetre diameter glued together. There are two separate elements, one of 20 centimetres long and one of 40 centimetres long, with a spacing of 40 centimetres. A layer of Duct tape is located at the water level to make sure the water only flows in over the desired height.

Two metres after the flow straightener, the flume expands from 25 centimetres to 50 centimetres. At this expansion, a mixing layer forms with its origin located at the tip of the expansion. At the end of the flume, there are two compartments: in the first compartment the pump is located and the second compartment functions as an overflow. The entrance of the second compartment is a weir to retain a constant water level in the flume. A small amount of water is additionally supplied at the inflow, which flows over the weir at the end of the flume. During the laboratory experiments, the flume was filled with 16 centimetres of water. The pump at the end of the flume circulated both the water and the sediment from the end of the flume back to the inflow compartment.

Looking at the requirements to the width-to-depth ratio explained in the previous section, the wide part of the flume has a ratio of 3.1, which means there is no problem with the flume being either too narrow or too wide. However, the width-to-depth ratio in the narrow part of the flume is 1.6, which could mean that some secondary circulations may occur in this part of the flume.

Sediment with a median diameter of 330 micrometres was selected for the experiments. Its sieve curve is given in Figure 3.1. Because the experimental set-up is much smaller than an actual sand closure, the sediment used for the experiments is relatively coarse. Due to this large grain diameter, the Shields number was much lower for the experiments than for MV2.
Two sets of experiments are conducted: one set with a non-erodible bed to study the flow patterns, and one set with a sediment layer of twenty centimetres placed on the bottom of the flume to study the morphology. For the first set of tests, a layer of sediment is glued to the bottom of the physical flume as shown in Figure 3.3. In this way, the same roughness is obtained as for the second set of tests, so the flow experiments are identical to the morphology experiments, except for the changes of the bed during the second set of tests. It actually turned out to be difficult to make the erodible bed completely straight over the entire five metres of flume. Variations with a maximum of one centimetre were allowed to occur in the bed height over the entire length of the flume.

During an experiment, water flows from left to right in Figure 3.4 at a certain flow velocity. The duration of a morphology experiment was two to three hours, until the bed level changes became negligible. Between the different experiments, only the flow velocity was varied.

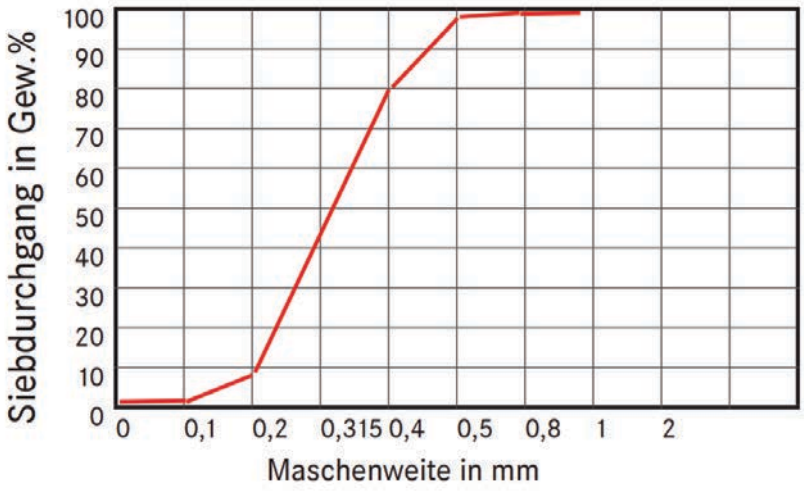

Figure 3.1: Sieve curve of the sediment used for the laboratory experiments. On the horizontal axis, the mesh size of the sieves is given in millimetres. On the vertical axis, the percentage of sediment with a smaller grain diameter is depicted. Figure from Quartzsand [11].

Figure 3.2: A photo of the flow straightener located at the beginning of the flume.

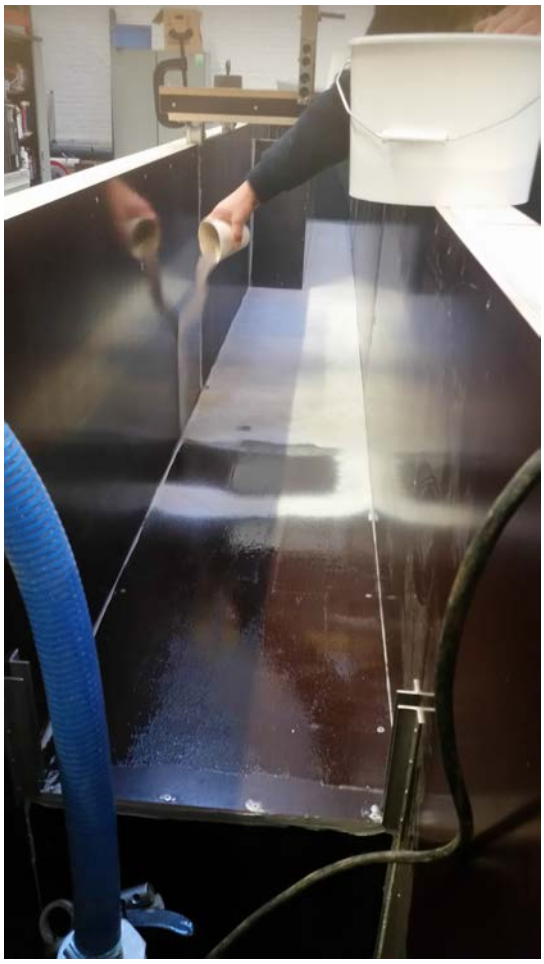

Figure 3.3: A photo of how epoxy was used to glue a layer of sediment to the bottom of the flume.

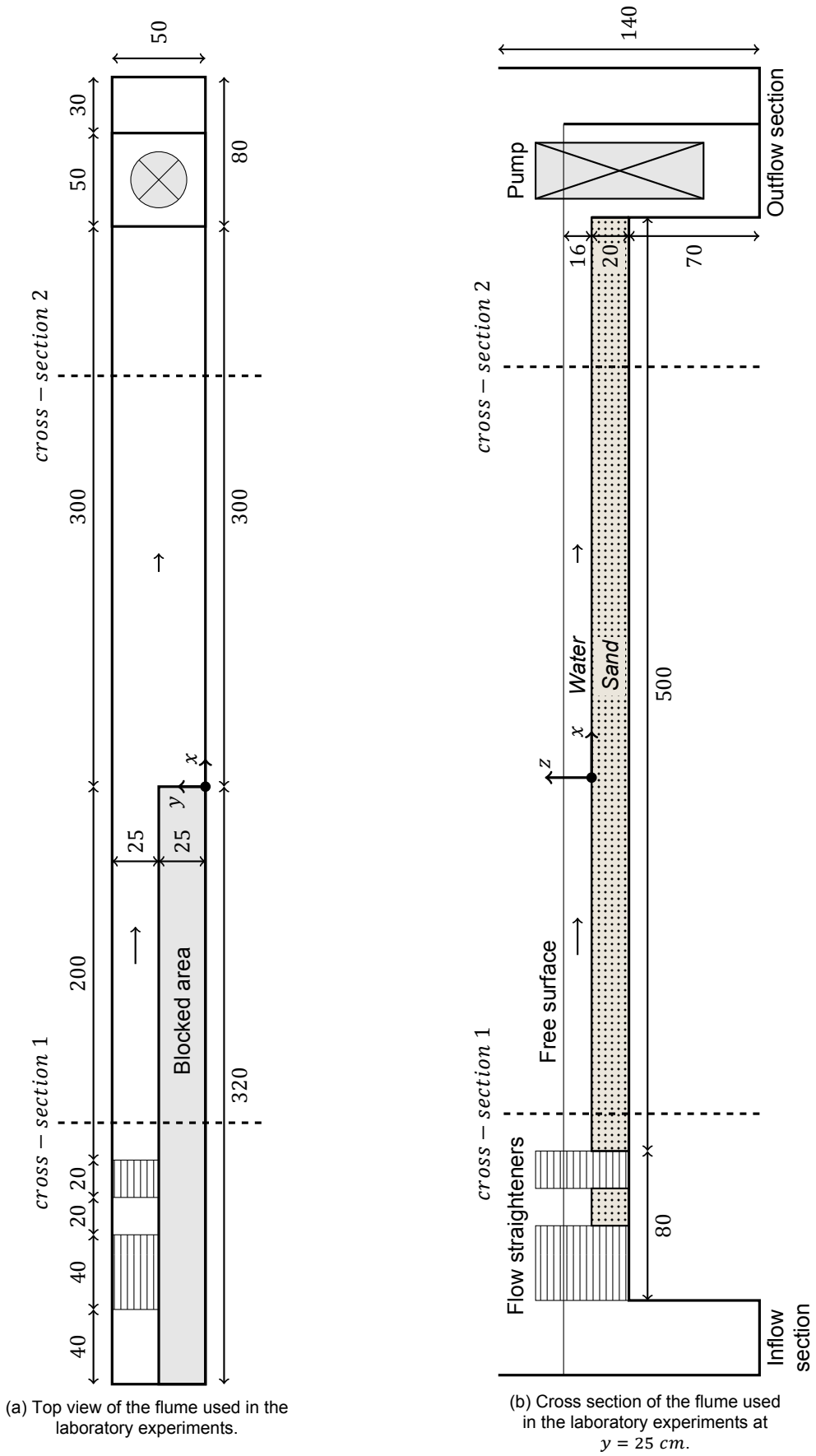

(a) Top view of the flume used in the laboratory experiments.

(b) Cross section of the flume used in the laboratory experiments at $y = 25\ cm$.

Figure 3.4: Layout of the flume used in the laboratory experiments. Lengths are given in centimetres.

3.3. Measurement techniques

To measure the discharge of water, a Proline Prosonic Flow 91W Ultrasonic flowmeter was placed on the pipe that led from the pump to the inflow. By measuring the discharge, the mean flow velocity can be computed for every experiment.

Because the goal of this study is to compare the flow pattern of the laboratory tests to the results from the numerical model, it was chosen to use an Acoustic Doppler Velocimeter (ADV) to obtain detailed point measurements of the flow. A Vectrino Profiler was chosen. It measures the flow in three dimensions over a range of three centimetres in depth. It turned out that the acoustic properties of the flume and the sand are important for the trustworthiness of the results obtained by the ADV. The acoustic signal send out by the ADV is scattered by hard objects, interfering with the measured signal. Unfortunately, this makes the ADV unusable for this laboratory set-up. Examples of measured signals are shown in Appendix A.

Other measurement techniques were considered, but rejected for various reasons. It was chosen to make a qualitative assessment of the flow, using dye and a flow vane. The dye was used to obtain a general image of the flow and to locate the reattachment point of the mixing layer. A flow vane was used to map the general direction of the flow throughout the flume in order to identify any secondary currents in the flow.

An attempt was made to track the bed level changes using stereoscopy. With stereoscopy, two or more photographs are combined to obtain a three dimensional image, in which height differences would be visible. Unfortunately, the lighting of the facility did not allow a sharp enough photo for this technique.

To make transects of the bed level over the length of the flume, three laser distance meters were used. The lasers were mounted on a measurement carriage, shown in Figure 3.5, so that they can be moved over the length of the flume to make a transect of the bed in the direction of the flow. The lasers were placed in PVC holders with a perspex bottom and were submerged just under the water surface to measure the bed level. On the carriage a wheel was mounted to track its position in x-direction. The lasers were mounted on the carriage at a y-position of 8.4, 27.4 and 38.7 centimetres. These locations were chosen because then laser 1 is positioned in the narrow part of the flume where the flow velocities are high, laser 2 is positioned directly underneath the mixing layer, and laser 3 is located where the return current occurs. This positioning of the lasers should give an overall view of the erosion and sedimentation patterns that occur during the experiments.

Figure 3.5: Photographs of the carriage placed on top of the flume. The left photo shows the positioning of laser 1 and the wheel that registers the location of the carriage. The right photo shows the positioning of laser 2 and 3.

3.4. Experimental cases

For the laboratory experiments, it was difficult to attain scenarios with high Froude numbers. An attempt was made to come as close to the Froude numbers of MV2 as possible. Furthermore, care was taken to make sure that the Reynolds number inside the flume was high enough to ensure turbulent conditions. For the lowest flow velocities in the experiment with the lowest discharge, the Reynolds number was still over $1.2 \cdot 10^4$, which is high enough to ensure turbulent flow.

Because the used sediment has a relatively large grain diameter, the Rouse numbers were larger, and the Shields parameters a lot smaller than for a sand closure. The Rouse number was between 28 and 5 for the experiments, so sediment was mostly transported in the form of bedload transport. This means that the water column was almost clear except for a thin layer of sediment rolling and sliding over the bed. This is different than for the final stage of a sand closure, where most of the eroded sediment is in suspension inside the mixing layers. The fact that most of the sediment transport consists of bedload may have some large implications on the morphology. When the governing transport mode is suspended sediment transport, no bedforms are present, as was found in Section 2.3.

The experiment had to be paused every half hour by turning off the pump in order to measure the bed level with the three lasers. This was necessary because the measurement signal was too scattered when the experiment was running. For the tests with the highest flow velocities, the experiment was paused every 15 minutes because the bed changed faster for these tests. The pausing of the experiments might impose some start-up effects; however, these effects are considered to be small because the morphological changes observed during the experiments acted on a completely different time scale than these start-up effects.

A complete overview of the executed experiments is given in Table 3.1. The values with subscripts 1 are located at the narrow part of the flume, the values with subscript 2 are located downstream of the expansion. To provide a quick comparison between the experiments and MV2, the Froude number varies between 0.25 and 1, the Reynolds number between $1 \cdot 10^6$ and $6 \cdot 10^6$, the Rouse number varies between 5.5 and 1, and the Shields parameter is between 0.3 and 7.7 for MV2.

Experiment 4 was repeated three times in the laboratory to ensure repeatability. The original plan was to repeat multiple experiments. However, as is shown in Chapter 4, the morphology of the various experiments is more or less similar so it was deemed unnecessary to repeat multiple laboratory experiments.

The experiments shown in Table 3.1 were selected in this manner to ensure that for experiments 1 and 2, which are the experiments with the lowest flow velocities, the Shields parameters in both the narrow and wide part of the flume are around incipient motion. The critical Shields parameter is 0.03 for all experiments.

It was chosen to do these experiments because the increase in flow velocity is small enough to detect the start of motion of the sediment particles, but also have some high flow velocities incorporated to study the morphological behaviour for higher Froude numbers. Experiment 8 is at the limit of the experimental set-up.

There were some stringent demands on the dimensions of the flume due to the available space, but mostly due to the measuring equipment. Because the water cannot become too turbid, it is chosen to use sediment with a relatively large grain diameter. This results in a larger Rouse number for the experiments than would be found during a sand closure. Although the dimensionless numbers of the laboratory experiments differ from a sand closure, the results can still be used to validate the numerical model.

Table 3.1: Overview of the conducted experiments with their corresponding dimensionless numbers. The experiments are numbered 1 to 8. The dimensionless numbers with subscripts 1 are located at the narrow part of the flume; the dimensionless numbers with subscripts 2 are located downstream of the expansion. Q is the discharge of the experiments.

$Nr.$	Q	U_1	Fr_1	Re_1	P_1	θ_1	U_2	Fr_2	Re_2	P_2	θ_2
	[l/s]	[m/s]	[-]	[-]	[-]	[-]	[m/s]	[-]	[-]	[-]	[-]
Low flow velocity experiments											
1	8	0.2	0.16	$2.5 \cdot 10^4$	13.9	0.02	0.1	0.08	$1.2 \cdot 10^4$	27.8	0.01
2	10	0.25	0.20	$3.0 \cdot 10^4$	11.1	0.03	0.13	0.10	$1.5 \cdot 10^4$	22.3	0.01
Moderate flow velocity experiments											
3	12	0.3	0.24	$3.7 \cdot 10^4$	9.3	0.05	0.15	0.12	$1.8 \cdot 10^4$	18.6	0.01
4	14	0.35	0.28	$4.3 \cdot 10^4$	8.0	0.06	0.18	0.14	$2.1 \cdot 10^4$	15.9	0.02
5	16	0.4	0.32	$4.9 \cdot 10^4$	7.0	0.08	0.2	0.16	$2.5 \cdot 10^4$	13.9	0.02
6	18	0.45	0.36	$5.5 \cdot 10^4$	6.2	0.10	0.23	0.18	$2.8 \cdot 10^4$	12.4	0.03
High flow velocity experiments											
7	20	0.5	0.40	$6.1 \cdot 10^4$	5.6	0.13	0.25	0.20	$3.1 \cdot 10^4$	11.1	0.03
8	21.4	0.54	0.43	$6.6 \cdot 10^4$	5.2	0.15	0.27	0.21	$3.3 \cdot 10^4$	10.4	0.04

4

Experimental results

The morphology under the mixing layers of a sand closure is investigated with the laboratory experiments. The experimental set-up was described in the previous chapter. The experimental results are presented and discussed in this chapter. The experimental results are used in chapter 5 to validate the numerical model.

The measurements consist out of two parts; qualitative measurements of the flow patterns, and quantitative measurements of the bed level changes. Dye was used to obtain an overview of the flow patterns. The dye was also used to find the reattachment point of the mixing layer. Furthermore, the direction of the flow was observed using a flow vane. The results of the determination of the flow patterns is discussed in Section 4.1. The bed level changes were tracked during the experiments by making streamwise transects with three lasers. This was done about every half hour in order to be able to track the development of the bed. The results of these measurements are discussed in Section 4.2.

4.1. Results flow patterns

The goal of the flow measurements is to obtain a qualitative image of the flow patterns and to verify the flow patterns simulated by the numerical model. This section starts with a general description of the flow patterns that were found, after which some special attention is given to two specific components of the flow pattern.

4.1.1. General flow pattern

The general flow pattern was similar to the one described in Subsection 2.2.3, showing fast flowing water in the narrow part of the flume, a return current downstream of the expansion, and a mixing layer in between. Figure 4.1 shows an example of how the flow patterns were investigated using dye. This was done at different locations in the flow to obtain a general image of the flow pattern. The dye was mostly convected in the narrow part of the flume. A large amount of diffusion in the mixing layer and a slow convection towards the expansion in the return current were found. When the dye was injected at the expansion, as shown in Figure 4.1, it was diluted by the mixing layer and part of the dye was taken up by the return current.

The difference between the experiments and the flow pattern shown in Figure 2.5 was that for the experiments, only one return current was observed, not two separate gyres rotating in opposite direction. Based on the experiments of Talstra [14], it is expected that this secondary gyre does not develop. During his experiments, the secondary gyre did not always develop and was easily disrupted by external factors. It is expected that the morphological changes that occur during the present experiments prevent the secondary gyre from forming.

Using dye and a flow vane, a general direction of the flow is obtained at several points in the flume. The flow pattern that resulted from these observations is given in Figure 4.2. It depicts the expected spreading of the mixing layer with the blue dotted lines and the return current behind the expansion

in black with the arrows indicating the flow direction. The point where the dotted line in the bottom of the figure reaches the sidewall of the flume is the reattachment point. This length decreased for an increasing flow velocity. The distance between this reattachment point and the location of the expansion is called the reattachment length.

In Figure 4.2, cross-section A-A' shows the horizontal flow pattern just downstream of the expansion. It is expected that a secondary current develops behind the expansion, but not in the main current. Both this secondary current and the reattachment lengths for each experiment are discussed separately in the next sections, because they stand out and provide a good comparison method for the numerical results.

Figure 4.1: Determination of the flow pattern inside the mixing layer using dye.

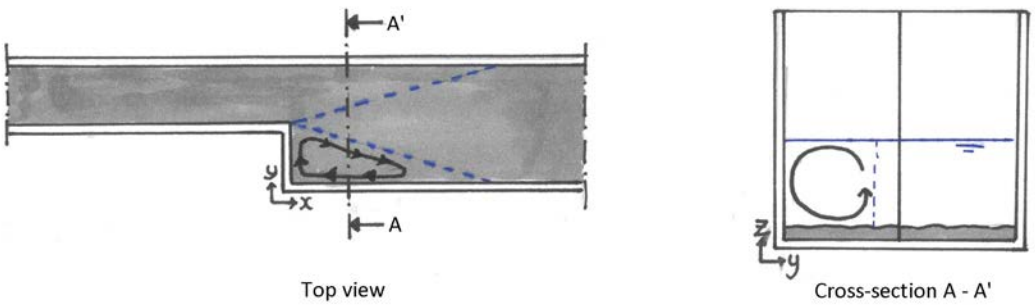

Figure 4.2: Observed flow pattern for the laboratory experiments, including a secondary circulation just downstream of the expansion. The blue dotted lines are the expected spreading of the mixing layer.

4.1.2. Reattachment length

The dye was used to determine the reattachment length of the mixing layer by observing the direction of the flow at the side wall after the expansion. At the point where the dye was transported both towards the expansion and towards the end of the flume, the reattachment point was located. The reattachment point varied in time due to turbulent eddies passing. An average value was obtained by doing multiple measurements during the experiment. It was found that the location of the reattachment point could vary over 20 centimetres due to the turbulent eddies. The average values of the measured reattachment lengths are given in Table 4.1.

As was stated in Subsection 2.2.3, Talstra [14] found a reattachment length between six and ten times the lateral expansion width. This would imply a reattachment length between 1.5 and 2.5 metres for the present experiment. However, the presently used experimental set-up lies outside the scope of Talstra's study, because it does not resemble the shallow lateral expansions investigated by Talstra, but a deep one. Talstra found an increasing reattachment length for an increasing water depth, and smaller reattachment lengths when the hydraulic roughness of the bed increased. The experiments of this research both have a larger water depth and larger bed roughness than the experiments of Talstra, so it is not sure what the theoretical reattachment length is for these experiments.

As can be seen in Table 4.1, the reattachment length is shorter for the experiments with high flow velocities. This actually contradicts the literature described in Subsection 2.2.3, where it was found that the reattachment length increases for an increasing discharge. This contradiction can be explained by the difference in measuring conditions between the experiments of Talstra [14] and the present experiments. During the laboratory experiments of Talstra, a fixed bed was used that was smooth and flat, while for the present experiments the reattachment length was determined for an erodible bed. So for the experiments of Talstra, the roughness of the bed did not vary between the different experiments, while for the present experiments the roughness was variable due to the presence of bedforms.

The reattachment length of the present experiments is influenced by both the flow velocity and the increase in roughness which is mainly determined by bedforms. It was observed that the height of the bedforms increased for an increasing flow velocity. The increasing flow velocity of the experiments should lead to an increase of the reattachment length, but it is concluded that the increase in bed roughness is in this case more important than the increase in flow velocity, leading to a decreasing reattachment length for higher flow velocities. Generally, the reattachment point stayed in between one and two metres downstream of the expansion. A jump in the reattachment length is observed between experiment 4 and 5.

Knowing the reattachment length of the mixing layers during a sand closure is not a necessaty, but some general comments are provided on the subject. The reattachment length depends on the expansion width, the flow velocity and the bed roughness. During a sand closure, the expansion width is the distance between the shore and the head of the dam. This distance increases as the heads of the dam are build up closer together.

For the first stage of a sand closure, when the flow velocities are low, the main transport mode is bedload transport and bedforms occur. However, due to the low flow velocities, the mixing layer will not be well developed. When the heads of the dam are build up closer together and the main transport mode is still bedload, it is possible that bedforms occur in combination with a strong mixing layer, which would result in a mixing layer with a short reattachment length. However, downstream of the dam, the water depth increases, which would result in a long reattachment length. Futhermore, the expansion width increases as the heads are build up closer together, which increases the reattachment length even further. It is expected that the increase in water depth and the increasing expansion width have a more significant influence on the reattachment length than the bedforms. During the final stage of a sand closure, it was found in Section 2.2 that the heads of the dam are build up so close together that the mixing layers start to interact. In this case, it is expected that the situation resembles more the case of a free mixing layer, which implies that there is no reattachment.

It seems like the reattachment length is only well pronounced somewhere between the first and the last stage of the sand closure. For this period, it is expected, based on the expected influence of the increasing depth and the increasing expansion width on the reattachment length, that bedforms play a relatively unimportant role on the reattachment length of a sand closure.

Table 4.1: Reattachment length given in metres downstream of the expansion.

$Nr.$	Q	U_1	U_2	Reattachment length
	[l/s]	[m/s]	[m/s]	[m]
Low flow velocity experiments				
1	8	0.2	0.1	1.8
2	10	0.25	0.13	1.75
Moderate flow velocity experiments				
3	12	0.3	0.15	1.7
4	14	0.35	0.18	1.65
5	16	0.4	0.2	1.35
6	18	0.45	0.23	1.2
High flow velocity experiments				
7	20	0.5	0.25	1.1
8	21.4	0.54	0.27	1

4.1.3. Secondary circulation

A vane was used to detect the flow direction in various parts of the flume. Most flow patterns matched the expectation described in Subsection 2.2.3 and what was observed with the dye. Interestingly, just downstream of the expansion, in the return current, a flow from the side wall towards the middle of the flume was observed near the bed. In theory, the inward flow near the bed should be accompanied by an outward flow, i.e. a flow from the mixing layer towards the side wall, at the surface. This outward flow was not observed with the flow vane. The dominant flow at the surface was directed towards the expansion. However, this does not mean that there is no outward flow present at the surface. The flow velocities near the surface were much larger than at the bed, so while the dominant flow direction was towards the expansion, there could be a smaller component directed towards the side wall.

Based on these observations, the expected flow pattern is depicted in Figure 4.2. The expectation is that there are both a return current and a secondary current located behind the expansion. The return current is driven by momentum exchange from the main current. The flow velocities of the main current, and thus the amount of momentum it carries, are smaller close to the bed, suggesting that the flow velocities in the return current are also smaller close to the bed. These lower flow velocities in the return current could explain why a secondary current is only observed close to the bed. It should be emphasized that there is no way of quantifying these flow patterns without detailed flow measurements.

It is expected that the occurrence of the secondary circulation depends on the expansion width. The circulation is driven by the main current, which adds a certain amount of momentum to the return current and the secondary circulation. When the area over which the secondary circulation is spread increases, it is expected that the strength of the circulation decreases. It is not known how delicate the balance is between the return current and the secondary circulation. It might be possible that the secondary circulation disappears all together when the expansion width increases. Both the dam and the shore have a sloping surface, which is not incorporated in these experiments. Because of these sloping surfaces and the expansion width being variable for a sand closure, the occurrence of the secondary current is unsure for a sand closure. If a secondary circulation occurs, it is probably temporary.

4.2. Results morphology

The bed level changes during the experiments were tracked by making transects with three laser distance meters at various times. Furthermore, photographs were made to get an overview of the outcome of the experiments.

Figure 4.3 shows an overview of the final layout of the bed after a typical experiment, in this case experiment 4. Most experiments show this general pattern with large bedforms of about two centimetres in height in the narrow part of the flume, and smaller bedforms of about one centimetre in the wide part of the flume. The bedforms are more or less perpendicular to the flow, but it can be seen that the bed-

forms are deflected underneath the location of the mixing layer. It seems that right after the expansion, the bedforms are joined together to form a streamwise bar that originates from the expansion.

Figure 4.3 depicts the layout of the bed after a typical experiment, but actually three different outcomes were observed for the different experiment that were conducted. For experiment 1 and 2, the experiments with the lowest flow velocities, there were barely any bed level changes. For experiment 3 to 6 an outcome comparable to the one shown in Figure 4.3 was observed. Only for experiment 5 and 6, additional bedforms were observed inside the return current. These bedforms travelled towards the expansion, which concurs with the direction of flow inside the return current. For experiment 7 and 8, the experiments with the highest flow velocities, the streamwise bar shifts towards the side wall where the return current is located and kept growing in height. The three different outcomes of the experiments are discussed in the remainder of this section. For each result, one typical experiment is explained in detail. All other results can be found in Appendix B.

Figure 4.3: Photograph gives an overview of a typical final erosion and sedimentation pattern for an experiment with a moderate flow velocity, in this case for experiment 4.

4.2.1. Low flow velocity experiments

For experiment 1 and 2, the bed level changes were negligible. This is because the Shields parameter was below the critical value for incipient motion. As was elaborated in Section 3.4, the critical Shields parameter was 0.03 for all experiments. From Table 3.1 it can be seen that for experiment 2, the Shields parameter was exactly equal to the critical Shields parameter in the narrow part of the flume. The results of the experiments are consistent with theory, because no bed level changes were observed during experiment 1. No bedforms were formed and after two hours and 15 minutes of running time the bed was still flat, without any bedforms.

Figure 4.4 shows the transect of the bed made by laser 1 over the course of an experiment. The expansion of the flume is located at $x = 0$. The negative values are locations in the narrow part of the flume and the positive x-values are located in the wide part of the flume. During experiment 2, some

small bedforms were observed, of which the development can be seen in Figure 4.4. But even after a running time of three hours, these did not result in the final morphology patterns which were observed during the other experiments at higher flow velocities. Figure 4.5 shows the final layout of the bed in the area between 0.5 and 1.5 metres downstream of the expansion after the completion of experiment 2. Bedforms are formed by initial instabilities in the bed and keep growing by a positive feedback mechanism until their final height is reached. It is expected that the initial bed had some larger pertubations in the area displayed in Figure 4.5 than in the surrounding areas, which caused these bedforms.

For the other experiments, the Shields parameter in the wide part of the flume is still around incipient motion, but they do exhibit a complete erosion and sedimentation pattern. Apparently the upstream Shields parameter is governing for the development of the bed level changes.

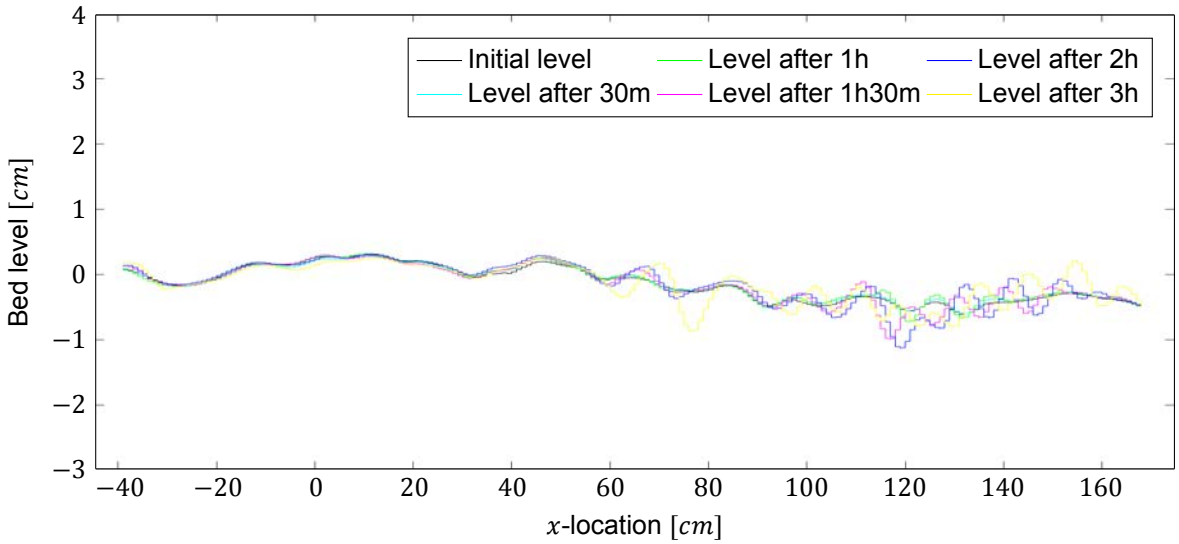

Figure 4.4: Bed level measured by laser 1 at different times after starting experiment 2.

Figure 4.5: Photograph of the final erosion and sedimentation pattern for experiment 2, which was an experiment with a low flow velocity. The photograph is made at the end of the flume, showing the bed between 0.5 and 1.5 metres downstream of the expansion.

4.2.2. Moderate flow velocity experiments

For experiments 3 to 6, a more or less similar erosion and sedimentation pattern is observed. In this section, the results of experiment 4 are used as an example. The results of the other experiments can be found in Appendix B.

Figure 4.6 shows the erosion and sedimentation patterns after experiment 4. The photograph shows the flume at the expansion and about the first 1.5 metres downstream of the expansion. As was discussed in the previous section, the final layout of the bed for the experiments with a moderate flow velocity consists out of relatively large bedforms at the beginning of the flume and smaller ones at the end. Furthermore, a streamwise bar is formed just after the expansion. In the return current, the bed shows no bedforms and little erosion and little sedimentation.

It can be seen in Figure 4.6 that the bedforms are more or less perpendicular to the flow direction in the narrow part of the flume and throughout the top half of the photograph. However, underneath the location of the mixing layer, the bedforms gradually bend off. This is because the flow velocities gradually decrease going from the main flow towards the return current, and the travelling speed of the bedforms depends on the flow velocities in the current above it. So the bedforms are deflected because their travelling speed varies over the width of the mixing layer.

Just behind the expansion, a bar is formed. It is expected that this bar is formed because the travelling bedforms in the main current are joined together due to the low flow velocities downstream of the expansion. During one of the experiments, a GoPro was placed in the flow to film the formation of the streamwise bar, it was observed that the bar was formed by passing bedforms from the upstream part. Each passing bedform bends around the expansion and increases the height of the bar. The expectation was that the sedimentation behind the expansion would be more spread out, but it seems that the presence of the secondary current prevented spreading of the sediment. The flow direction of this secondary current is outward at the top of the water column and inwards at the bottom, keeping the bar at a fixed location.

Figure 4.6: Photograph of the final erosion and sedimentation pattern for experiment 4, which was an experiment with a moderate flow velocity. The photograph shows the flume at the expansion and about the first 1.5 metres downstream of the expansion.

Laser transects

The largest bed level variations were observed in the transects of laser 1. This laser measures the bed level over a transect starting about 40 centimetres into the narrow part of the flume up to almost 160 centimetres downstream of the expansion. Laser 2 and 3 were mounted to the other side of the carriage and measure the bed level from the location of the expansion up to 220 centimetres downstream of the expansion. Laser 2 makes a transect at the location of the bar and laser 3 is located over the return current. It should be noted that the transects do not span the entire length of the flume, because the carriage could not reach it;however, these transects span a large enough part of the flume to capture the most important erosion and sedimentation patterns.

Laser 1 - development of bedforms

Figure 4.7 shows the transects made by laser 1 during experiment 4. It can be seen that the bedforms grow in time, but at some point an equilibrium is reached; during the last part of the experiments, the bedforms do not grow in size anymore. After one hour, the bedforms are higher in the narrow part of the flume compared to the wide part. The amplitude of the bedforms being larger in the fast flowing part of the flow is in accordance with theory. For experiment 4, the corresponding average flow velocity was 0.35 metres per second in the narrow part of the flume and 0.175 metres per second after the expansion. The bedforms for this experiment had an amplitude of about two centimetres before the expansion, so for the negative x-values. After the expansion, the pattern is much less consistent because there is some sedimentation as well, but the amplitude of the bedforms is between one and two centimetres. After one hour, the bedforms downstream become of equal height in the wide part and the narrow part. It is expected that this is because the bedforms generated in the narrow part of the flume travel into the wide part of the flume.

Another observation is that when the height of the bedforms increases, the length increases accordingly. After one hour, the bedforms in the narrow part of the flume have a height of about two centimetres and a length of about 20 centimetres. After 3 hours, the height of the bedforms has increased to three centimetres and the length of the bedforms is about 30 centimetres. Comparing this results to the bedforms that were found for experiment 2, a low flow velocity experiment, it can be seen that the length and height of the bedforms depend on the average flow velocity, since the bedforms have a height of about 0.5 centimetre and a length of about 10 centimetres for experiment 2.

Laser 1 - morphology

In Figure 4.8, the transects of laser 1 were smoothened to observe the average erosion and sedimentation. In order to obtain this plot, a moving average is taken with enough points to smoothen out most of the bedforms. It can be seen that the upstream part of the flume experiences sedimentation first. This is expected because it was observed during the experiments that the upstream part of the flume shows mostly erosion, and the downstream part shows sedimentation. The sediment needs time to travel towards the downstream part of the flume. This can be observed in Figure 4.8. It can be seen that there are little changes between the last two measurements, suggesting that the system has reached an equilibrium. This would mean that this specific experiment takes two and a half hours to reach equilibrium.

Another observation from Figure 4.8 is that the highest point of sedimentation forms in the upstream part of the flume and travels in downstream direction, gaining height. Looking at the other experiments, the same phenomenon occurs. This sedimentation wave seems to act like a very long bedform that travels downstream slowly due to its large wavelength. The sedimentation wave transports the sand eroded in the narrow part of the flume effectively in downstream direction.

Laser 1 - beginning of the flume

Figure 4.9 shows a transect of the narrow part of the flume, starting ten centimetres downstream of the flow straighteners until about 40 centimetres before the expansion, where the transect of Figure 4.8 begins. Only two transects were made, one at the beginning of the experiment, and one at the end. This measurement was executed during experiment 4, to investigate the morphology in the entire narrow part of the flume. Since sedimentation was observed in the entire downstream part of the flume, as can be seen in Figure 4.8, it was suspected that this sediment came from the upstream part of the flume. This suspicion was confirmed by the measurements because they show an erosion of four centimetres at the beginning of the flume. It is expected that the largest erosion is observed at the beginning of the flume because the flow straighteners are used to break up large turbulent structures in the flow, but also generate some accelerations and a small amount of turbulence in the flow. This results in erosion of the sediment behind the flow straightener. Furthermore, the sediment carrying capacity of the flow is much higher at the beginning of the flume than at the end. Because sediment is recirculated during the experiment, there is a small amount of sediment in the water at the inflow, but not enough for an equilibrium sediment profile. This also results in extra erosion at the beginning of the flume, until an equilibrium is reached.

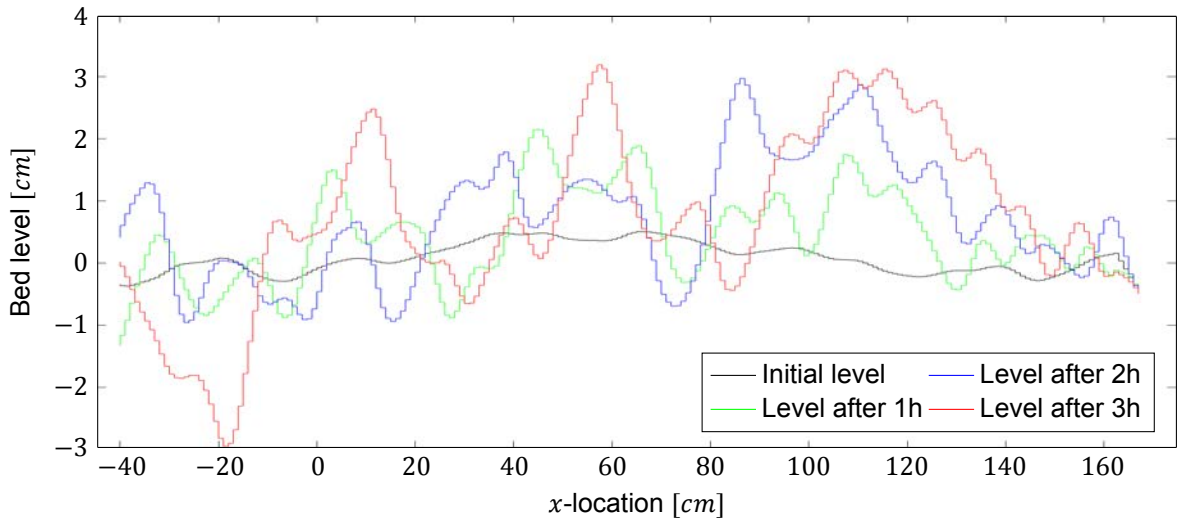

Figure 4.7: Bed level measured by laser 1 at different times after starting experiment 4.

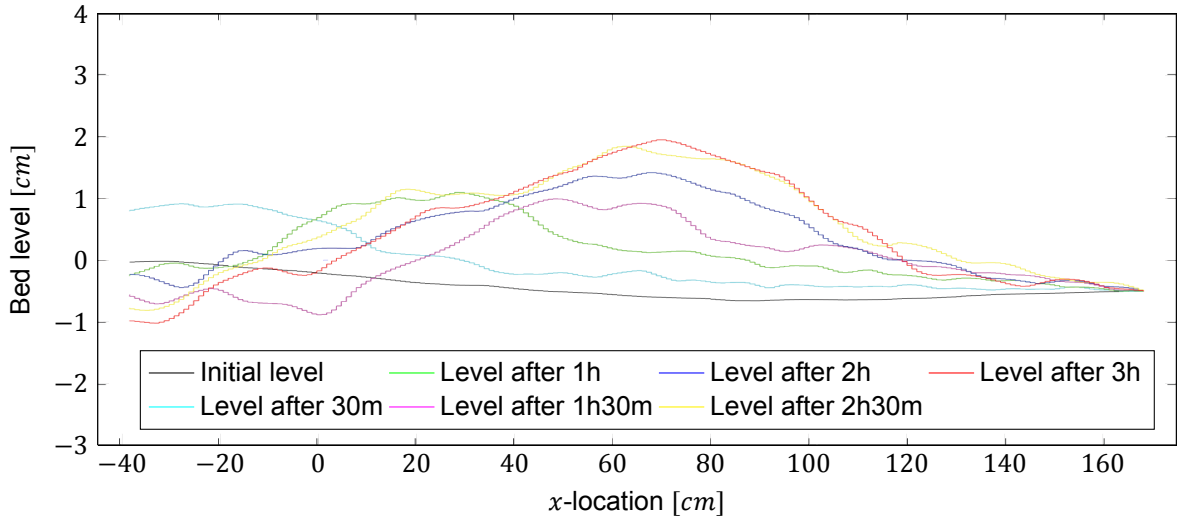

Figure 4.8: Bed level measured by laser 1 at different times after starting experiment 4. The results are smoothened to even out most of the bedforms.

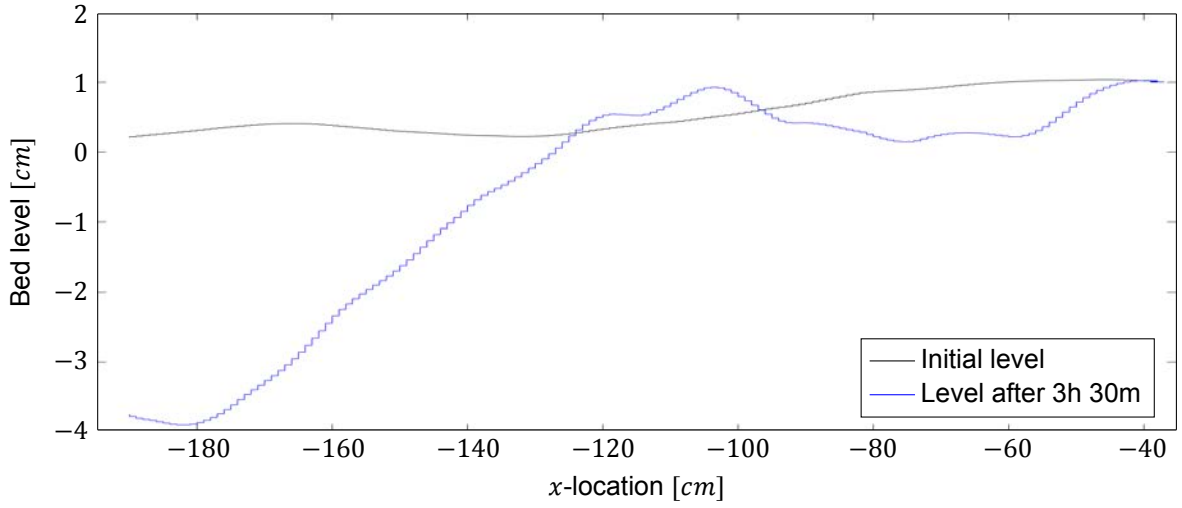

Figure 4.9: Bed level measured by laser 1 in the narrow part of the flume. Transects were measured at the beginning and end of experiment 4. The results are smoothened to even most of the bedforms out.

Laser 2 - bar development

Figure 4.10 shows the development of the bed for experiment 4 underneath laser 2. The laser originates somewhere near the tip of the expansion and makes a transect until almost 220 centimetres downstream of the expansion. Laser 2 makes a transect more or less at the location of the streamwise bar. It should be noted that this does not necessarily represent the highest point of the bar. 30 minutes after the start of the experiment, a small amount of erosion is observed. For the later measurements, a continuous increase of the bed is observed, especially at the first part after the expansion. From the photographs taken during the experiment, the bar is already visible, so it is possible that the bar was shifted just outside the track of the laser.

As was mentioned above, it can be seen in Figure 4.8 that the transects of laser 1 show no significant changes between the last two measurements. However, the transects of laser 2 demonstrate that the bar is still under development at this time, suggesting that the experiment has not reached an equilibrium yet.

Laser 3 - return current

Figure 4.11 shows the bed level changes measured by laser 3, which makes a transect through the return current. The results are marginally smoothened; only some small irregularities are evened out. Inside the recirculation zone, a small amount of sedimentation of about 0.5 centimetres is observed. Another observation from the bed level changes under laser 3 is that the initial state of the bed might have some influence on the morphology during the experiments. It can be seen that the locations with the lowest bed exhibit the largest amount of sedimentation. However, this effect seems to be small compared to the total amount of erosion and sedimentation in the rest of the flume.

Experiment 4 was conducted three times to ensure repeatability. For the repeat tests, the location of the highest peak shifted about 30 centimetres in downstream direction; however, the general patterns were equal. The largest differences in the measured erosion and sedimentation are about 0.5 centimetre. The experiments are similar enough to conclude that the experiments are repeatable.

Bedforms in return current

There was one visible difference between experiments 5 and 6 and the other typical experiments. For experiments 5 and 6, the flow velocities in the return current apparently became high enough to form small bedforms that propagate in the direction back towards the expansion. These bedforms originated somewhere near the reattachment point and propagated in the direction of the expansion during the experiment. The formation of bedforms in the return current coincides with a jump in the reattachment length as can be seen in Table 4.1. This additional shortening of the reattachment length can be explained by the increase in bed roughness due to the presence of bedforms. Figure 4.12 shows an overview of the final layout of the bed for experiment 5.

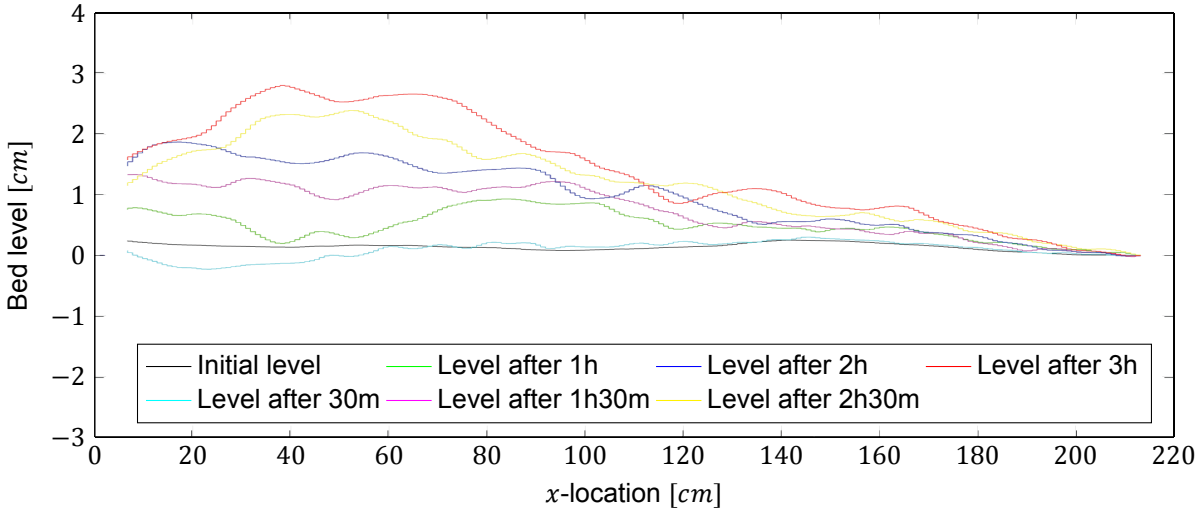

Figure 4.10: Bed level measured by laser 2 at different times after starting experiment 4. Results are smoothened to even out the smallest bedforms.

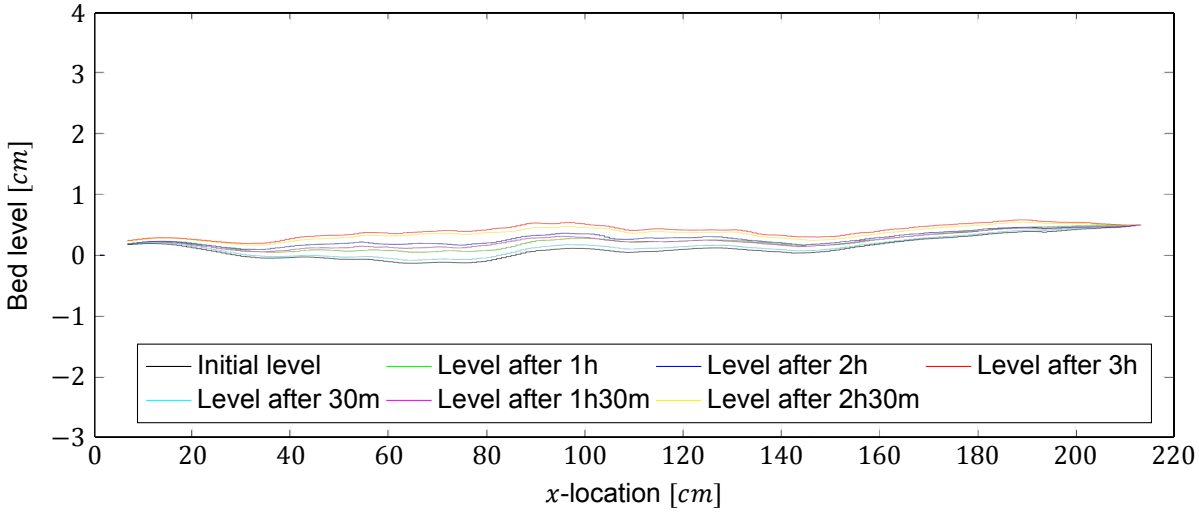

Figure 4.11: Bed level measured by laser 3 at different times after starting experiment 4. Results are smoothened to even out the smallest bedforms.

Figure 4.12: Photograph of the final erosion and sedimentation pattern for experiment 5, which was an experiment with a moderate flow velocity. The photograph shows the flume from just upstream of the expansion and the first metre downstream of the expansion.

4.2.3. High flow velocity experiments

For the two experiments with the highest flow velocities, a different erosion and sedimentation pattern was observed. The streamwise bar that forms downstream of the expansion moves to the side of the flume, into the recirculation area. Figure 4.13 shows the final layout of the bed for experiment 7. The shaded area in the photograph parallel to the side wall is the streamwise bar. To emphasize the size of this bar, a second photograph is shown in Figure 4.14. This photograph is taken from the wide part of the flume towards the narrow part. On the left of this photograph, the size of the formed bar is clearly visible. It can also be seen that on the left side of the bar, the bed level goes down again, but is still higher than in the main current on the right side of the flume.

At the start of the experiment, the reattachment length of the mixing layer was 1.1 metres. During the course of the experiment, the bar shifted to the side of the flume and the reattachment point moved upstream towards the expansion. At the end of the experiment, the reattachment length was reduced to only 42 centimetres.

Shift of the streamwise bar

The reason why the bar shifts towards the side wall of the flume is not clear. There are a number of possible explanations for the bar to shift, of which the most plausible are discussed, namely bedforms in the return current, large turbulent eddies in the flow, and water level fluctuations.

Bedforms in return current

It is expected that for the typical experiments the bar is kept in place by the secondary circulation that was described in Section 4.1.3. It is possible that for experiments 7 and 8, the secondary circulation is disrupted by the bedforms travelling back towards the expansion in the return current. In the previous section, it was shown that these bedforms already occur in experiments 5 and 6, but somehow these did not result in a shift of the streamwise bar. This can be explained by the size of the bedforms depending on the flow velocity. When the flow velocities in the main current increase, the strength of the return current increases as well. This would result in higher bedforms in the return current. If the secondary circulation is overruled, it is possible that the bar is not held in place anymore and it has the possibility to travel to the side of the flume.

Large turbulent eddies in the flow

Another explanation for the bar shifting towards the sidewall where the return current in located, is that an increase in flow velocity also increases the size of the turbulent eddies in the flow. These eddies could cause instabilities in the secondary circulation that occurs behind the expansion. It is possible that these instabilities become too large for the high flow velocity experiments, eliminating the secondary circulation. Since it is expected that the secondary circulation holds the bar in place, the elimination of this circulation could cause the bar to move towards the sidewall.

Water level fluctuations

Larger flow velocities do not only increase the size of the turbulent eddies, but also result in larger water level fluctuations. Just like the increase in size of the turbulent eddies, the water level fluctuations could cause instabilities in the secondary circulation, eliminating the restriction that causes the bar to stay in place.

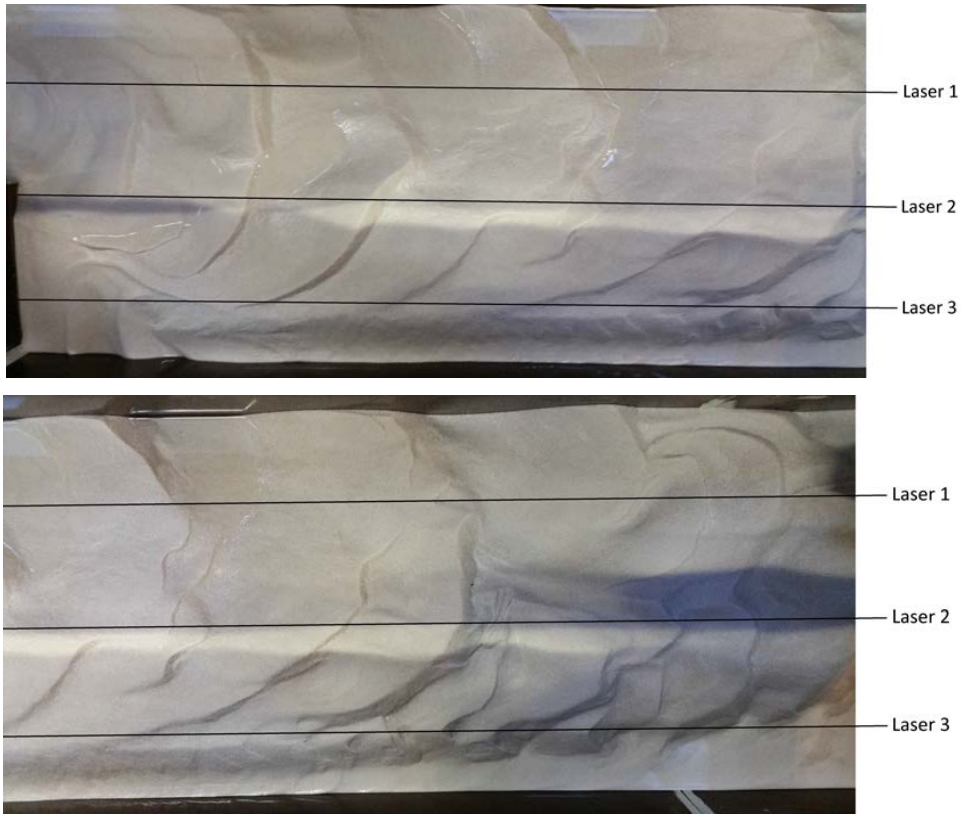

Figure 4.13: Photographs of the final erosion and sedimentation pattern for experiment 7, which was an experiment with a high flow velocity. The photograph in top shows the flume at the expansion and the first metre downstream of the expansion. The other photograph depicts the flume somewhere between 0.5 and 1.5 metres downstream of the expansion.

Figure 4.14: Photograph of the final erosion and sedimentation pattern for experiment 7, which was an experiment with a high flow velocity. The photograph is taken from the back of the flume, facing the expansion.

Laser transects

Generally, large amounts of erosion and sedimentation were found for the experiments with the highest flow velocities. During experiment 8 a similar pattern as for experiment 7 was found, but with larger bed level changes.

Laser 1 - morphology

Figure 4.15 shows the transects of laser 1 made during experiment 7. Large amounts of erosion are observed in the first part of the flume, even until after the expansion. In the wide part of the flume, large amounts of sedimentation are observed. As for the typical experiments, a peak with the largest amount of sedimentation seems to build up gradually while it travels in downstream direction. For the last three measurements, the system seems to be in equilibrium underneath laser 1 since the changes in erosion and sedimentation have become small.

Laser 3 - bar development

Due to the shift of the bar, the transect of laser 3 is now located at the position of the streamwise bar. Figure 4.16 shows the transects made by laser 3. It depicts the development of the bar over time. Large amounts of sedimentation are observed, which are expected by looking at the photographs. Again, a sedimentation peak travels through the flume, but in opposite direction from the sedimentation peaks found underneath laser 1. This is because the flow velocities in the return current are directed towards the expansion. Just as for the typical experiments, the bar is still growing after the morphology underneath laser 1 has already reached an equilibrium.

While the highest point of the bar shifts towards the expansion, it was observed that the reattachment length also shifts towards the expansion. It is not clear why this is happening. It seems like the morphology influences the reattachment length. The reattachment point is moved towards the expansion significantly. It is possible that the increase in bed roughness due to the bar development is responsible for this.

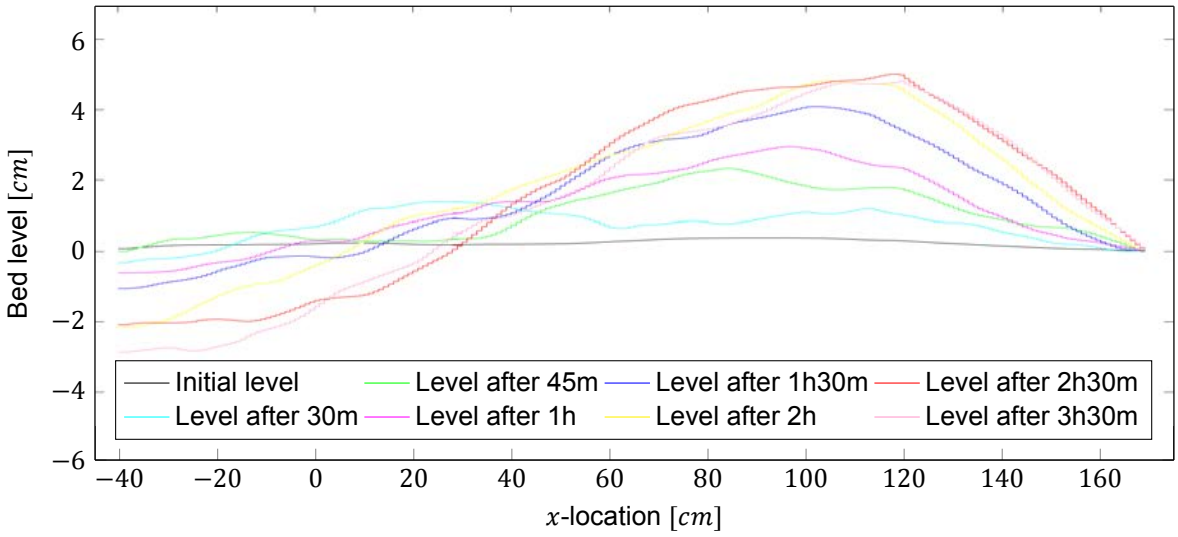

Figure 4.15: Bed level measured by laser 1 at different times after starting experiment 7. Results are smoothened to even out most of the bedforms.

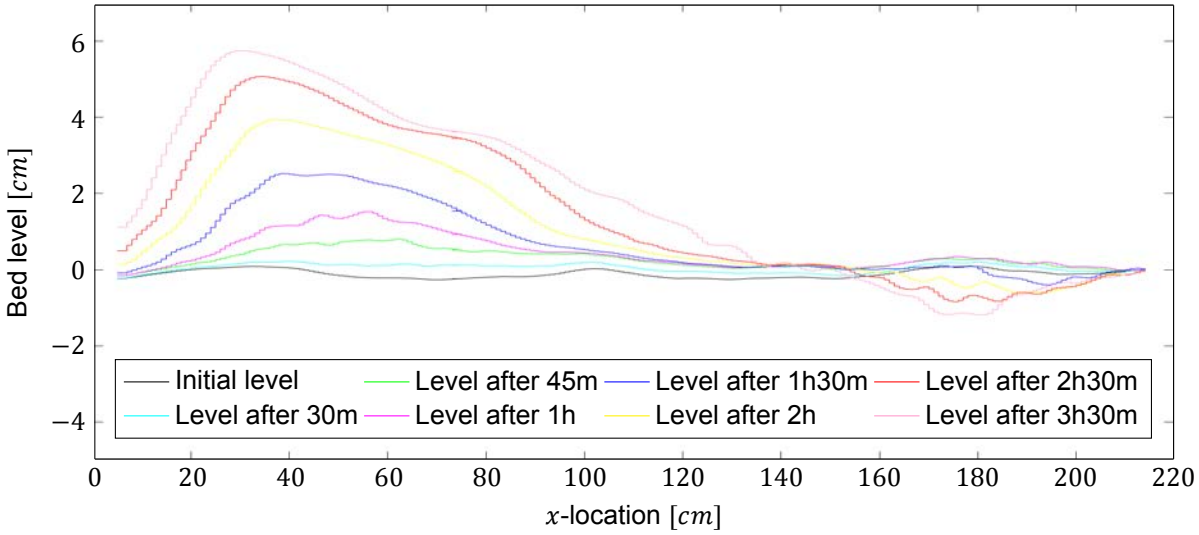

Figure 4.16: Bed level measured by laser 3 at different times after starting experiment 7. Results are smoothened to even out the smallest bedforms.

4.3. Discussion

There are three different flow regimes distinguished for the morphological results of the laboratory experiments. For the experiments with the lowest flow velocities, little bed level changes were observed. For the experiments with moderate flow velocities, a typical flow pattern was found with large bedforms at the start of the flume, lower bedforms after the expansion with a streamwise bar originating from the tip of the expansion. For the high flow velocity experiments, the streamwise bar moved to the side of the flume and grew in size.

The bedforms had a large influence on both the flow pattern and the morphology of the experiments. The bed roughness turned out to have the largest influence on the reattachment length for these experiments. Since bedforms significantly increase the bed roughness, these had the largest influence on the reattachment length. The bedforms seemed to cause most of the morphological changes during the experiments. Large bedforms were found in the narrow part of the flume, propagating in downstream direction. When these bedforms reached the expansion, they bend around it to form a streamwise bar.

A difference between the experiments and a sand closure is that the main transport mode during the experiments was bedload transport, while for the final stage of a sand closure the main transport mode is suspended transport. When the experiments of the present study would be repeated for suspended sediment transport, by reducing the grain diameter, a very different outcome is expected. This is because the bedforms seemed to have a large impact on the morphological changes and are not present for suspended sediment transport. When investigating the erosion of sand during the final stage of a sand closure, it might be interesting to set-up an experiment that investigates suspended sediment transport.

The experiments were designed to recirculate the sediment that reached the end of the flume and settled into the pump compartment. However, since there was so much sedimentation in the wide part of the flume, most of the sediment never reached the pump compartment and thus never got recirculated. It is expected that, if the sediment would start out higher into the water column at the beginning of the flume, the suspended sediment would have stayed in suspension after the expansion due to the high turbulence intensities. Furthermore, for an upper flow regime with lots of suspended sediment, a plane bed would have been present instead of bedforms. If the bed would have been flat, bedforms that originated in the narrow part of the flume would not have bend around the expansion and settled there. Possibly, the bed under the mixing layer would have eroded if the sediment was more in suspension during the experiments. In general, it is expected that the erosion and sedimentation patterns would have differed substantially.

To make sure that the sediment remains in suspension, sediment with a smaller grain diameter should be used. However, it is not feasible to use the laser distance meters for such an experiment.

For the high flow velocity experiments, a waiting time of 20 minutes was required after the pump was shut off before the water was clear enough to measure the bed level with the lasers. When more particles are in suspension, this waiting time increases significantly, and it is possible that the water never becomes clear enough to measure through.

Another difference between the executed experiments and a sand closure, is that the present experiments only exhibit an expansion of the flow, while for a sand closure the flow first contracts towards the gap and then expands. Furthermore, the mixing layers of a sand closure originate on a sloping, erodible surface. Finally, the amount of contraction and expansion of the flow varies greatly during a sand closure. The set-up of the experiments should therefore be designed very carefully.

The secondary current that kept the streamwise bar in place during the experiments is not necessarily present during sand closures. It is possible that the secondary circulation is eliminated when the expansion width is increased. According to Talstra [14], a widening of the flume downstream of the expansion moves the reattachment point downstream. Since it is undesirable to end the flume before the reattachment point, the flume should be longer. It is possible that a different morphology would be observed for these experiments.

To be able to replicate the present experiment and extend the research to different layouts and morphological conditions, a numerical model is set up. To validate the model, the laboratory experiments are replicated and the results are compared in Chapter 5.

5

Numerical modelling

To predict the sand loss during a sand closure, a numerical model is needed to simulate the flow and the resulting erosion and sedimentation. As was stated in the introduction of this thesis, the present models do not predict the sand loss accurately. This thesis provides a first step towards improving this prediction by investigating the erosion and sedimentation under mixing layers. It was chosen to use a three-dimensional model for the present study, instead of the two-dimensional model FINEL2D that was used to predict the sand losses for MV2. The results from the laboratory experiments are used to validate this three-dimensional model, so the model may be used in the future to simulate the erosion and sedimentation patterns of other turbulent flows. Ultimately, the goal is to improve the sand loss prediction of a sand closure. It is investigated if this is feasible with the numerical model used in this thesis.

The laboratory experiments are simulated with the numerical model by making the layout as similar as possible in order to validate the model. After the numerical simulation of the laboratory experiments, it is interesting to use the abilities of the numerical model to simulate a situation that has more resemblance to a sand closure. It was found in the previous chapter that the transport mode of the sediment seems to have a large influence on the morphological changes. The numerical model allows us to extrapolate the results to a case where the sediment is transported as suspended load, like during a sand closure, to investigate the implications on the morphological outcome. This is done by a numerical simulation using sediment with a grain diameter of 100 micrometres instead of the 330 micrometres that was used during the experiments.

The decision-making regarding the choice of the numerical model is discussed in Section 5.1. Then, Section 5.2 treats the specifics of the selected model. How the numerical domain is set up to replicate the laboratory experiments as accurately as possible, is treated in Section 5.3. The outcomes of the simulations for the flow pattern are treated in Section 5.4 and in Section 5.5 the morphological results are presented. A sensitivity analysis towards the model and important properties of sand closures is presented in Section 5.6. Finally, a discussion about the found results will be started in Section 5.7.

5.1. Numerical model

Care was taken to make sure that the set-up of the numerical model replicated the laboratory experiments as much as possible. This meant it had to comply with some stringent demands. As stated in Section 2.2.2, turbulence is a three-dimensional phenomena. To be able to model a turbulent environment correctly, a three-dimensional model is required. The problem with using a two-dimensional model is that it does not involve vortex stretching, which means it only models energy dissipation as the result of viscous forces. When the modelled environment becomes more turbulent, and the Reynolds number thus becomes larger, larger vortices are present in the flow. These larger vortices are more prone to stretching by the current, resulting in more energy dissipation by vortex stretching. For the Reynolds numbers presented in Section 3.2, vortex stretching is definitely important for energy dissipation. This implies that a three-dimensional numerical model with an accurate turbulence description is needed to simulate the flow. It is necessary to solve the Navier-Stokes equations in three directions,

which are given by

$$\frac{\partial u_i}{\partial x_i} = 0 \,, \tag{5.1a}$$

$$\frac{\partial \rho u_i}{\partial t} + u_j \frac{\partial \rho u_i}{\partial x_j} = -\frac{\partial p}{\partial x_i} + \frac{\partial}{\partial x_j}\left(\rho \nu_e \frac{\partial u_i}{\partial x_j}\right) + (\rho - \rho_w)\, g_i \,, \tag{5.1b}$$

where ρ is the local density of the water taking into account the sediment concentration, u_i are the Cartesian flow velocity components, x_i are the Cartesian coordinates, t indicates time, p is the pressure, ν_e is the local eddy viscosity, ρ_w is the density of water, and g_i is the gravitational acceleration. The subscripts i and j can have a value 1, 2, or 3 to represent the Cartesian coordinates x_1, x_2 or x_3, and their corresponding velocity components u_1, u_2, u_3. In this case the three dimensions are denoted as x, y and z, their corresponding velocity components are u, v and w.

There are two differences between the above equations and the original Navier-Stokes equations: the eddy viscosity ν_e is used instead of the molecular viscosity to account for the sub-grid viscous forces caused by turbulent eddies. The second difference is in the gravitation term. Normally, this term states the local density of water times the gravitational acceleration, i.e. ρg_i. In TUDflow3d, the relative differences in density are used for the gravitation term, which enhances the numerical stability of the model without changing the influence of the gravity term.

Equation (5.1b) is the momentum equation. In this equation the first term represents the time derivative of the velocity. The second term denotes the short notation of the three advection terms. Combined, the terms on the left-hand-side of Equation (5.1b) are the inertia forces. The first term on the right-hand-side of Equation (5.1b) is the pressure force. The second term describes the viscous forces. This term accounts for the dissipation of energy as a result of vortex stretching. The last term represents the external forces on the flow, in this case the gravitational force.

To numerically model the sediment transport, the advection-diffusion equation (2.6) needs to be solved using a pick-up equation and a sedimentation equation. The selection of these equations is discussed in the following section.

The stringent demands on the model lead to the decision to use TUDflow3d, which was developed by De Wit [1], to numerically model the laboratory experiments. The downside of using this model is that it uses a rigid lid for the water surface, which may become a problem for higher Froude numbers. Despite the rigid lid, it seems to be the most suitable model to simulate the experiments. The specifications of TUDflow3d are treated in the following section.

5.2. TUDflow3d

TUDflow3d is a three-dimensional numerical model that uses the finite volume method and Large Eddy Simulation (LES) to solve the Navier-Stokes equations on a staggered grid in three directions. To calculate the sediment transport, the model solves the transport equation using a pick-up equation which can be selected by the user, and the sedimentation equation (2.25). The most important features of the model are discussed in this section. For all the details of the model, the reader is referred to De Wit [1].

5.2.1. Discretization schemes

Each term of the Navier-Stokes equations requires its own discretization scheme. To discretize the momentum equation, several discretization schemes are used. For the time integration, the Adam-Bashforth scheme is used, with a pressure-correction algorithm to update the pressure. The use of this scheme makes it possible to use a variable timestep which allows the model to take a smaller timestep when the flow velocities are temporarily higher. Ultimately, this improves the results near boundaries. For the advection terms, the sixth-order hybrid difference scheme (HYB6) is used. For the other terms in the momentum equations, a second-order central difference scheme (CDS2) is applied.

For the discretization of the transport equation (2.6), the Adam-Bashforth scheme is again used for the time integration. For the second term, the advection of volume fractions, a total variation diminishing (TVD) flux limiting scheme is used. For the diffusion term, CDS2 is used.

5.2.2. Turbulence closure

The viscous forces are the hardest to discretize since they require a description of all eddies in the flow. When the Reynolds number increases, the amount and the size of the eddies present in the flow increase accordingly. For the laboratory experiments, the Reynolds numbers are too high to solve the Navier-Stokes equations directly using Direct Numerical Simulation (DNS). TUDflow3d uses the principle of Large Eddy Simulation (LES) to model the flow. LES solves the largest eddies in the flow directly, but the eddies with a diameter smaller than the grid size are lumped into an extra term added to the Navier-Stokes equations. This extra term contains the viscous forces of the eddies smaller than the grid size. Because these smaller eddies are not solved directly, an error is made in the amount of dissipated energy, but because the smallest eddies hold a small amount of energy, this error is small. In TUDflow3d, Wall-Adapting Local Eddy-Viscosity (WALE) is used as the LES model.

5.2.3. Sediment transport and bed update

To model the morphology of the laboratory experiments accurately, it is expected that the pick-up formula of Okayasu et al. [9], Equation (2.15), is the most suitable formula to describe the pick-up of sediment underneath a mixing layer, as was discussed in Section 2.3.1. This equation was validated by Okayasu et al. with laboratory experiments for grid turbulence. This chapter attempts to validate this pick-up equation for mixing layers in combination with a three-dimensional numerical model.

In TUDflow3d, the bed is updated every timestep by tracking which cells are solid cells and which are fluid cells. A schematic overview of the incorporation of the bed update in TUDflow3d is provided in Figure 5.1. In the cells filled with water, the concentration of solid particles is calculated. When the concentration becomes 0.6, which is a typical concentrations for particles in a bed, the cell is categorized as a solid cell. For the solid cells, the flow velocities are kept zero.

To model the sediment transport, use is made of the transport equation (2.6). This equation is used to describe the advection and diffusion of sediment particles in the flow. At the bed, a boundary condition is implied with a pick-up flux in the form of the equation of Okayasu et al. and a sedimentation flux. These fluxes cause the bed level changes. In the other fluid cells, the gravitational pull that the particles experience towards the bed is implemented into the vertical velocity component in the advection term of the transport equation.

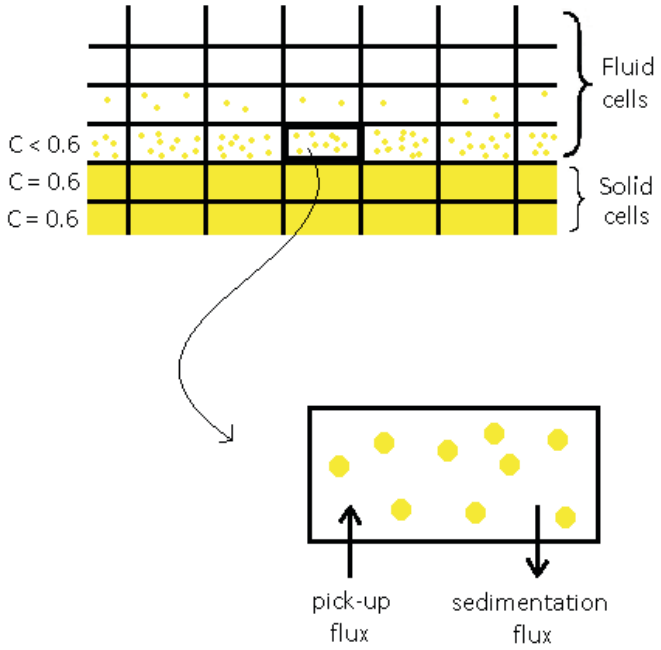

Figure 5.1: Visualization of the incorporation of the transport equation, the pick-up flux and the sedimentation flux in TUDflow3d.

5.3. Set-up of the numerical domain

To validate the results of the numerical model, the results from the laboratory experiments are used. To make sure that the results from the laboratory experiments and the numerical model are comparable, the layout of the physical experiments and the numerical simulations are made as similar as possible. This section describes how the numerical domain is set up to achieve this.

5.3.1. General set-up

Figure 5.2 shows the layout used for the numerical simulations. Essentially, the numerical simulations have the same layout as the laboratory experiments, Figure 3.4. For the numerical simulations, the end of the domain is situated just before the compartment of the pump. The domain starts just behind the flow straighteners; an inflow condition is applied there.

TUDflow3d makes use of a radial grid; however, by taking a very large value for the radius of the grid, the set-up stays rectangular over the five metres length of the flume. Obstacles can be placed in the domain. Inside these obstacles, the flow velocities can be set to zero. In this way the expansion is implemented into the numerical set-up.

At the bed, a layer of sediment of four centimetres is added to accommodate the erosion and sedimentation occurring during the experiment. During the laboratory experiments, the sediment consisted out of several fractions as given by the sieve curve in Figure 3.1. It is possible to implement all the sediment fractions of the sand used in the laboratory experiments; however, since the sieve curve is relatively steep and adding fractions to the numerical model increases simulation time, only the mean grain diameter of the sediment, which is 330 micrometres, is used during the numerical simulations.

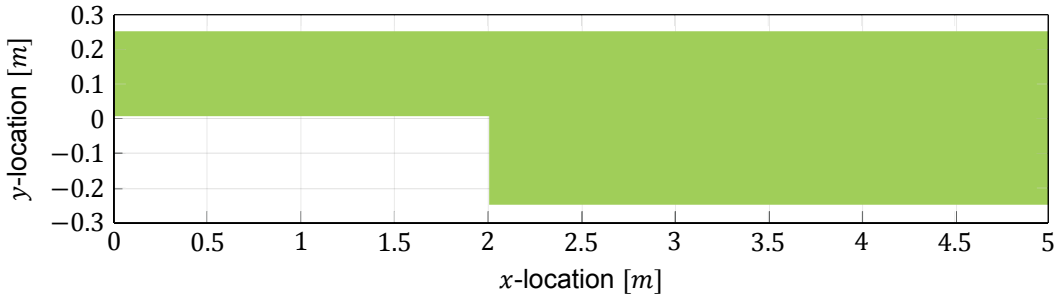

Figure 5.2: Top view of the layout used for the numerical simulations. The numerical domain is coloured green in the figure.

5.3.2. Boundary conditions

At the inflow of the numerical domain, a boundary condition for the flow velocity is imposed. This is a logarithmic velocity profile of which the mean velocity can be given as a constant to the numerical model. This logarithmic profile is lifted to start at the top of the bed. For the side walls of the flume, a no-slip boundary condition is used.

TUDflow3d does not implement a free surface to model the water level, instead a rigid lid is imposed. This sets the water level at one certain height for the entire domain. This might impose a problem for higher Froude numbers, because the water level variations are larger then.

5.3.3. Spatial resolution and time stepping

When choosing the grid size and corresponding time step, the accuracy of both the flow results and the morphological results should be taken into account. In this case, the maximum grid size is governed by the sediment transport. The numerical model with corresponding pick-up equation was developed for suspended sediment transport by De Wit [1], while the laboratory experiments were primarily bedload transport. Because bedload transport takes place close to the bed, a very small grid size is required in vertical direction in order to solve the transport of sediment accurately. Because the aspect ratio of grid cells can not differ too much in the three Cartesian directions, the grid size in both horizontal directions needs to be small as well. It is expected that when the grid size is chosen small enough, there should

be no difference between using a pick-up equation or a bedload transport formula to model bedload transport.

A grid size of about one centimetre in the x- and y-direction and 0.4 centimetre in the z-direction is used. For this small grid size, the description of the velocity field should be quite accurate, since both the accuracy of the solution of the Navier-Stokes equations and of the LES approximation improve with a decreasing grid size.

The time stepping is solved by the numerical model itself. The proper timestep to solve the governing equations depends on the spatial grid resolution and the flow velocity through the Courant Friedrichs Lewy (CFL) condition:

$$C = \frac{u\Delta t}{\Delta x} \leq C_{max} \, . \tag{5.2}$$

where C is the Courant number, u is the flow velocity, Δt is the timestep, Δx is the spatial resolution, and C_{max} is a constant which represents the stability requirement. In order to ensure numerical stability, this Courant number should be smaller than the value of C, which depends on the used discretization scheme. TUDflow3d calculates the required time step based on a Courant number of 0.7.

5.3.4. Calibration parameters

The numerical model uses some calibration parameters that have an effect on both the computed velocity field and the morphological outcomes. To calibrate both the flow results and the morphological results, the roughness of the bed can be adjusted. This roughness depends on the grain diameter and is typically chosen with a value between one and five times the median grain diameter. For the numerical simulations of the laboratory experiments, a value of three times the median grain diameter was chosen.

The main transport mode for the laboratory experiments was bedload transport. This means that most of the sediment is rolling and sliding over the bed, and does not get picked-up into the water column. This means that it is possible that for the present grid size, most of the morphological processes occur within the grid cell closest to the bed. Furthermore, the bedforms seemed to have a large impact on the morphology during the laboratory experiments and it is unsure if the flow and the morphology of these bedforms is solved accurately enough by the numerical model in order to capture all the important mechanisms occurring around these bedforms.

To calibrate the morphological results, three equations can be altered; the transport equation (2.6), the pick-up equation (2.15) and of calibrating the morphological results, two tuning parameters were implemented in the numerical model. Both parameters are incorporated into the pick-up equation, because it is expected that the bedload transport and the bedforms not being accurately solved has the largest effect on the pick-up of sediment.

First, the critical Shields parameter, as was treated in Section 2.3.1, can be altered to allow the sediment particles to be picked-up from the bed more easily. The second tuning parameter is a pick-up factor, which multiplies the pick-up equation (2.15) with a certain factor in order to scale the pick-up from the bed. It is expected that both the transport mode being bedload transport and the incomplete modelling of the bedforms result in a lower prediction of the sediment transport than is occurring in reality. For this reason, it is chosen to increase the amount of pick-up artificially with the two calibration parameters. A value of 0.5 is used for the critical Shields parameter, and the pick-up factor is set to 2.

5.3.5. Numerical cases

The numerical cases that were simulated are based on the cases that were executed for the laboratory experiments. Again, two sets of simulations are executed, one with a non-erodible bed to observe the flow patterns without the interference of morphology, and one that incorporates a bed update to model the morphology of the experiments. The simulations with a non-erodible bed are used to validate the model with the flow patterns found during the experiments, but also to gain more insight into the characteristics of the flow. The simulations including morphology were used to validate the model for the experimental set-up.

For the simulations of the flow patterns, all eight experiments are simulated with the numerical model. For the morphological simulations, only the three most relevant experiments were simulated,

namely experiments 1, 4 and 7. For completeness, an overview of the numerical simulations is given in Table 5.1. The experiments that were chosen for the morphological simulations are printed bold.

Flow simulations
The simulated time of the flow simulations was five minutes. This was sufficient to observe all the relevant flow patterns and average them over a long enough period to obtain a mean flow pattern. For experiment 4, the simulated time was also doubled to ten minutes to check if five minutes of simulated time was sufficient. There were no significant differences found between both simulations. Their results are given in Appendix C. A simulated time of five minutes was sufficient for the flow simulations.

Morphological simulations
In Chapter 4, the results of the experiments are split up into the three groups that all have fundamentally different results. Experiments 1 and 2 had the lowest flow velocities, and showed negligible morphological changes. Experiments 3 to 6 were the most typical experiments, each with a similar morphological outcome. The experiments with the highest flow velocities, experiments 7 and 8, were treated separately because their results diverted from the mean flow velocity experiments again. To discuss the outcome of the numerical simulations in this chapter, the same division is made, taking the same experiments as examples as was done in Chapter 4.

Most laboratory experiments had a duration of about three hours. A simulated time of one hour was chosen for the morphological simulations. This is justified because it was found during the laboratory experiments that the general features of the final morphology, like the bedforms and the streamwise bar, had already developed after an hour and only grew in height and length after this time. To check if the simulated time of one hour is sufficient, the numerical simulation of experiment 4 was repeated for a simulated time of three hours. It was found that the morphological patterns were similar to the simulation of one hour and only increase in time, so it can be concluded that a simulated time of one hour is sufficient for the morphological simulations. The results from the three hour simulation can be found in Appendix D.

Table 5.1: An overview of the numerical simulations with their corresponding dimensionless numbers. The simulations that were chosen for the morphological simulations are printed bold. Table adapted from Table 3.1.

$Nr.$	Q	U_1	Fr_1	Re_1	P_1	θ_1	U_2	Fr_2	Re_2	P_2	θ_2
	[l/s]	[m/s]	[-]	[-]	[-]	[-]	[m/s]	[-]	[-]	[-]	[-]
Low flow velocity experiments											
1	**8**	**0.2**	**0.16**	**$2.5 \cdot 10^4$**	**13.9**	**0.02**	**0.1**	**0.08**	**$1.2 \cdot 10^4$**	**27.8**	**0.01**
2	10	0.25	0.20	$3.0 \cdot 10^4$	11.1	0.03	0.13	0.10	$1.5 \cdot 10^4$	22.3	0.01
Moderate flow velocity experiments											
3	12	0.3	0.24	$3.7 \cdot 10^4$	9.3	0.05	0.15	0.12	$1.8 \cdot 10^4$	18.6	0.01
4	**14**	**0.35**	**0.28**	**$4.3 \cdot 10^4$**	**8.0**	**0.06**	**0.18**	**0.14**	**$2.1 \cdot 10^4$**	**15.9**	**0.02**
5	16	0.4	0.32	$4.9 \cdot 10^4$	7.0	0.08	0.2	0.16	$2.5 \cdot 10^4$	13.9	0.02
6	18	0.45	0.36	$5.5 \cdot 10^4$	6.2	0.10	0.23	0.18	$2.8 \cdot 10^4$	12.4	0.03
High flow velocity experiments											
7	**20**	**0.5**	**0.40**	**$6.1 \cdot 10^4$**	**5.6**	**0.13**	**0.25**	**0.20**	**$3.1 \cdot 10^4$**	**11.1**	**0.03**
8	21.4	0.54	0.43	$6.6 \cdot 10^4$	5.2	0.15	0.27	0.21	$3.3 \cdot 10^4$	10.4	0.04

5.4. Results flow patterns

This section treats the results of the simulations with a non-erodible bed. All the experiments from the previous chapter were simulated using TUDflow3d in order to investigate if the numerical results are similar to the flow patterns found during the laboratory experiments. The general flow patterns are assessed, but also the specific characteristics that were found in Section 4.1, such as the reattachment length and the secondary circulation, are considered.

In the previous chapter, the morphology found for a typical experiment was presented using experiment 4 as an example. To obtain a good comparison between the laboratory experiments and the

numerical simulations, experiment 4 is again used as an example. The results of the other experiments can be found in Appendix C. Some resilience checks were executed to validate the results for the current simulation duration and grid resolution, these can be found in Appendix C as well.

5.4.1. General flow patterns

In this section, the general flow patterns of the numerical simulations are compared to what was found during the laboratory experiments. Furthermore, the numerical simulations are used to obtain a more complete image of the flow, since it was not possible to make flow measurements during the laboratory experiments.

The average flow velocities as plotted in Figure 5.3 follow the same pattern as the laboratory experiments. In the narrow part of the flume, high flow velocities are observed. At the location of the return current, the flow velocities are almost zero. Inside the mixing layer the flow velocities linearly decline between the main current and the mixing layer, which concurs with the literature presented in Subsection 2.2.3.

Figure 5.4 shows the turbulence intensity, plotted by dividing the local root-mean-square value of the flow by the overall mean flow velocity. The turbulence intensity at the inflow are uniformly distributed and about 0.05, which is quite low. It is expected that the turbulence intensities were somewhat higher for the laboratory experiments due to the presence of the flow straighteners, which break up the large eddies in the flow but also generate a small amount of turbulence. It can be seen that the mixing layer observed in Figure 5.4 spreads in a similar fashion as the mean flow. At the start of the mixing layer, the turbulence intensity slightly increases. While the mixing layer spreads, the turbulence intensity increases until it reaches a value of 0.45. Further downstream, the maximum value of the turbulence intensity decreases again while the mixing layer spreads further. At the end of the flume, the turbulence intensity is more or less uniformly distributed again, at a value of about 0.25.

In general, the mean flow velocities agree with the literature presented in Subsection 2.2.3. During the laboratory experiments, large eddies were observed at the location of the mixing layer. Although it was not possible to quantify the turbulence intensities during the laboratory experiments, the image presented in Figure 5.4 agrees with the observations made during the experiments. It seems that the flow patterns of the numerical simulations resemble the laboratory experiments well and concur with the literature presented in Chapter 2.

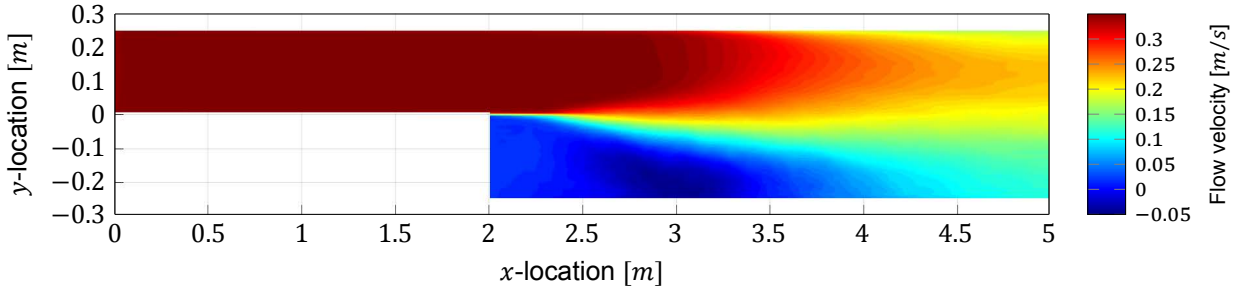

Figure 5.3: Time-averaged flow velocity for experiment 4 at eight centimetres above the bed.

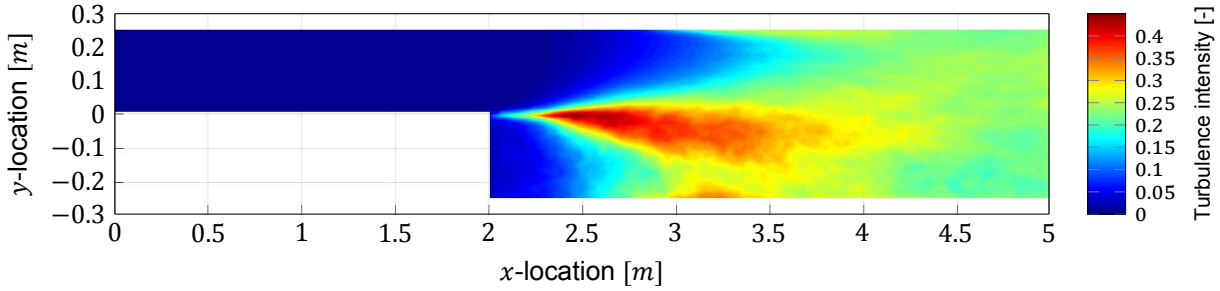

Figure 5.4: Time-averaged turbulence intensity throughout the flume for experiment 4 at eight centimetres above the bed.

5.4.2. Reattachment length

For the laboratory experiments, the reattachment length was determined by inserting dye into the flow near the side wall at which the return current is located. For the numerical simulations, an attempt is made to replicate the way in which this reattachment length was obtained as well as possible. The first four centimetres of the water column are averaged, which is the expected penetration depth of the dye. Then, the location at which the flow becomes zero at the side wall is determined. This is the location of the reattachment point for the numerical simulations.

Table 5.2 compares the reattachment lengths of the laboratory experiments to the ones modelled by TUDflow3d. It can be seen that while the reattachment length of the laboratory experiments starts at a value of 1.8 metres and gradually decreases with increasing flow velocity, the reattachment length of the numerical simulations only varies marginally around a value of 1.45 metres. The difference in reattachment length can have various reasons, both physical and numerical. The difference could be caused by the used LES model, by a difference in turbulence at the inflow of the flume, by the rigid lid the model uses for the water level, and by a difference in roughness between the experiments and the numerical model of both the bed and the side walls.

Since the grid size was very small for the numerical simulations, it is expected that the influence of the used LES model is relatively small. This suspicion was verified by simulating experiment 1 again, but this time using the direct dynamic Smagorinsky model (DSmag) instead of the WALE model. DSmag is generally accepted as an accurate LES model and provides a good comparison for verification. The reattachment length for this simulation was 1.5 metres, so the difference in reattachment length for both LES models is small in this case.

For the side walls of the flume, a no-slip boundary condition is applied; this means that the flow velocities are set to zero at the boundary. No additional roughness was applied to these boundaries. Since the side walls of the laboratory experiments were made of smooth shuttering plywood, it is expected that the no-slip boundary condition is a proper representation of the flow at the wall.

The rigid lid could have a large effect on the reattachment length for the higher flow velocities. Using the formula of Bernoulli as a first estimate to assess the effect of the high flow velocities on the water level changes over the mixing layer, a difference in water level of one centimetre is expected between the fast flowing part and the return current. It is unsure if this has a significant contribution to the reattachment length. Looking at the difference in reattachment length for the low flow velocity experiments, where the rigid lid has little to no influence on the result, it can be seen that there is a large difference between the reattachment length of the laboratory experiments and the numerical simulations. The rigid lid is not the main cause for the discrepancy in the reattachment length, another cause for the difference should be sought.

At the start of the laboratory flume, flow straighteners are placed to break up the turbulence at the inflow. However, these flow straighteners in itself also cause some turbulence at the inflow of the flume. Since the numerical model imposes a logarithmic velocity profile at the inflow, it is possible that there is some difference between the inflow conditions of the experiments and the numerical model. It is possible to impose additional eddies at the inflow using the synthetic eddy method (SEM). The numerical simulation of experiment 1 was repeated with a turbulent inflow using SEM. This resulted in a reattachment length of 1.4 metres. The influence of the inflow condition on the reattachment length seems to be small.

During the laboratory experiments, the reattachment length decreased for an increasing flow velocity. In Subsection 4.1.2, it was concluded that this shortening of the reattachment length was caused by an increase in bed roughness as the flow velocities of the experiments increased. For the numerical model, this change in bed roughness is not taken into account in the numerical simulations, which would cause a difference in the reattachment point between the laboratory experiments and the numerical simulations. However, for experiment 1, no bedforms were present and the difference in bed roughness between the experiments and the numerical model should be negligible.

Experiment 4 was repeated with a simulated time of ten minutes. The corresponding reattachment length was 1.45 metres. Furthermore, a grid refinement was applied to experiment 4 and the resolution of the grid was doubled in all directions. For this simulation, the reattachment length was 1.5 metres. Neither the simulated time, nor the grid refinement influenced the reattachment length significantly. It can thus be concluded that the simulated time of the simulations was sufficiently long, and the grid size was sufficiently small. Finally, the reattachment length during the morphological simulations, which will be treated in Section 5.5, was computed. A reattachment length of 1.45 metres was found for experi-

ment 4 and 1.55 metres for experiment 1. So although the bed level changes were small for experiment 1, the morphological changes thus seem to have some influence on the found reattachment length for the experiment. However, the reattachment length still does not agree with the values found during the laboratory experiments.

It is unsure what the reason is for the discrepancy between the reattachment lengths of the laboratory experiments and the numerical simulations. The bedforms seem to be the mechanism with the most significant impact on the results, but do not explain the large difference in reattachment length for experiment 1. A different explanation thus has to be sought for the discrepancy.

Figure 5.5a shows the flow velocities in x- and z-direction for a cross-section over the depth adjacent to the side wall from the expansion to the end of the flume. The location and orientation of this cross-section is shown in Figure 5.5b. It can be seen that the flow velocities are more or less zero in the left side of the plot, just after the expansion, at the top of the water column. The flow velocity again becomes zero at the reattachment point. For this experiment, it can be seen that the reattachment point is at x-location 3.5, which is 1.5 metres downstream of the expansion.

It is observed that the reattachment point is closer to the bed further downstream, up to two metres downstream of the expansion at the bed. It is not sure why the reattachment length is variable over the depth, but the same lengthening over depth was observed for all the simulations. The influence of bed roughness can not explain this longer reattachment length close to the bed, since an increase in bed roughness only decreases the reattachment length. Possibly, the increase in reattachment length can be explained by the decrease in flow velocity over depth. It was found from literature that an increase in flow velocity causes an increase of the reattachment length. Because the flow velocity decreases towards the bed, a decrease in the reattachment length is a logical result.

Table 5.2: Reattachment length given in metres downstream of the expansion for both the laboratory experiments and the numerical simulations.

$Nr.$	U_1	U_2	Laboratory	TUDflow3d
	[m/s]	[m/s]	[m]	[m]
Low flow velocity experiments				
1	0.2	0.1	1.8	1.45
2	0.25	0.13	1.75	1.45
Moderate flow velocity experiments				
3	0.3	0.15	1.7	1.5
4	0.35	0.18	1.65	1.5
5	0.4	0.2	1.35	1.45
6	0.45	0.23	1.2	1.5
High flow velocity experiments				
7	0.5	0.25	1.1	1.4
8	0.54	0.27	1	1.4

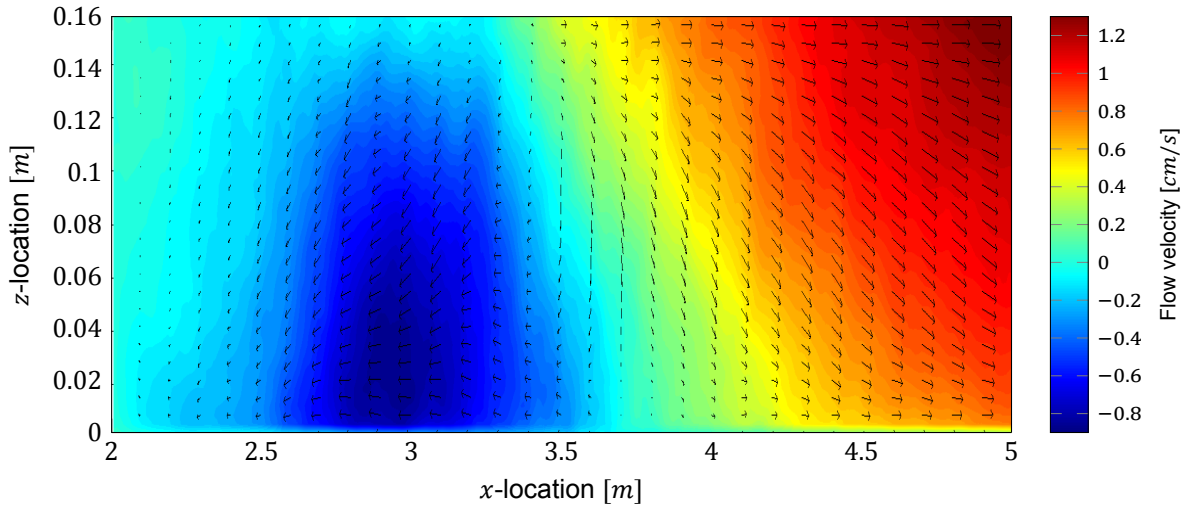

(a) Time-averaged flow pattern in a slice adjacent to the side wall at which the return current is located.

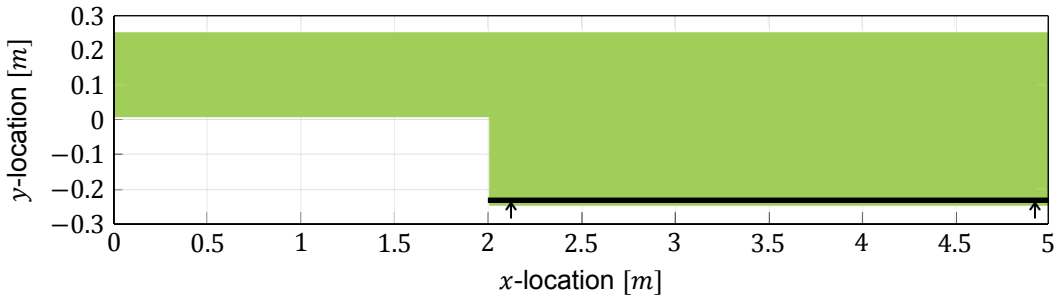

(b) Plot showing the top view of the flume layout. The location and orientation of the cross-section of Figure 5.5a is indicated.

Figure 5.5: Flow pattern for the numerical simulation of experiment 4 in a slice adjacent to the side wall at which the return current is located.

5.4.3. Secondary circulation

In Figure 5.6a, a plot is depicted of the flow velocities in y- and z-direction for a cross-section perpendicular to the flume 35 centimetres behind the expansion. On the right side of the figure, the main current is located. In the main current, the flow velocities in x-direction are the highest, and as can be seen from this plot, the flow velocities perpendicular to the main current are negligible.

Behind the expansion, the flow velocities in x-direction are low, as can be seen from Figure 5.5a. Figure 5.6a depicts relatively large flow velocities in y- and z-direction. The secondary circulation that was suspected during the laboratory experiments seems to be confirmed by the numerical model, although the outward flow near the surface is low. As was explained in the previous chapter, this secondary circulation explains the streamwise bar that was observed during the experiments.

It was investigated how the secondary circulation would change when the expansion width was increased. This was done by doubling the expansion width of the flume, while keeping the narrow part of the flume and all other parameters the same. Figure 5.7b shows the layout of the numerical set-up that was used for this simulation. Note that the expansion is not located at a zero y-location, but at 0.125 metres. In Figure 5.7a, the results of the simulation of experiment 4 with a twice as large expansion width are depicted. It can be seen that the flow velocities have the same range as for the simulation of experiment 4, which is depicted in Figure 5.6a. The return flow from the mixing layer to the side wall at the surface is less pronounced than in Figure 5.6a, but the flow velocity towards the location of the mixing layer is not reduced. A widening of the flume thus seems to have a small effect on the strength of the secondary circulation.

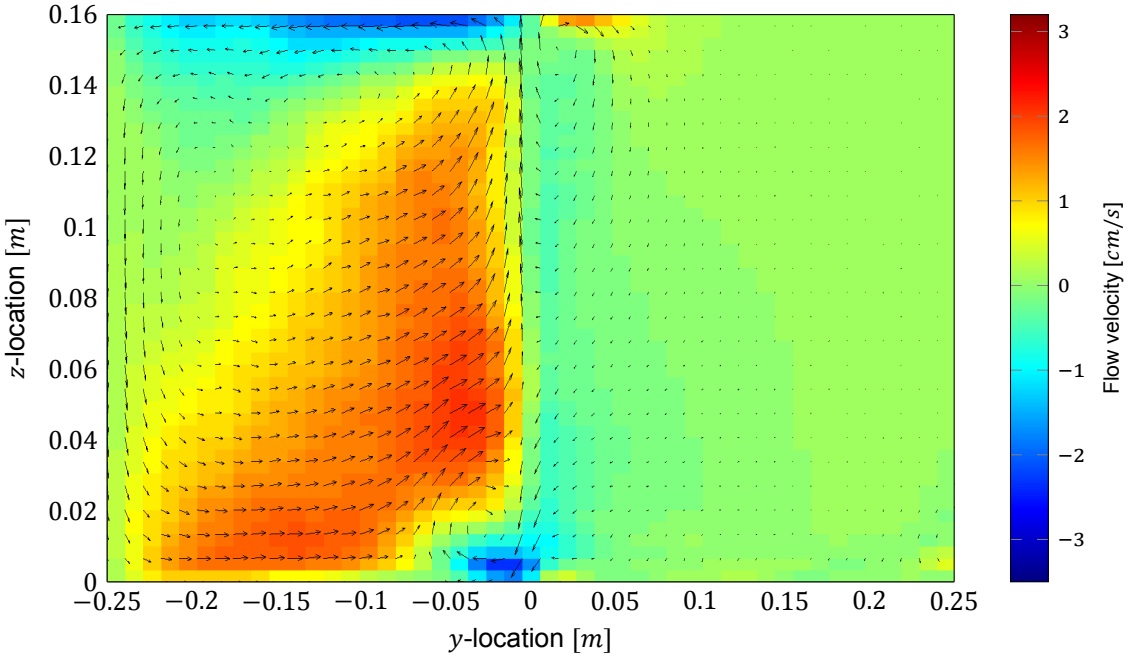

(a) Flow pattern in a cross-section perpendicular to the flume 35 centimetres downstream of the expansion.

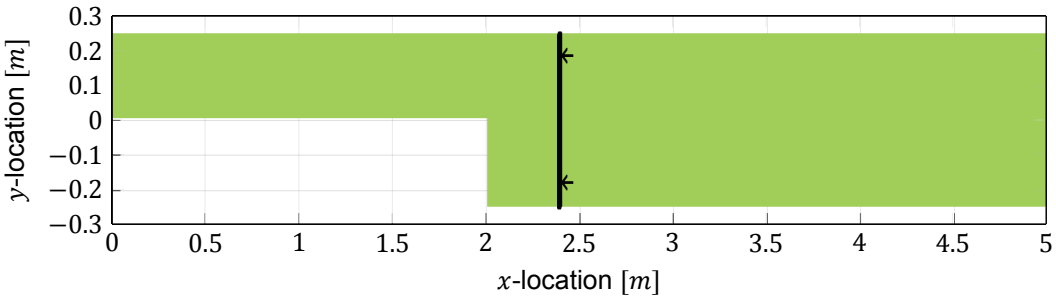

(b) Plot showing the top view of the flume layout. The location and orientation of the cross-section of Figure 5.6a is indicated.

Figure 5.6: Flow pattern for the numerical simulation of experiment 4 in a cross-section perpendicular to the flume 35 centimetres downstream of the expansion.

5.4.4. Conclusion

The flow patterns computed by TUDflow3d largely agree with the flow patterns that were observed during the laboratory experiments. The flow velocities decrease linearly over the mixing layer, which concurs with literature, and a secondary circulation is simulated that was observed qualitatively during the laboratory experiments. However, the predicted reattachment lengths do not match the values that were found during the experiments. During the laboratory experiments, the reattachment length started out at 1.8 metres and decreased when the flow velocity increased, while the numerical model predicts a more or less constant value for the reattachment length. It is possible that this is partially caused by the rigid lid, but this does not explain why they do not match for the low flow velocities. It is thus expected that the discrepancy between the laboratory experiment and the numerical results originates from the presence of bedforms in the laboratory experiments, which increase the roughness of the bed.

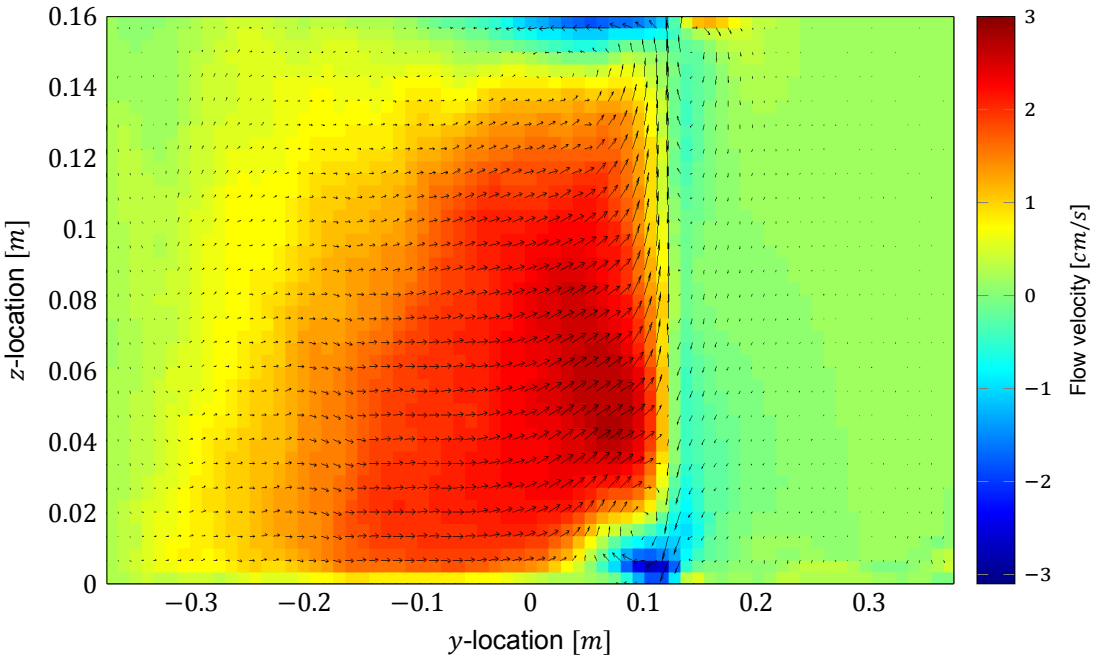

(a) Flow pattern in a cross-section perpendicular to the flume 35 centimetres downstream of the expansion.

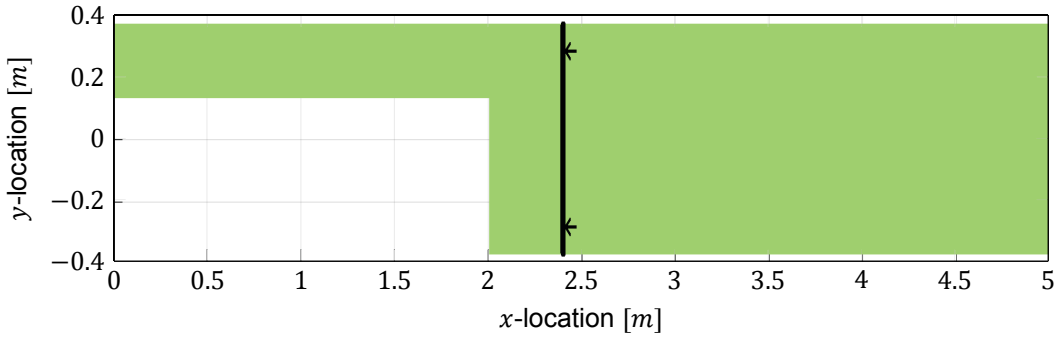

(b) Plot showing the top view of the flume layout. The location and orientation of the cross-section of Figure 5.7a is indicated.

Figure 5.7: Flow pattern for the numerical simulation of experiment 4 with a twice as large expansion width in a cross-section perpendicular to the flume 35 centimetres downstream of the expansion.

5.5. Results morphology

The morphological results of the numerical simulations are treated in this section. It is investigated if the numerical model TUDflow3d can be used to predict the morphology of the laboratory experiments, using the pick-up formula of Okayasu [9]. The figures that showed the final layout of the bed for the laboratory experiments are displayed under the morphological results obtained with the numerical model to offer an easy comparison. It should be noted that the numerical model had a shorter running time, so the general patterns should be equal but the magnitude of the morphological changes varies.

The transport mode of the laboratory experiments was bedload transport. As discussed in Section 2.3, the Rouse profile reduces to a small layer of sediment rolling and sliding over the bed for bedload transport. It is possible that this layer became too thin for the present numerical study, and all the sediment transport took place in the first cell above the bed. As was discussed in Section 5.3.5, the grid size is small, but possibly still too large to describe the detailed flow patterns that take place around bedforms which were about one centimetre in height for experiment 4, while the height of a grid cell is 0.4 centimetre.

Bedforms originate due to a instability in the bed. When the first onset of a bedform is formed, the bedforms keep growing until they reach an equilibrium height and length. For the laboratory experiments, it was impossible to make the initial bed completely flat, so there were some initial imperfections present in the bed. In the numerical set-up, these initial imperfections are not present which could hamper the development of the bedforms.

The remainder of this section treats the results of the morphological simulations. Just as for the laboratory experiments, experiment 1, 4 and 7 are treated in more detail. Opposed to the flow simulations, the other experiments are not simulated. Instead, a sensitivity analysis is performed on the model and the most important properties of sand closures, and is discussed in Section 5.6. Only the figures that were most relevant to interpret the numerical results are treated in this section. A complete overview of the numerical results can be found in Appendix D.

5.5.1. Low flow velocity experiment

It was chosen to numerically model laboratory experiment 1 with TUDflow3d, because this experiment showed no bedforms or other morphological changes during the laboratory experiments. Ideally, the numerical simulation does not show any bed changes as well. From Figure 5.8 it can be seen that the numerical model predicts some negligible bed level changes in the order of half a millimetre after a simulated time of one hour of which the erosion in the first part of the flume are inflow effects. There is one spot at the tip of the expansion with bed level changes of about one millimetre, but overall it can be concluded that the bed level changes are negligibly small.

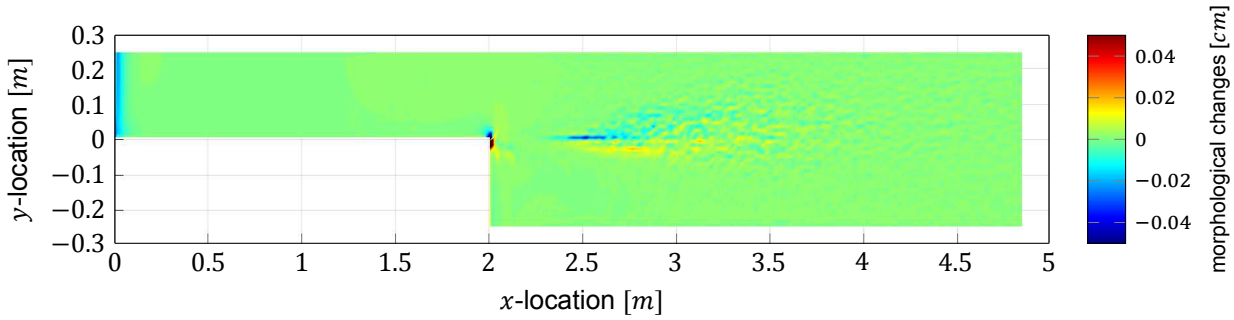

Figure 5.8: Simulated bed level changes for experiment 1.

5.5.2. Moderate flow velocity experiment

Just like for the laboratory experiments, experiment 4 is used as an example. In this section the results of Chapter 4 are compared to the results of the numerical simulation.

In the laboratory experiments that were described in Chapter 4, some general characteristics of the morphology were found. The experiment showed erosion and bedforms with a height of about two centimetres in the narrow part of the flume. Further, a streamwise bar originated from the expansion with bedforms of about one centimetre on the fast flowing side of the bar, and negligible bed level changes under the return current as can be seen in Figure 5.10.

Figure 5.9 shows the final erosion and sedimentation pattern for experiment 4 after a simulated time of one hour. The erosion pit at the tip of the expansion that was found for the low flow velocity experiment is still visible, but is less pronounced. The numerical simulation displays a bar that is similar to the laboratory experiments, but this bar is not attached to the tip of the expansion, as it was for the laboratory experiments. However, the location of the bar seems to agree with its location during the laboratory experiments. The height of the bar is about one centimetre, which concurs with the height measured after one hour during the laboratory experiments.

The numerical simulation differs further from the laboratory experiments because it shows an erosion pit underneath the fast flowing part of the mixing layer. Furthermore, no bedforms are present in the numerical simulation. The narrow part of the flume exhibits much less erosion than during the laboratory experiments. It is expected that the lack of bedforms in the narrow part of the flume result in a drastic decrease in the amount of observed erosion. This is because bedforms increase the roughness

of the bed and create small scale turbulent eddies in the wake of the bedforms. The presence of bedforms potentially increases the transport capacity of the flow, so the absence of them in the numerical model has a large impact on the outcome of the numerical simulations. Because the bed underneath the fast flowing part of the mixing layer is not fed by the sediment transported by the bedforms in the same way as for the laboratory experiments, the bed erodes for the numerical simulations.

The morphology predicted by the numerical simulation shows some analogy with the damage pattern found by Zuurveld [23] as treated in Section 2.4. The largest amount of erosion is found under the fast flowing part of the mixing layer and since the sediment is pebble-sized for the research of Zuurveld, no bedforms were present in those laboratory experiments. This analogy shows that the above theory about the bedforms feeding the downstream part of the flume might be correct.

To investigate if the flow patterns are altered by the bed level changes, the mean flow velocity and turbulence intensity near the bed are plotted. Figure 5.11 depicts the root-mean-square value of the two horizontal velocity components in the first cell above the bed, averaged over the duration of the simulation. The plot actually shows the value of the first cell above the bed, regardless of which cell this is, so the showed result is not a flat slice but follows the bed. Comparing this plot to Figure 5.3, it can be seen that the flow velocities are lower close to the bed. This is due to the friction of the bed. The flow pattern near the bed more or less follows the flow patterns shown in Figure 5.3, with the exception of a slight increase in flow velocity in the return current near the wall. This increase in flow velocity could explain the bedforms in the return current, as were described in Subsection 4.2.2, for laboratory experiments 5 and 6.

Figure 5.12 shows the average turbulence intensity of the flow near the bed. When this is compared to the turbulence intensities at a depth of eight centimetres for the flow simulation that is shown in Figure 5.4, it can be seen that the high turbulence intensities are much wider spread near the bed. The range of the turbulence intensities in the flow is not altered close to the bed, which means that the magnitude of the fluctuations in the flow decreases at the same rate as the mean flow velocity. It also suggests that turbulence is not negligible for the pick-up of sand underneath a mixing layer.

Altogether, it can be concluded that for the moderate flow velocities, the model requires some extra attention towards the incorporation of the bedforms, but the flow patterns that were found in the laboratory experiment seem to be captured well. Both the laboratory experiment and the numerical results showed the presence of a streamwise bar of which the height was simulated correctly by the numerical model.

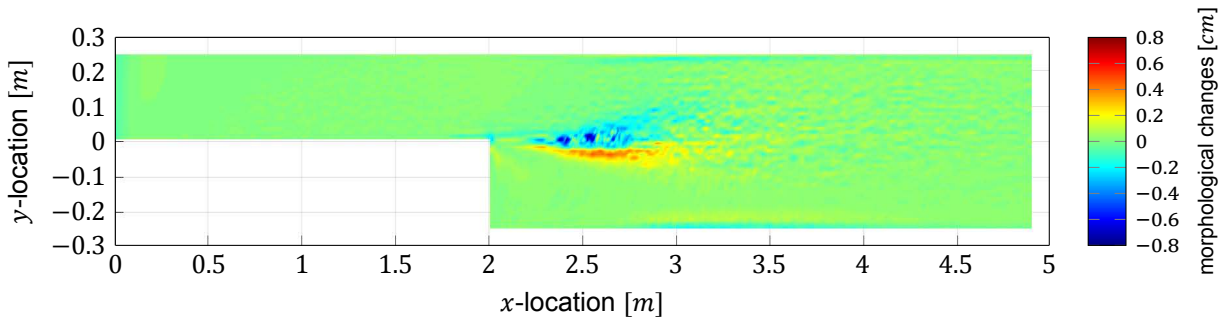

Figure 5.9: Simulated bed level changes for experiment 4.

Figure 5.10: Photograph of the final erosion and sedimentation pattern for experiment 4. The photograph shows the flume at the expansion and about the first 1.5 metres downstream of the expansion. This is the same photograph as Figure 4.6.

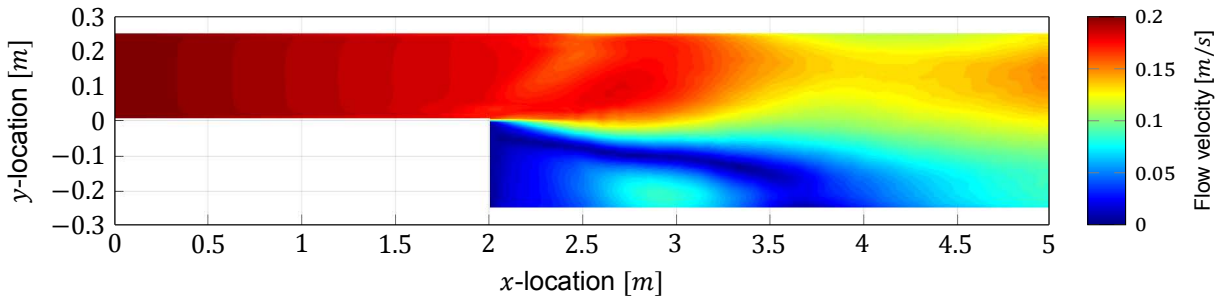

Figure 5.11: Time-averaged flow velocity in the first cell above the bed for experiment 4.

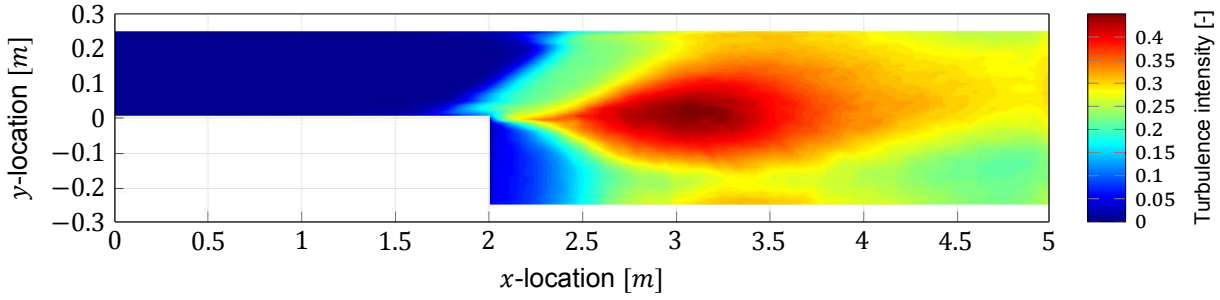

Figure 5.12: Time-averaged turbulence intensity throughout the flume in the first cell above the bed for experiment 4.

5.5.3. High flow velocity experiment

For the high flow velocities, experiment 7 is used as an example. Figure 5.13 shows the result of the simulation of experiment 7. The simulated time was again one hour.

During the laboratory experiments, the morphology of experiment 7 and 8 varied from the other experiments. The streamwise bar that developed during the experiments shifted to the location of the return current and grew in size dramatically after it reached its final location as can be seen again in Figure 5.14. During the laboratory experiments, large water level variations were observed, so it is expected that the rigid lid assumption will have a large influence on the results of this simulation.

The results of the numerical simulation are depicted in Figure 5.13. It can be seen that the small erosion pit found for the low flow velocities has completely disappeared. The numerical simulation shows a

growth of the streamwise bar, both in height and width. The height of the bar is about 1.5 centimetres, which concurs with the height of the bar after one hour during the laboratory experiments. The bar is mostly expanded in the direction of the return current. However, the bar does not shift towards the side of the flume and attaches to the side wall in the way it did during the laboratory experiments. The erosion pit under the fast flowing part of the mixing layer is deepened for these large flow velocities compared to the results that were found for experiment 4. Just downstream of this erosion pit three ridges are visible that can be identified as bedforms.

There are two possible causes for the absence of the bar shift towards the return current. Section 4.2.3 suggests that the occurrence of bedforms travelling towards the expansion could cause an imbalance in the secondary circulation that causes the bar to shift. The numerical simulation showing no bedforms in the return current could be the reason that the bar shift does not occur. It is also possible that fluctuations in the water level cause the streamwise bar to shift towards the side wall. The rigid lid would prevent these water level changes, which would preclude the bar shift.

Figure 5.15 shows the simulated mean flow velocities near the bed, averaged over the duration of the experiment. As would be expected for an experiment with a larger mean flow velocity, the flow velocities near the bed are larger than for experiment 4. Again, an increase in the mean flow velocity is observed in the return current.

Figure 5.16 depicts the average turbulence intensities near the bed that were simulated by the numerical model. The results are more or less similar to the turbulence intensities found for experiment 4, but larger turbulence intensities are found in the narrow part of the flume, and inside the mixing layer, the area with high turbulence intensities is somewhat larger.

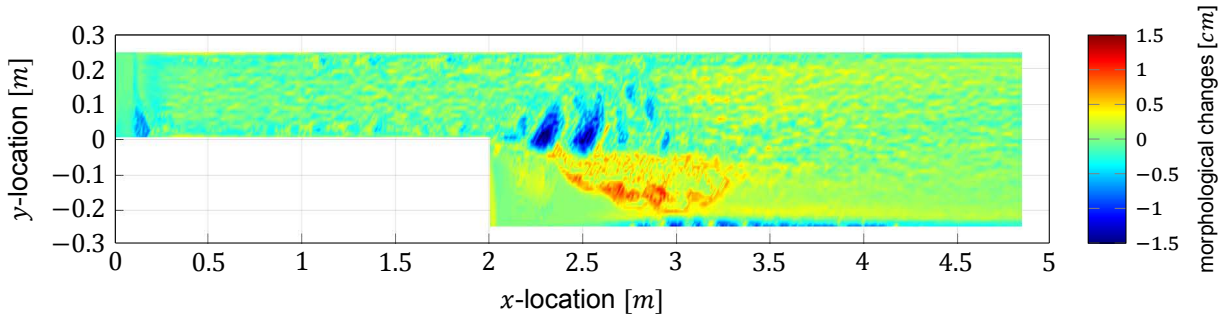

Figure 5.13: Simulated bed level changes for experiment 7.

Figure 5.14: Photograph of the final erosion and sedimentation pattern for experiment 7. The photograph shows the flume at the expansion and the first metre downstream of the expansion.
This is the same photograph as Figure 4.13.

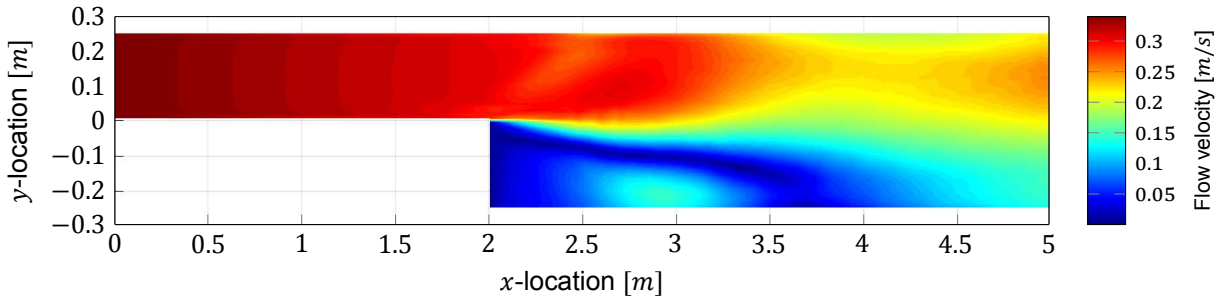

Figure 5.15: Time-averaged flow velocity in the first cell above the bed for experiment 7.

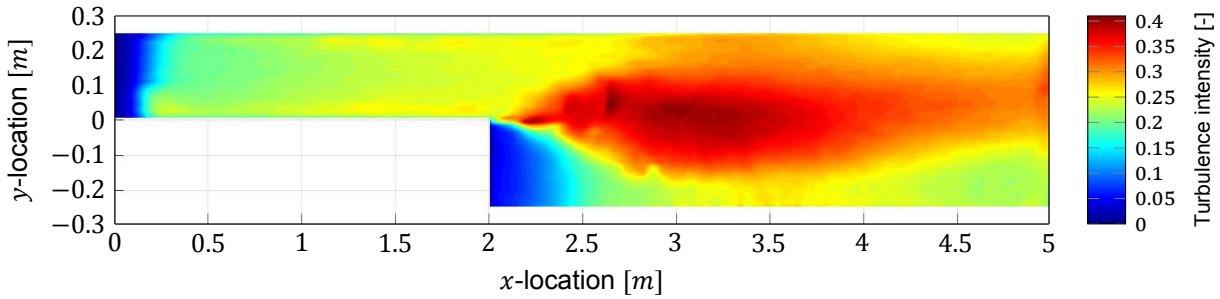

Figure 5.16: Time-averaged turbulence intensity throughout the flume in the first cell above the bed for experiment 7.

5.5.4. Conclusion

The results of the numerical simulations concur with the laboratory experiments in terms of the sedimentation prediction. However, the numerical simulations also show a large erosion pit under the fast flowing part of the mixing layer and do not contain the bedforms or bar shift that occurred during the laboratory experiments. Because the main transport mode for the laboratory experiments was bedload transport, using a bedload formula would possibly have been a better choice to model the experimental set-up.

5.6. Sensitivity analyses

This sections aims to obtain more insight into the sensitivity of the model on important properties of sand closures. In the first subsection, experiment 4 is repeated with the pick-up formula of Van Rijn [20] instead of the formula of Okayasu et al. [9], in order to investigate the importance of taking turbulent properties into account in the pick-up equation. In the Section 5.5, it was found that the streamwise bar that developed during the laboratory experiments is well captured by the numerical model. However, it was found that the bedforms that occurred during the laboratory experiments are not well captured by the numerical model. In Subsection 5.6.2, it is attempted to obtain more insight into the onset and formation of these bedforms. Finally, the laboratory experiments exhibited bedload transport as the main transport mode of the sediment. Subsection 5.6.3 expands the research to investigate suspended sediment transport.

5.6.1. Pick-up formula Van Rijn

To assess the influence of the pick-up equation of Okayasu et al. [9] on the results, the simulation of experiment 4 was repeated using the pick-up equation of Van Rijn [20], keeping all other settings equal. Since the pick-up equation of Van Rijn is widely used, it functions as a good comparison. Furthermore, it was shown in Section 2.3 that the pick-up formulas of Van Rijn and Okayasu are similar, apart from the incorporation of turbulent parameters. This makes a simulation of experiment 4 using the pick-up equation of Van Rijn a good test to asses the influence of incorporating turbulent parameters on the result. It should be noted that both equations are better suited to model suspended sediment transport, but the simulation still provides insight into the mutual differences between the pick-up equations.

The results of using the pick-up formula of Van Rijn [20] instead of Okayasu et al. [9] are depicted in Figure 5.17. The plot shows about the same morphology pattern as the simulation with the pick-up equation of Okayasu, of which the results are depicted in Figure 5.9. The amount of sedimentation and erosion are about equal. However, some differences can be distinguished between the outcomes of the two pick-up equations. In Figure 5.17, the origin of the bar is located further downstream from the tip of the expansion. Furthermore, the bar is shorter and seems to be lower than for the simulation were the pick-up equation of Okayasu was used.

TUDflow3d uses the local flow velocities in the first cell above the bed to determine the pick-up, both for the pick-up equation of Van Rijn and the one of Okayasu. This means that in this case, the model did not use a mean flow velocity to determine the pick-up with the equation of Van Rijn, as was stated in Subsection 2.3.1. Using a numerical model provides the possibility to use the local flow velocities in any pick-up equation. The only difference now between the pick-up calculated by the equation of Van Rijn and the Okayasu formula is the incorporation of the inertia and lift force on the sediment grains. The inertia force represents the resistance force of sediment grains against changing flow conditions. This force hampers the erosion of sediment from the bed. The lift force is an upwards force on the particles and increases the erosive force. It is expected that these forces cause the small differences observed between the simulations with the two different pick-up equations.

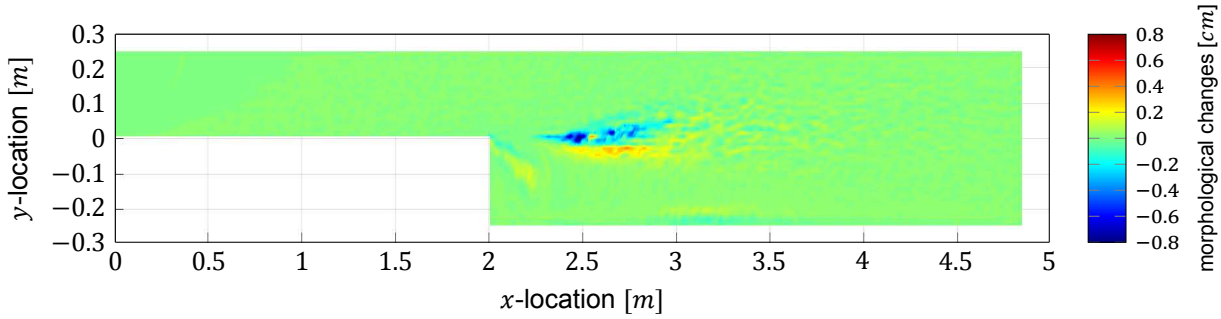

Figure 5.17: Simulated bed level changes for experiment 4 using the pick-up equation of Van Rijn [20].

5.6.2. Initial instabilities in the bed

It was expected that the lack of initial imperfections to the bed might hamper the onset and the development of bedforms. A simulation is set up that investigates the influence of these initial imperfections on the development of bedforms. The initial bed of the numerical simulation was given a randomly spread initial perturbation with the height of one grid cell as can be seen in Figure 5.18, while all other parameters are kept the same as for experiment 4, so making use of the pick-up equation of Okayasu et al. again. It is expected that this is enough to trigger the development of bedforms.

Figure 5.19 shows the morphological changes at the end of the simulation. It can be seen that the random perturbations have formed bedforms of about one centimetre in height and a length of about 20 centimetres, which is about the same as the bedforms of the laboratory experiments after a simulation of one hour. Strangely these bedforms did not spread out through the domain, as they did during the experiments. The bedforms were mostly formed during the first thirty minutes of the simulation, after that the location and the height of the bedforms barely changed. It is expected that the bedforms did not travel through the domain due to a combination of two reasons: firstly, the bedforms are apparently formed due to local instabilities, preventing the initiation of bedforms in the wide part of the flume; secondly, it is expected that the bedforms do not travel through the domain because the model does not resolve the flow patterns around the bedforms accurately enough.

The presence of bedforms apparently increases the turbulence intensities near the bed. Figure 5.20 shows the mean value of the turbulence intensities in the first cell above the bed. It can be seen that the turbulence intensities are up to 0.35 in the narrow part of the flume. It is thus expected the numerical model does simulate eddies around the bedforms, but it is possible that the simulation is not accurate enough to resolve all the relevant processes around the bedforms.

At the location of the mixing layer, it can be seen that the turbulence intensities have a maximum

value of about 0.35 instead of 0.4, which was the maximum value for the original simulation of experiment 4, of which the results are shown in Figure 5.4. The area in which these high turbulence intensities are found is larger than for the original simulation. The higher turbulence intensities at the location of the bedforms seems to have an influence on the downstream turbulence characteristics.

Finally, Figure 5.19 shows a wider bar and deeper erosion pit than the original simulation of experiment 4, caused by the bedforms and locally increased turbulence intensities. It is possible that the influence of using the pick-up equation of Van Rijn or the one of Okayasu et al. would be bigger for this case.

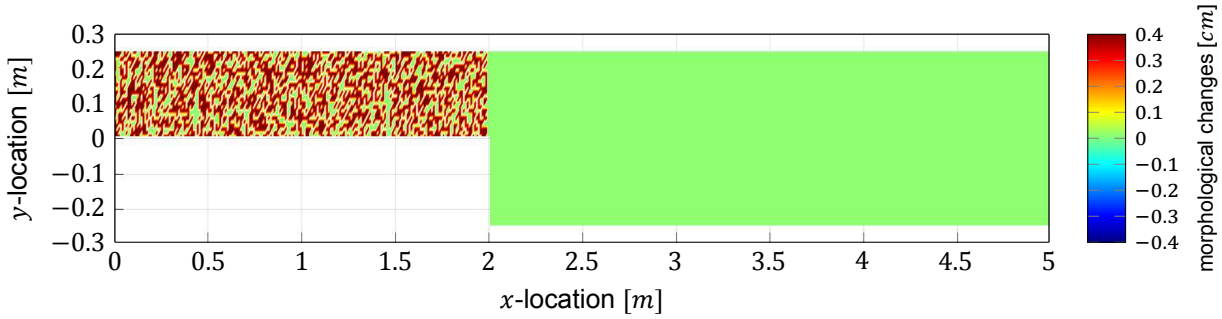

Figure 5.18: Initial layout bed for experiment 4 with a random perturbation of the bed with a height of one grid cell in the narrow part of the flume.

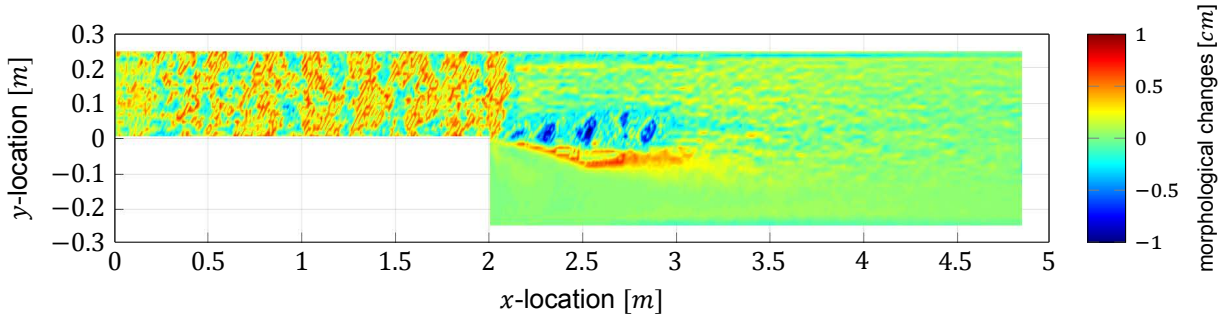

Figure 5.19: Simulated bed level changes for experiment 4 with an initial random perturbation of the bed with a height of one grid cell in the narrow part of the flume.

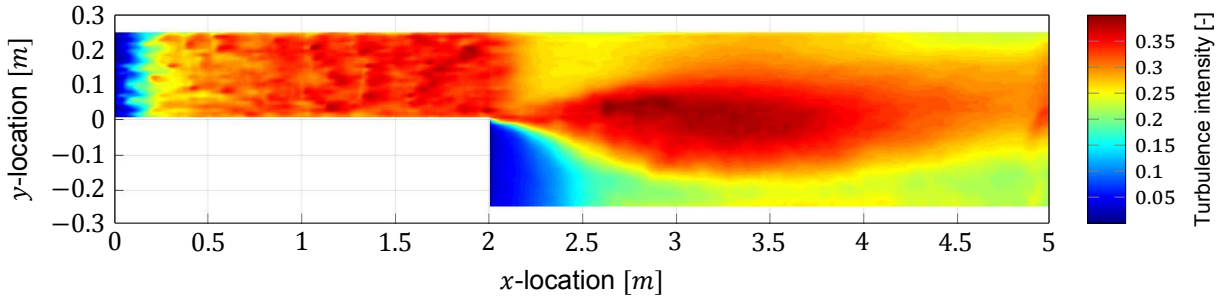

Figure 5.20: Time-averaged turbulence intensity throughout the flume in the first cell above the bed for experiment 4 with an initial random perturbation of the bed with a height of one grid cell in the narrow part of the flume.

5.6.3. Suspended sediment transport

In Chapter 2, it was found that the main transport mode during the last stage of a sand closure is suspended sediment transport. The laboratory experiments exhibited bedload transport. The numerical model makes it possible to simulate a situation that represents the sediment transport mode during a sand closure better. TUDflow3d was originally designed to simulate the suspended sediment transport due to the overflow of dredging vessels. It is interesting to investigate the influence of suspended sediment transport on the numerical results, since it was not possible to investigate this during the laboratory experiments. It was chosen to lower the Rouse number to a value of 2, which is a typical value for the final stage of a sand closure, by decreasing the grain diameter from 300 micrometres to 100 micrometres. Experiment 4 was repeated with this grain diameter while all other parameters remained unchanged.

In Subsection 5.5.2, it was already stated that the numerical results show some resemblance with the results found by Zuurveld [23], who investigated the damage pattern of gravel downstream of a shallow lateral expansion. An explanation for this similarity is the lack of beforms in both the experiments of Zuurveld and the numerical simulations. The results of the simulation are shown in Figure 5.21. The erosion and sedimentation pattern can be divided into four different areas. In the narrow part of the flume, the flow velocities are high and the turbulence intensities are low. In this area, a moderate amount of erosion is found. The second area is located at the fast flowing part of the mixing layer, with high flow velocities and high turbulence intensities. This area exhibits large amounts of erosion, supporting the theory that turbulence plays an important role for erosion. The third area is the part of the mixing layer where the flow velocities are low, but the turbulence intensities are high. This area does not show any erosion, only sedimentation due to the formation of the bar. The last area is located at the return current, which exhibits low flow velocities and turbulence intensities. A negligible amount erosion and sedimentation is observed in this area. This may resemble the actual morphology of a sand closure, because bedforms should play a less significant role for suspended sediment transport.

The turbulence intensities of the simulation are shown in Figure 5.22. The general pattern is similar to the results of the original experiment 4, of which the turbulence intensities were given in Figure 5.12. However, the results of the present simulation show an increased value for the turbulence intensities in the narrow part of the flume. The triangular shape at the beginning of the flume is caused by inflow effects, but does show the dependency between the turbulence intensity near the bed and the erosion of the bed.

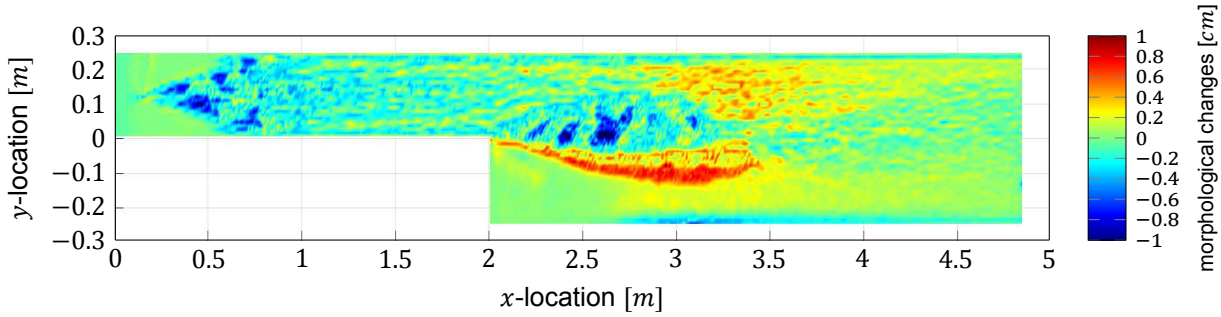

Figure 5.21: Simulated bed level changes for experiment 4 with a grain diameter of 100 micrometres.

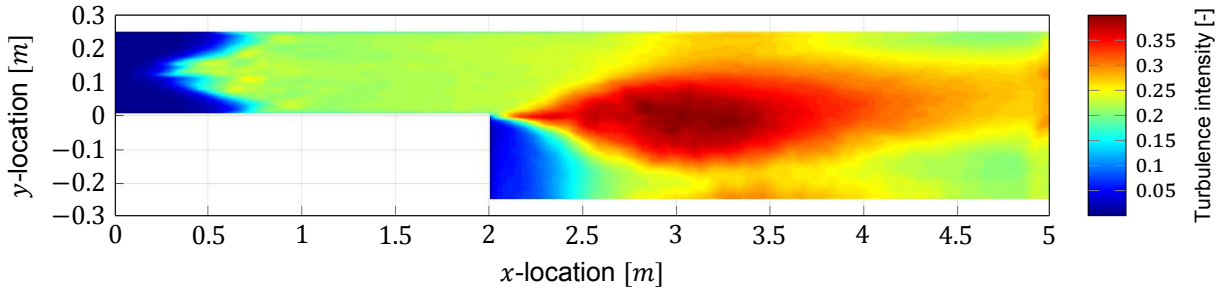

Figure 5.22: Turbulence intensity throughout the flume in the first cell above the bed for experiment 4 with a grain diameter of 100 micrometres.

5.7. Discussion

In Section 5.4, it was found that the secondary circulation, of which the occurrence was expected based on the laboratory experiments, is well captured by the numerical model. However, the reattachment length of the numerical simulations did not agree with the reattachment lengths measured during the laboratory experiments.

Generally, the numerical results are not completely comparable to the results of the laboratory experiments. The predicted morphology did not agree. It is expected that the main reason for this is that the main sediment transport mode is bedload transport instead of suspended load transport. The numerical model was selected to simulate the morphology under a mixing layer exhibiting suspended sediment transport. This is why a pick-up equation was implemented into the model. For the purpose of modelling the laboratory experiments, better results are expected when a bedload transport formula is implemented. However, for the purpose of modelling suspended sediment transport, it is still suspected that a pick-up formula is more suitable.

The presence of bedload transport and bedforms plays an important role on morphology. For the simulation of experiment 4, it was found that the bedforms did not arise, and that the lack of bedforms are associated with much lower erosion rates than those found during the laboratory experiments.

An attempt was made to trigger the onset of the formation of the bedforms by applying an initial perturbation to the bed. It was found that the initial perturbation was effective in the onset of the formation of bedforms, but the bedforms did not travel through the domain like they did for the laboratory experiments. It was found that the bedforms increased the turbulence intensities near the bed.

It is expected that the formula of Okayasu et al. [9] becomes more interesting to use when the degree of turbulence in the flow increases. This is because the relative importance of the inertia and lift forces on the grains increases for an increasing degree of turbulence, which are not taken into account in the pick-up equation of Van Rijn [20].

If bedforms can not be modelled by this three-dimensional LES model on this small scale, it is doubtful that any other currently available model is able to do so on a scale that makes it useful for large-scale simulations. It can be concluded that it is very important to incorporate the effect of the bedforms on the bed roughness, since they can not be solved by numerical models correctly. For the numerical simulation of any physical situations, it is important to know the presence and the dimensions of bedforms in order to parametrize them in the numerical simulations.

6

Discussion

This chapter reviews the found results on their quality and discusses the results with respect to the research question. The goal of this thesis is to make the first step towards a better prediction of the sand loss during a sand closure than the presently used models provide. After conducting an additional MSc thesis [5], the expectation was that most of the inaccuracy of the current predictions are caused by the modelling of the complicated morphology under the mixing layers of a sand closure. Therefore, it was chosen to focus this research on this area of the complete sand closure.

During the closure of the gap, the main transport mode changes from bedload transport to suspended load transport. During final stage of the closure, the main transport mode is suspended sediment transport. Most of the sand losses occur during this period, which is why this thesis mostly focusses on the final stage of a sand closure.

For this thesis, both laboratory experiments were conducted and a numerical model was set up. For practical reasons, the laboratory experiments were conducted with bedload as the main transport mode. The numerical model, on the other hand, was selected to improve the prediction of sand loss for the final stage of a sand closure. The model incorporated a pick-up equation and was thus more suitable to simulate the morphological changes for suspended sediment transport. An attempt was made to verify the model using the results from the laboratory experiments, but the model was not able to capture the morphological changes that occur for bedload transport. For bedload transport, bedforms have an important contribution to the erosion and sedimentation patterns that occur. It is possible to initiate the formation of bedforms in the numerical model by an initial perturbation; however, due to the small scale of the bedforms, it is not possible to completely solve them and their effect on the morphology with the numerical model.

To be able to verify TUDflow3d for the use of predicting the morphological changes that occur under mixing layers of a sand closure, it is advised to conduct laboratory experiments incorporating suspended load transport as the main transport mode. The layout of this experiment could be similar to the experiment of this thesis. To achieve suspended sediment transport, only the grain diameter of the sediment has to be smaller. To be able to reach the Rouse numbers that occurred for Maasvlakte 2 (MV2), sediment with a grain diameter between 70 and 170 micrometres should be used. Conducting measurements in a flow accommodating suspended sediment transport poses some new challenges. To conduct depth measurements with lasers, the water has to be clear. When more sediment is brought into suspension, the water becomes more turbid, which makes the lasers unusable. A possible measurement method to quantify erosion and sedimentation for an experiment with suspended sediment transport is by using Sound Navigation And Ranging (SONAR).

Since the experimental set-up is a schematization, not all features of an actual sand closure are taken into account. For example, the mixing layers of a sand closure originate from a dam, which often holds both a horizontal and a vertical contraction. Furthermore, the dams of a sand closure have an erodible slope, which is not incorporated in the set-up of the experiments. Although not all features are taken into account, a general idea of how the different features influence the flow patterns can be given.

In Section 5.4.3, it was found that the strength of the secondary circulation does not seem to be influenced by the width of the flume. Since it is expected that the secondary circulation keeps the streamwise bar in place and has no effect on the flow velocities and the degree of turbulence inside the mixing layer, it is expected that a widening of the flume does not cause significant changes to the morphology.

When a erodible slope is incorporated into the experimental set-up, it is expected that the origin of the mixing layer is located somewhere on the slope. Depending on the steepness of this slope, the erosion and sedimentation that was found during the present study could affect the sloping surface. When the slope is steep, it is expected that the slope is eroded because instabilities cause avalanching of the sand. When the slope is mild, it is expected that the streamwise bar originates at the surface of the slope. It is unsure where the bar forms, because the location of the origin of the mixing layer is not known for a sloping surface either. When the flow is additionally contracted, for instance, by building the head of a dam in the flume, it is possible that the location of the origin of the mixing layer changes even further. This would again lead to a different location of the erosion and sedimentation. Furthermore, it is expected that the sloping surface and the contraction change the turbulent properties of the flow, which in turn could have an effect on the pick-up of the sediment from the bed, changing the erosion and sedimentation pattern. Possibly, the anisotropy of the turbulent eddies increases for these alterations. It is suspected that the amount of sediment being picked-up increases under anisotropic turbulence.

During a sand closure, the flow is oscillatory due to the changing tide, propagating in and out of the basin. During the experiments, the flow velocity was constant. During the final stage of a sand closure, it is attempted to close the gap in the hours around slack water. This implies that the flow could come from both directions through the gap.

Finally, a sand-water-mixture is added to the gap at the heads of the dam during a sand closure. This means that more sand is in suspension than just the sand that erodes from the bed. When the sediment concentrations in the flow are high, this could lead to hindered settling and hindered erosion of the bed, which influences the morphology during a sand closure.

When the experiments were numerically simulated using sediment with a grain diameter of 100 micrometres instead of the 330 micrometres that was used during the laboratory experiments, the main transport mode became suspended sediment transport instead of bedload transport. An erosion and sedimentation pattern was found that looks similar to the damage pattern that was found by Zuurveld [23] during his experiments towards determining the damage pattern of gravel under a mixing layer. It can not be concluded that the erosion and sedimentation predicted by the numerical model is accurate, for that a dataset should be available on the morphology of sand under a mixing layer during suspended sediment transport. However, it is expected that the pattern will be similar to the results found with the numerical model, since both the experiments of Zuurveld, and the erosion of sand during suspended sediment transport depict a situation where bedforms do not play a role in the found morphology.

During a sand closure, the flow velocities through the gap are caused by a water level difference between the sea and the basin on either side of the gap. Furthermore, the contraction of the flow causes an additional water level drop inside the gap. This means that the rigid lid incorporated in TUDflow3d makes the model currently unusable for a sand closure. However, when a free surface is implemented in the model, it would be theoretically possible to model a sand closure using TUDflow3d. It should be noted that the computational effort of a three-dimensional model will be much larger than the presently used two-dimensional model FINEL2D. To describe the pick-up of sediment accurately, a certain resolution of the grid over the depth is necessary. It was shown in Section 2.3 that the suspended sediment becomes more uniformly distributed over depth when the Rouse number decreases. For the Rouse numbers that are encountered during a sand closure, the concentration near the bottom is still significantly higher than at the surface, and the grid resolution of the three-dimensional model should be chosen fine enough in order to capture the sediment profile well. This would result in a relatively small grid size over depth, and since the aspect ratio between the different dimensions can not be too large, the grid size of the x- and y-direction has to be small too. This makes the model computational costly.

To decrease the computational effort of the calculations, it is possible to conduct flow simulations with a three-dimensional model, and use the turbulence values of this model to improve the predictions of a two-dimensional morphodynamic model. However, it should be noted that the morphological

changes will in turn influence the flow patterns and turbulence properties, so this method is still a simplification. It would be interesting to simulate the erosion and sedimentation patterns of a sand closure using a three-dimensional morphodynamic model. It is expected that when the computational capacities keep growing, this is definitely possible in the future.

For both the laboratory experiments and the numerical simulations, a streamwise bar was formed that originated at the tip of the expansion. During a sand closure, the tip of the expansion is in fact one of the heads of the dam. These heads are constantly changing in location while the gap is closing. When a streamwise bar also develops during an actual sand closure, it could be interesting to use this as an additional source of sand to aid the closure. This can be done by picking-up the sand with a dredging vessel and re-feeding it into the gap. This way, the dredging vessels do not have to sail back to the borrow pit every time, but can sometimes pick-up sediment from this nearby location in order to speed up the closure progress. However, it should be investigated how sensitive this bar is to the geometry of a sand closure, and if it is not an artefact of the layout of the experiments. Furthermore, during a sand closure, the mixing layers originate from the heads of the dams, which are constantly being build up closer together over the course of the closure. This means that, if the erosion-sedimentation pattern that was found with the numerical simulations is correct, the bar only fills up the erosion pit that was formed next to it when the head of the dam shifts. It is thus uncertain if the bar forms and leaves additional sand to aid the sand closure. Finally, if the bar forms and leaves a significant amount of sediment to use during the closure, it should be investigated how to use this sand most efficiently. It is expected that the sediment can be used best during the last hours of a sand closure, when the closure of the gap is most critical.

7

Conclusions and recommendations

In this thesis, the morphological development under the mixing layers of a sand closure was investigated. The research focusses on the following main- and sub-questions:

How are the morphological processes under the mixing layer of a sand closure described and how can these be modelled numerically?

The following sub-questions were formulated:

1. What are the important characteristics of the mixing layers that occur during sand closures?
2. What is the morphological development under a mixing layer in a laboratory experiment that resembles a mixing layer of a sand closure?
3. Is TUDflow3d a suitable numerical model to simulate the morphology for the mixing layers that occur during a sand closure?

This chapter aims to answer these questions based on the findings of this thesis. After this, some recommendations are given in Section 7.2.

7.1. Conclusions

To answer the main question of this study, this section answers the three sub-questions that were formulated:

1. *What are the important characteristics of the mixing layers that occur during sand closures?*
   - The mixing layers of sand closures are caused by the sudden expansion downstream of the closure gap. The flow is contracted into the gap, and the mixing layers originate at the sloping surface of the heads of the dam.
   - The mixing layers of a sand closure mostly resemble the theoretical case of a lateral expansion. For an experimental set-up, this is the most appropriate layout.

2. *What is the morphological development under a mixing layer in a laboratory experiment that resembles a mixing layer of a sand closure?*
   - During a laboratory experiment that involves a lateral expansion with bedload as the main transport mode, bedforms are formed which are higher in the narrow part in the flume than in the wide part, a streamwise bar originates from the tip of the expansion and under the return current little bed level changes occur.
   - When the Shields parameter is lower than the critical value of the Shields parameter throughout the entire flume, no bed level changes occur.
   - For high flow velocities, in this case higher than 0.5 metres per second in the narrow part of the flume, the streamwise bar originating from the tip of the expansion shifts towards the sidewall of the flume where the return current is located.

- During a laboratory experiment with bedload as the main transport mode, bedforms have a large influence on the final erosion and sedimentation pattern.

3. *Is TUDflow3d a suitable numerical model to simulate the morphology for the mixing layers that occur during a sand closure?*
- When the main transport mode is bedload transport, TUDflow3d is not a suitable model to describe the morphological changes for a lateral expansion, because it can not capture the bedforms well.
- It is possible to initiate bedforms by applying an initial perturbation to the bed, but they do not travel through the domain. It is not possible to model bedforms accurately with a set-up of the numerical model used during this study.
- For the numerical simulation of suspended load transport, four areas are distinguished: a main current with high flow velocities and low turbulence intensities with a moderate amount of erosion; an area in the mixing layer with high flow velocities and high turbulence intensities with large amounts of erosion; an area inside the mixing layer with low flow velocities and high turbulence intensities where no erosion occurs but only sedimentation due to the formation of the streamwise bar; and an area in the return current with low flow velocities and low turbulence intensities where a negligible amount erosion and sedimentation is observed.
- Even though the main transport mode during the last stage of a sand closure is suspended sediment transport, the rigid lid prevents the use of TUDflow3d for a sand closure at this point.

7.2. Recommendations

Based on the insights gained during this thesis, the following recommendations are made for further research on the experimental and numerical investigation of sand closures and associated topics:

- Before new laboratory experiments are conducted, it is advised to first conduct a numerical study to assess the influence of a slope and a contraction in the geometry on the flow patterns. This could limit the amount of experiments that have to be conducted during experimental research.

- To validate TUDflow3d for the set-up that was investigated in the present thesis, a laboratory experiment that has suspended sediment transport as the main transport mode should be conducted. Care should be taken to use the proper measuring equipment, it is expected that SONAR is an appropriate method to measure the bed level changes.

- The grid size used for the numerical simulations of the present study was very small. In order to apply the model on a large scale problem like a sand closure, the first step is to increase the grid size and to investigate the accuracy of the results for suspended sediment transport. It is expected that the accuracy of the sediment pick-up prediction will be the limiting factor on the maximum grid size.

- It is advised to look into the possibility to use the sand deposited as a streamwise bar during a sand closure as an additional borrow pit to aid the closure process. Firstly, it should be investigated how sensitive the development of the bar is to the geometry with a numerical model; secondly, it should be investigated if the bar develops when the origin of the mixing layer is moving in time; and finally, it should be studied how to use the sand as efficiently as possible for the final stage of a sand closure.

- For modelling sediment transport during the first stage of a sand closure, it is advised to use a two-dimensional model that incorporates a bedload transport formula to model the sediment transport, because turbulence does not play a significant role yet during this stage of the closure. It is important to use a parametrization of the bedforms that occur during bedload transport. This parametrization should incorporate both the increased bed roughness due to the dimensions of the bedforms and the additional sediment transport due to small scale flow patterns around the bedforms.

- For modelling sediment transport during the final stage of a sand closure, which is the most critical phase due to the high flow velocities and the time restriction, it is advised to use a three-dimensional model with a pick-up equation that takes the influence of turbulence on the grains into account, such as the pick-up formula of Okayasu et al. [9]. A three-dimensional model is advised, because for this stage of the closure, the turbulence inside the mixing layers plays a significant role on the amount of erosion. This model can not make use of a rigid lid, and the simulation should have a sufficiently fine grid for an accurate prediction of the sediment pick-up.

Bibliography

[1] L. de Wit. *3D CFD modelling of overflow dredging plumes*. PhD thesis, Delft University of Technology, 2015.

[2] H.A. Einstein and E.A. El-Samni. Hydrodynamic forces on a rough wall. *Reviews of modern physics*, 21(3):520–524, 1949.

[3] J. Fredsøe and R. Deigaard. *Mechanics of coastal sediment transport*. World Scientific, Singapore, 1992.

[4] L.E. Frostick, S.J. McLelland, and Mercer T.G. *Users Guide to Physical Modelling and Experimentation: Experience of the HYDRALAB Network*. CRC Press/Balkema, Leiden, The Netherlands, 2011.

[5] N. Huppes. *Erosion during a sand closure - A literature study*. Additional MSc thesis, Delft University of Technology, 2016.

[6] M.N. Le Couturier, N.T. Grochowski, A. Heathershaw, E. Oikonomou, and M.B. Collins. Turbulent and macro-turbulent structures developed in the benthic boundary layer downstream of topographic features. *Estuarine, Coastal and Shelf Science*, 50:817–833, 2000.

[7] E. Michaelides. *Particles, bubbles and drops: their motion, heat and mass transfer.* World Scientific, Singapore, 2006.

[8] The national commitee for fluid mechanics films. Turbulence, 1972. URL `https://www.youtube.com/watch?v=1_oyqLOqwnI&t=10s`.

[9] A. Okayasu, K. Fujii, and M. Isobe. Effect of external turbulence on sediment pickup rate. In *Proceedings of Coastal engineering conference*, 2010.

[10] N.D. Pope, J. Widdows, and M.D. Brinsley. Estimation of bed shear stress using the turbulent kinetic energy approach - A comparison of annular flume and field data. *Elsevier*, 26:959–970, 2006.

[11] Quarzsande. Sieve curve Dorsilit Nr. 9, 2017. URL `http://www.quarzsande.at/produkte/kristallquarzsand_feuergetrocknet.php`.

[12] H. Rouse. Modern conceptions of the mechanics of fluid turbulence. *Transactions of the American Society of Civil Engineers*, 102:463–541, 1937.

[13] P. Struik, R. 't Hart, R.E.A.M. Boeters, H.P.J. Mulder, H. Postma, F. van Roode, and H. van Rossum. *CUR Report 157 - Sand closures*. A.A. Balkema, Gouda, 1993.

[14] H. Talstra. *Large-scale turbulence structures in shallow separating flows*. PhD thesis, Delft University of Technology, 2011.

[15] H. Tennekes and J.L. Lumley. *A first course in turbulence*. The Massachusetts Institute of Technology, Cambridge, 1972.

[16] C.E.L. Thompson, C.L. Amos, T.E.R. Jones, and J. Chaplin. The manifestation of fluid-transmitted bed shear stress in a smooth annular flume - a comparison of methods. *Journal of Coastal Research*, 19(4):1094–1103, 2003.

[17] J. Tukker. *Turbulence structures in shallow free-surface mixing layers*. PhD thesis, Delft University of Technology, 1997.

[18] B. van Prooijen. *Shallow mixing layers*. PhD thesis, Delft University of Technology, 2004.

[19] C. van Rhee. Sediment Entrainment at High Flow Velocity. *Journal of Hydraulic Engineering*, 136 (9):572–582, 2010.

[20] L.C. van Rijn. Sediment pick-up functions. *Journal of Hydraulic Engineering*, 110(10):1494–1502, 1984.

[21] H. van Rossum, P. Struik, H. Lodder, R.E.A.M. Boeters, R. 't Hart, and H.P.J Mulder. Zandsluitingen - State of the art, nota BCZ-88-20.002, 1988.

[22] X. Zhang, W. Yang, and J. Xia. Bed shear stress in non-uniform flow. *Environmental Fluid Mechanics*, 16(4):777–792, 2016.

[23] J. Zuurveld. *Hoofdstroming contra menglaag - De invloed van een menglaag op het begin van bewegen van bodemmateriaal*. MSc thesis, Delft University of Technology, 1998.

A

Results Acoustic Doppler Velocimeter

This appendix treats the problems that occurred during the measurements with the Vectrino Profiler. The results are presented to aid future users in their choice of appropriate measuring equipment. The encountered problem was that the measured profiles showed a significant amount of noise. The manufacturer, Nortek, was contacted and some tests were conducted of which the results are given in this appendix.

Figure A.2 shows the result of a measurement at location 1, depicted in Figure A.1, in the laboratory flume for a discharge of 23.3 litres per second. The Acoustic Doppler Velocimeter (ADV) measured the flow velocities in three directions in 15 points over a span of three centimetres. Each dot in Figure A.2 represents a measurement point of the ADV. For the plot depicted in Figure A.2, four separate measurements were conducted. The ADV was placed at four different z-locations and measured the flow velocities over a period of one minute. The z-location of the measurement points is given on the vertical axis, it represents the height of the measurement point above the bed. The measured velocity profile as depicted in Figure A.2 is more or less logarithmic, apart from a large drop in the average flow velocity at about eight centimetres water depth. When the measurement was repeated, a similar pattern was found. The same measurement was also conducted in the narrow part of the flume, and a similar drop in the average flow velocity was found at eight centimetres water depth.

Figure A.3 shows the velocity signal of one measuring point of the ADV, in this case located at 8.8 centimetres above the bed. The blue line depicts the instantaneous flow velocities, and the red line represents the mean flow velocity averaged over the entire measuring period. It can be seen that the velocity signal shows some fluctuations around a mean flow velocity due to turbulent eddies in the flow, but this is normal for a flow velocity signal. Figure A.4 depicts the velocity signal in the peak of Figure A.2, at 7.8 centimetres above the bed. It can be seen that the average flow velocities in this signal are much lower, and that there are much more fluctuations around the mean flow velocity. It should be noted that the magnitude of the fluctuations does not increase, but the amount of fluctuations over time does.

When the discharge of the pump was decreased, the distortions in the velocity signal increased. Furthermore, they were not only occurring at eight centimetres water depth, there were distortions visible throughout the entire profile.

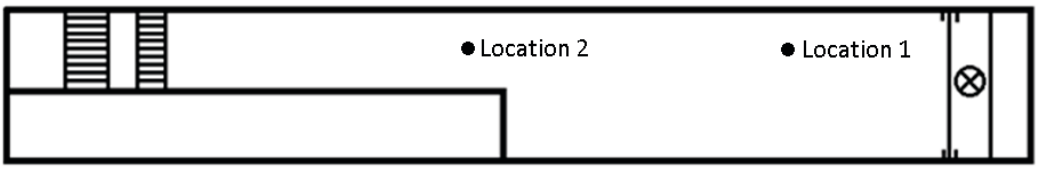

Figure A.1: Locations of the ADV in the flume used during the ADV measurements.

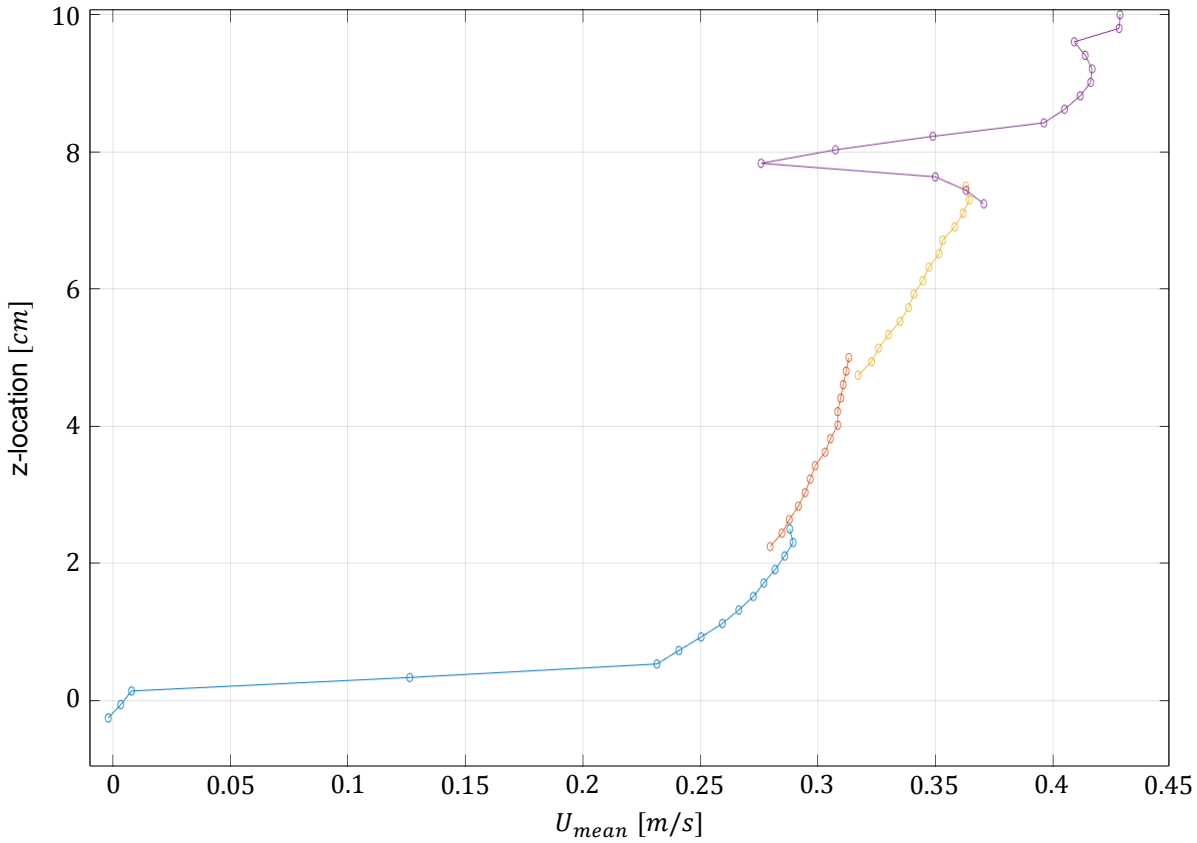

Figure A.2: Plot of mean velocity measured by the ADV over a period of 1 minute for a discharge of 23.3 litres per second.

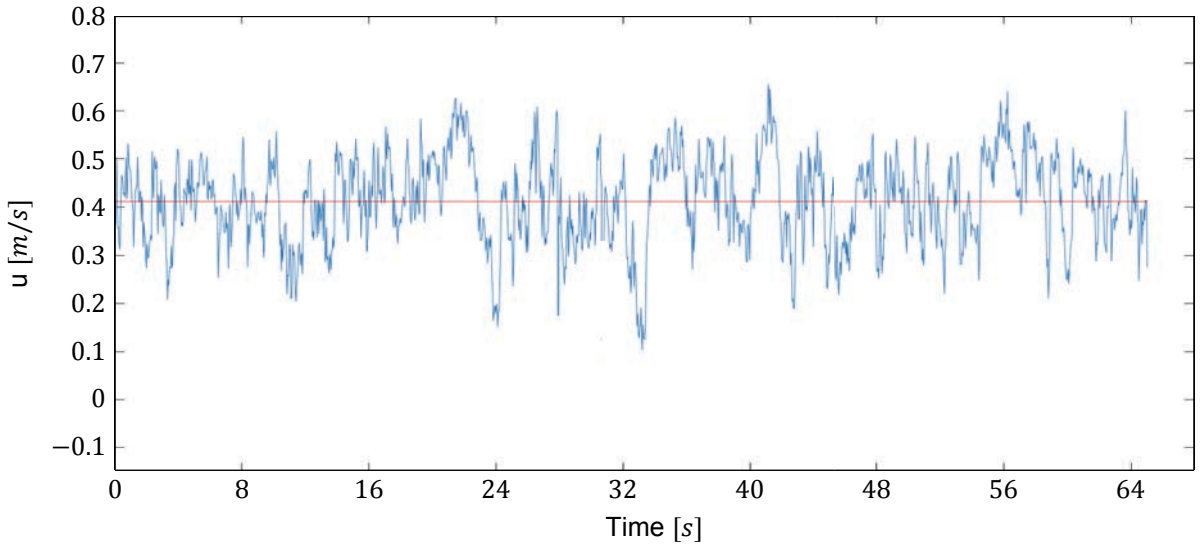

Figure A.3: Plot of mean velocity measured by the ADV over a period of 5 minutes for a discharge of 23.3 litres per second.

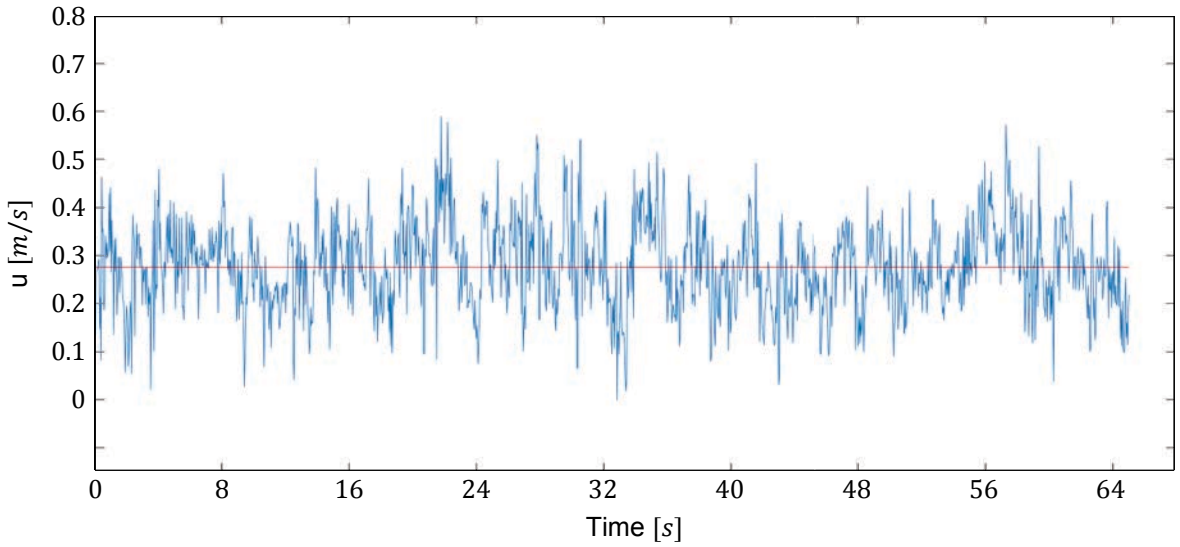

Figure A.4: Plot of mean velocity measured by the ADV over a period of 5 minutes for a discharge of 23.3 litres per second.

The measurement was repeated for different settings of the ADV. The power level was altered between high and low, the velocity range was adapted, and the transmit pulse size was changed. None of these settings resulted in an undisturbed velocity profile.

After this an attempt was made to alter the acoustic properties of the bed. It is expected that, because the ADV uses acoustic signals for its measurements, the acoustic properties of the surroundings are important. Figure A.6 shows the set-up that was used to assess the influence of the acoustic properties of the surroundings. A wooden board wrapped in a cloth was used to dampen the signal of the ADV, and avoid reflection of the signal back to the receiver of the ADV. Figure A.7 shows the mean flow velocity that was measured for this set-up at location 2. The discharge of the pump was set at 6.6 litres per second, which resulted a scattered measurement above the original bed, of which the result is shown in Figure A.5. It should be noted that the wooden board had a height of about two centimetres and the cloth may have lifted up during the measurement, so the actual bed was located at a depth of about 2.5 centimetres. It can be seen from the plot that an undisturbed logarithmic velocity profile develops.

This test shows that the acoustic properties of the surrounding play a significant role during the measurement with an ADV. Another test was conducted with a layer of sediment on the bottom of the flume. Unfortunately, the signal of this test was scattered, making the ADV unusable for the laboratory experiments that were conducted for this thesis.

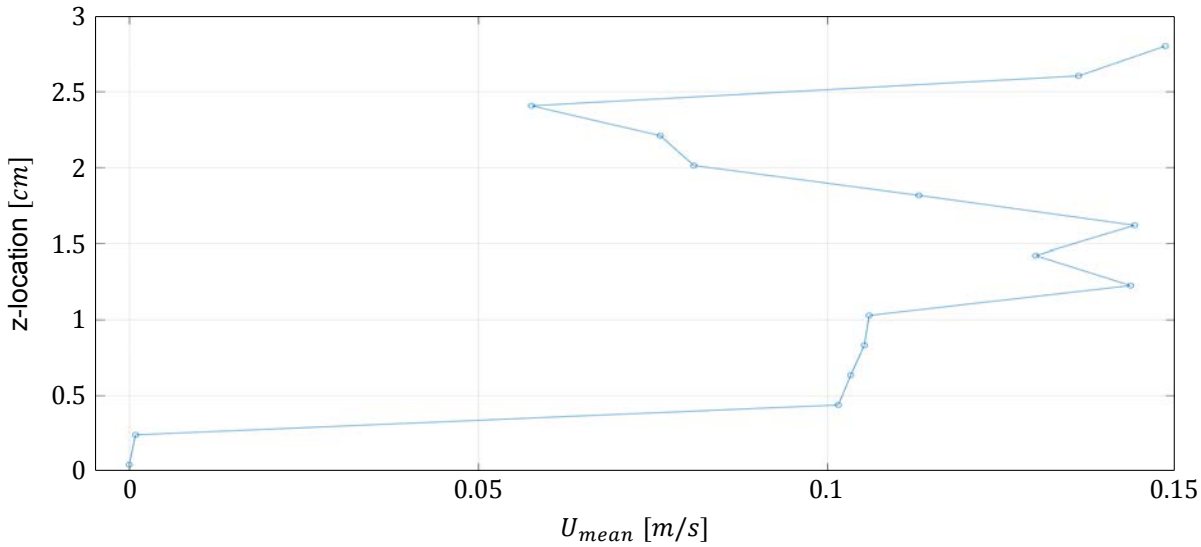

Figure A.5: Plot of mean velocity measured by the ADV over a period of 1 minute for a discharge of 6.6 litres per second.

Figure A.6: Photograph of the set-up of the ADV and wooden board with cloth wrapped around it on the bottom of the flume.

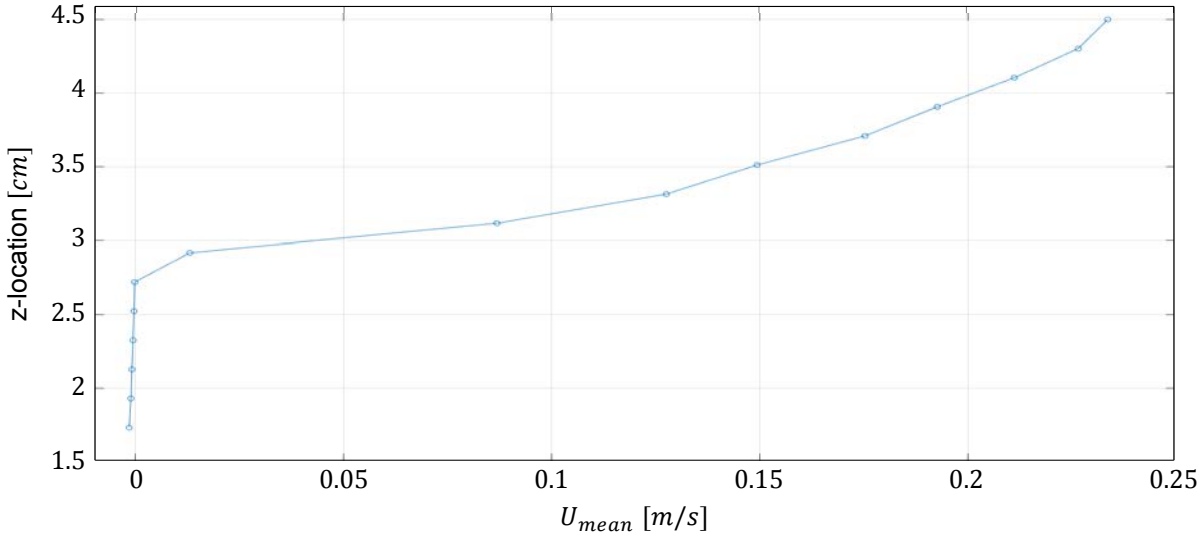

Figure A.7: Plot of mean velocity measured by the ADV over a period of 1 minute for a discharge of 6.6 litres per second with a wooden board with a cloth wrapped around it on the bottom of the flume.

B

Experimental results

This appendix gives the results of the laboratory experiments. In each section, the overview of the bed at the end of the experiment is given with one or more photographs. After these photographs, the laser transects of respectively laser 1, 2, and 3 are depicted in separate plots. Table B.1 provides an overview of the executed experiments.

Table B.1: Overview of the executed laboratory experiments.

$Nr.$	Q	U_1	U_2
	[l/s]	[m/s]	[m/s]
1	8	0.2	0.1
2	10	0.25	0.13
3	12	0.3	0.15
4	14	0.35	0.18
5	16	0.4	0.2
6	18	0.45	0.23
7	20	0.5	0.25
8	21.4	0.54	0.27

Experiment 1

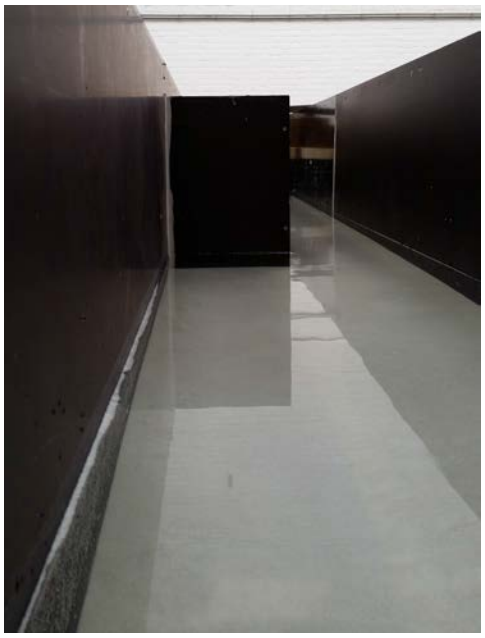

(a) Photograph of the final erosion and sedimentation pattern for experiment 1. The photograph is made at the end of the flume, facing in the direction of the expansion.

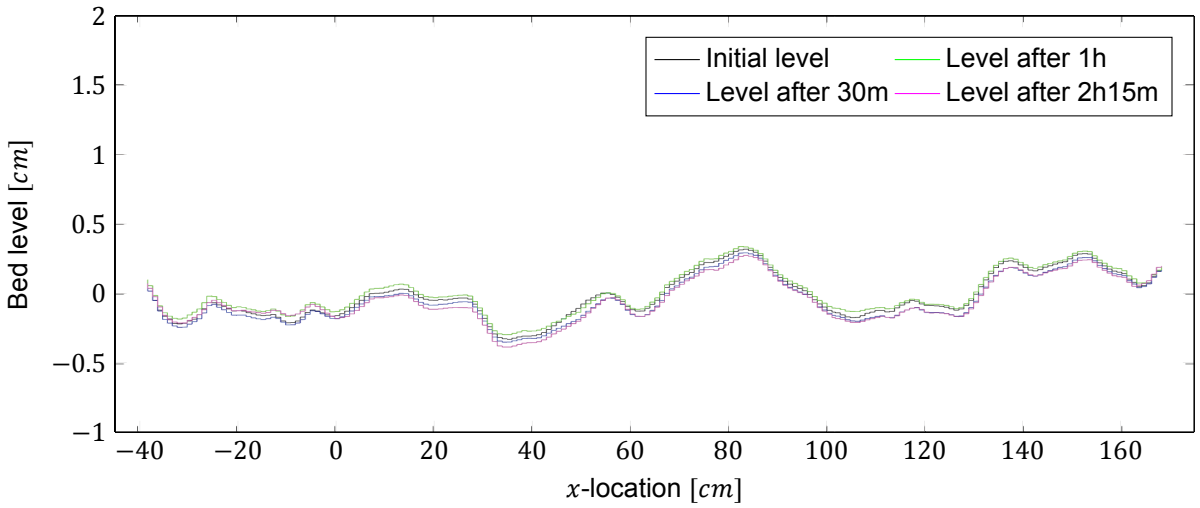

(b) Bed level measured by laser 1 at different times after starting the experiment.

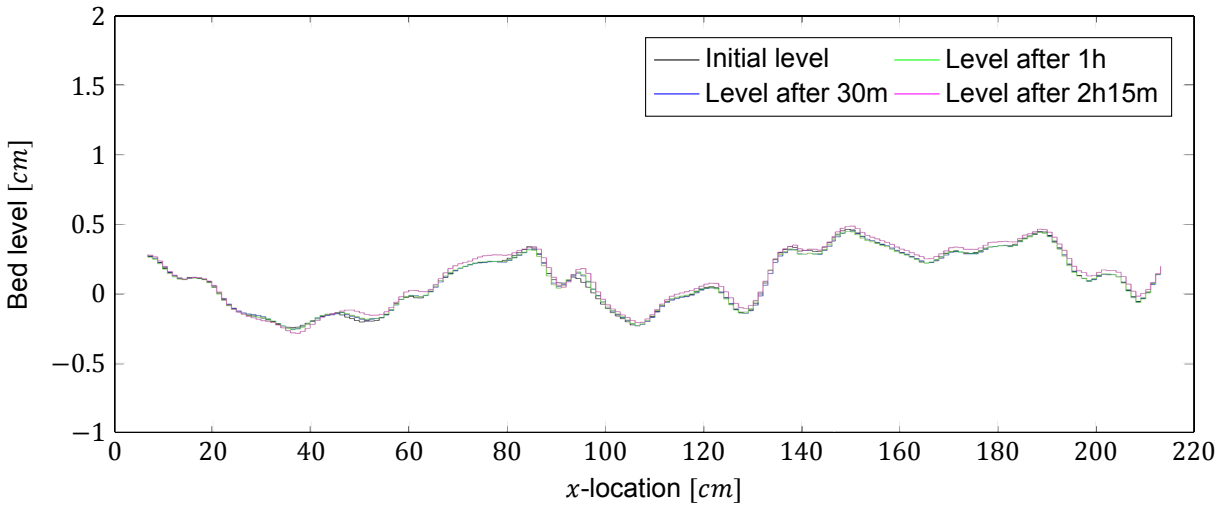

(c) Bed level measured by laser 2 at different times after starting the experiment.

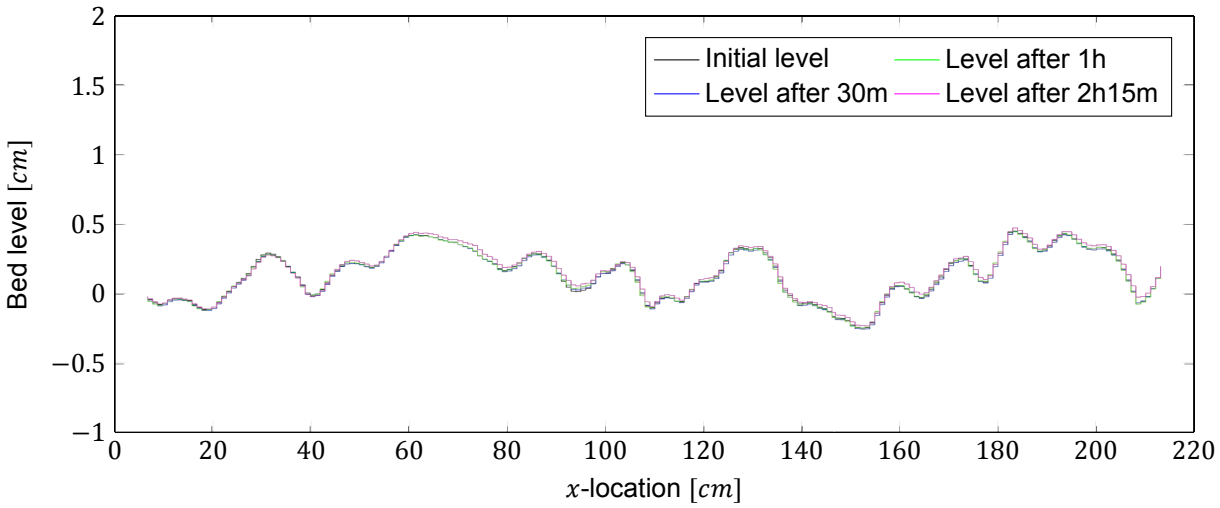

(d) Bed level measured by laser 3 at different times after starting the experiment.

Figure B.1: Bed level changes for experiment 1, measured by the different lasers. Laser 1 is located at y=38.7cm Laser 2 is located at y=27.4cm Laser 3 is located at y=8.4cm

Experiment 2

(a) Photograph of the final erosion and sedimentation pattern for experiment 2. The photograph is made at the just after the expansion, showing the bed until about one metre downstream of the expansion.

(b) Photograph of the final erosion and sedimentation pattern for experiment 2. The photograph is made at the end of the flume, showing the bed between 0.5 and 1.5 metres downstream of the expansion.

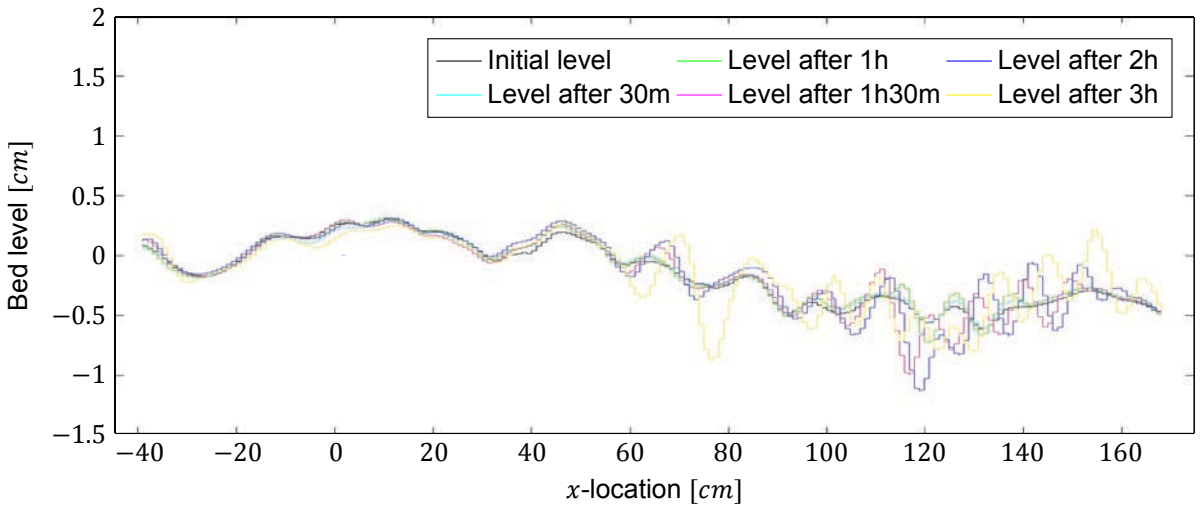

(c) Bed level measured by laser 1 at different times after starting the experiment.

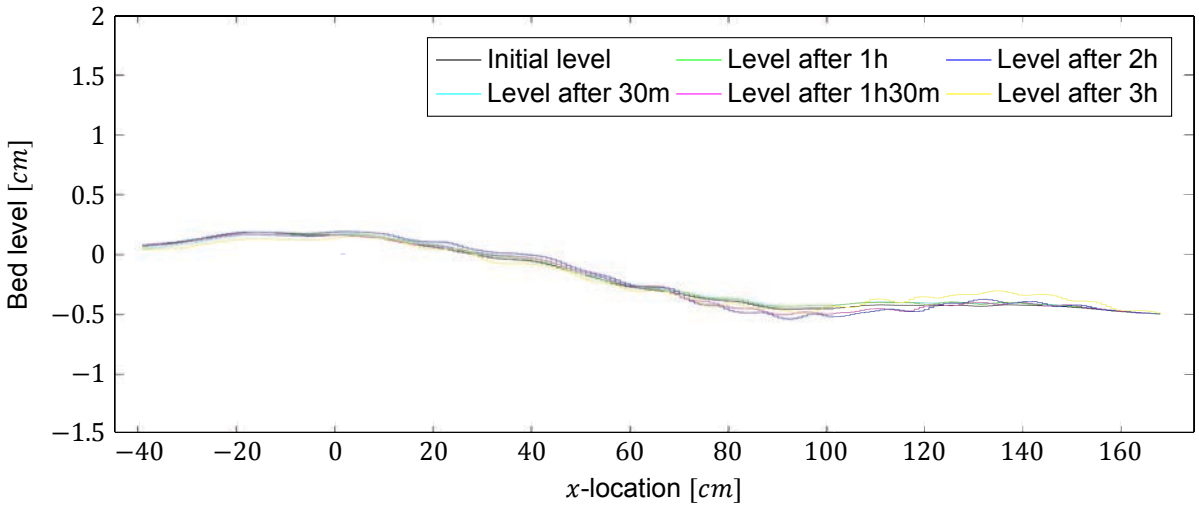

(d) Smoothed bed level measured by laser 1 at different times after starting the experiment. Results are smoothened to even out most of the bedforms.

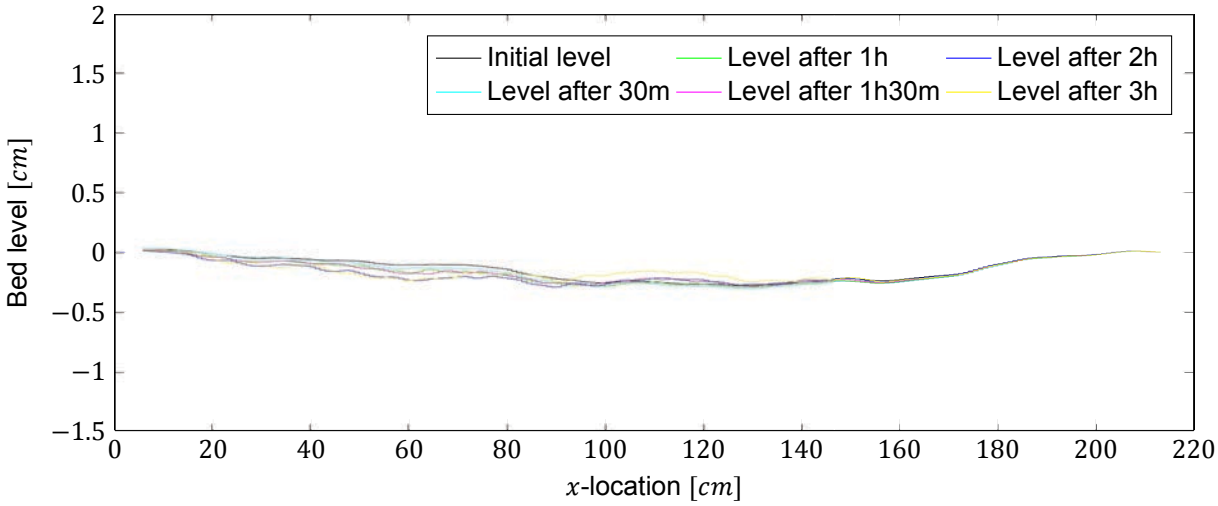

(e) Smoothed bed level measured by laser 2 at different times after starting the experiment.

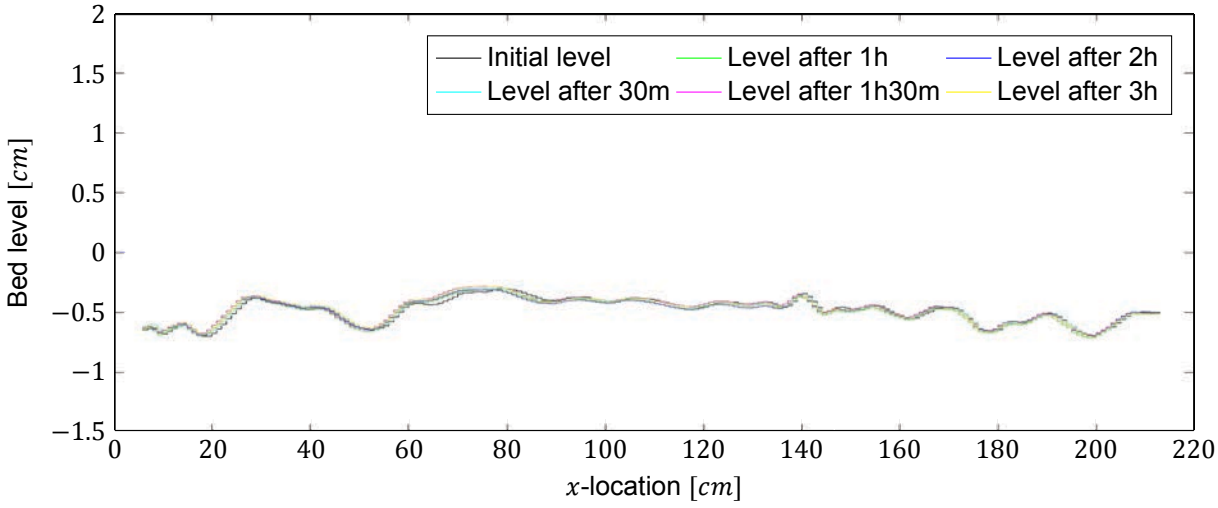

(f) Bed level measured by laser 3 at different times after starting the experiment.

Figure B.2: Bed level for experiment 2, measured by the different lasers. Laser 1 is located at y=38.7cm Laser 2 is located at y=27.4cm Laser 3 is located at y=8.4cm

Experiment 3

(a) Photograph of the final erosion and sedimentation pattern for experiment 3. The photograph is made at the just after the expansion, showing the bed until about one metre downstream of the expansion.

(b) Photograph of the final erosion and sedimentation pattern for experiment 3. The photograph is made at the end of the flume, showing the bed between 0.5 and 1.5 metres downstream of the expansion.

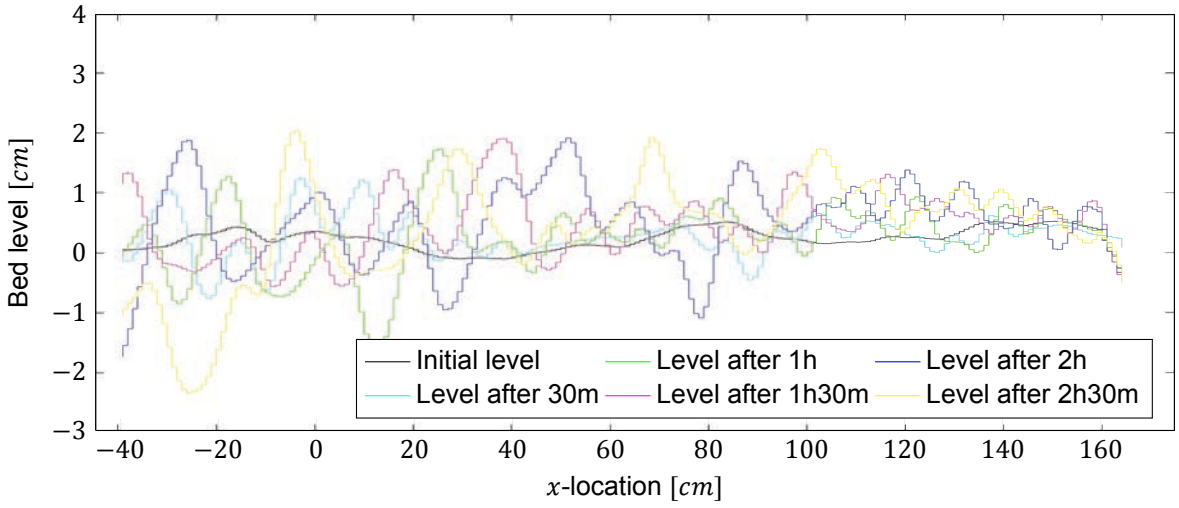

(c) Bed level measured by laser 1 at different times after starting the experiment.

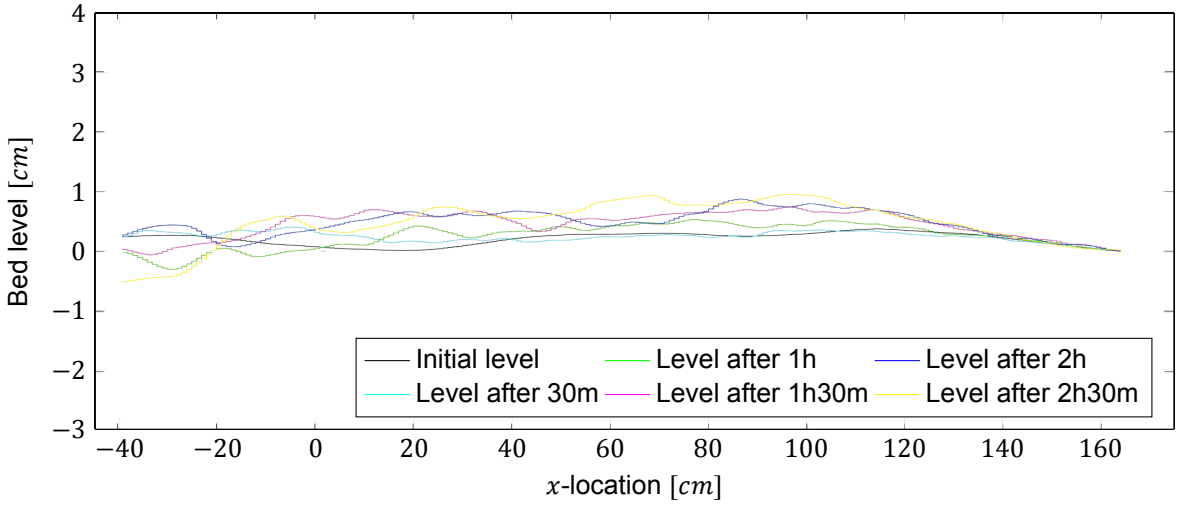

(d) Smoothed bed level measured by laser 1 at different times after starting the experiment. Results are smoothened to even out most of the bedforms.

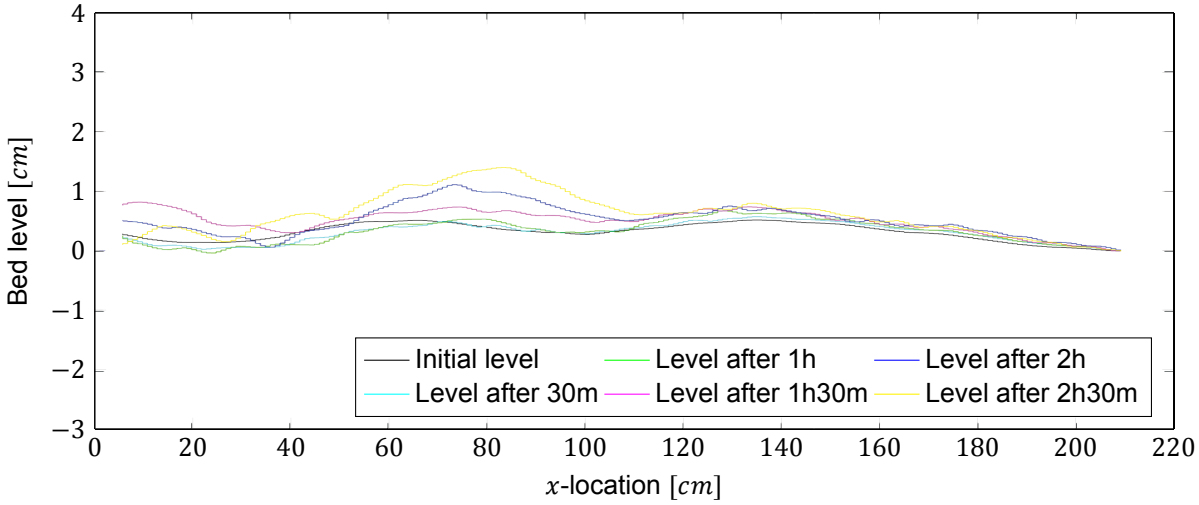

(e) Bed level measured by laser 2 at different times after starting the experiment.

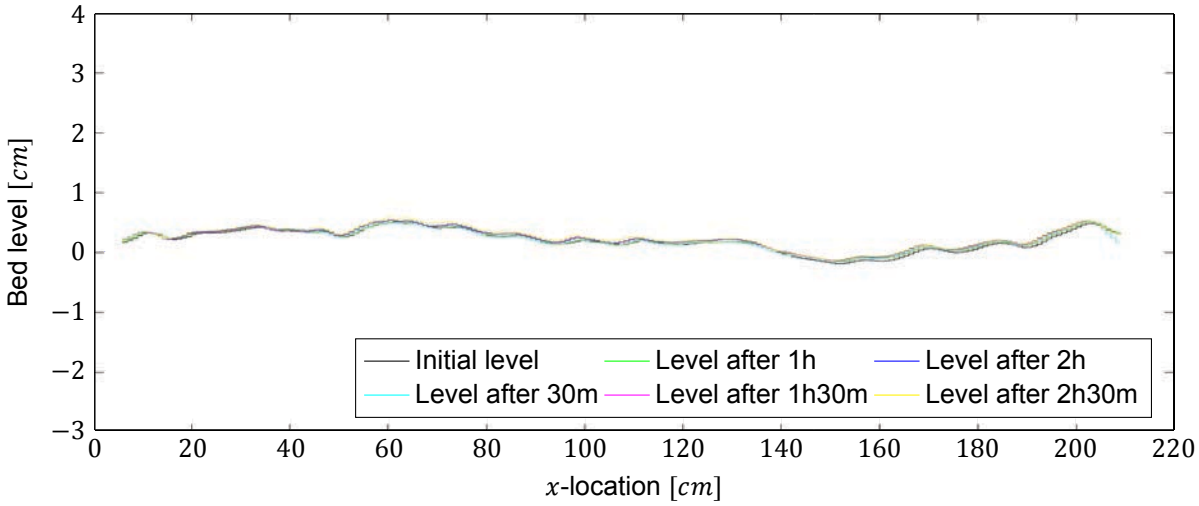

(f) Bed level measured by laser 3 at different times after starting the experiment.

Figure B.3: Bed level for experiment 3, measured by the different lasers. Laser 1 is located at y=38.7cm Laser 2 is located at y=27.4cm Laser 3 is located at y=8.4cm

Experiment 4

(a) Photograph of the final erosion and sedimentation pattern for experiment 4. The photograph is made at the just after the expansion, showing the bed until about 1.5 metre downstream of the expansion.

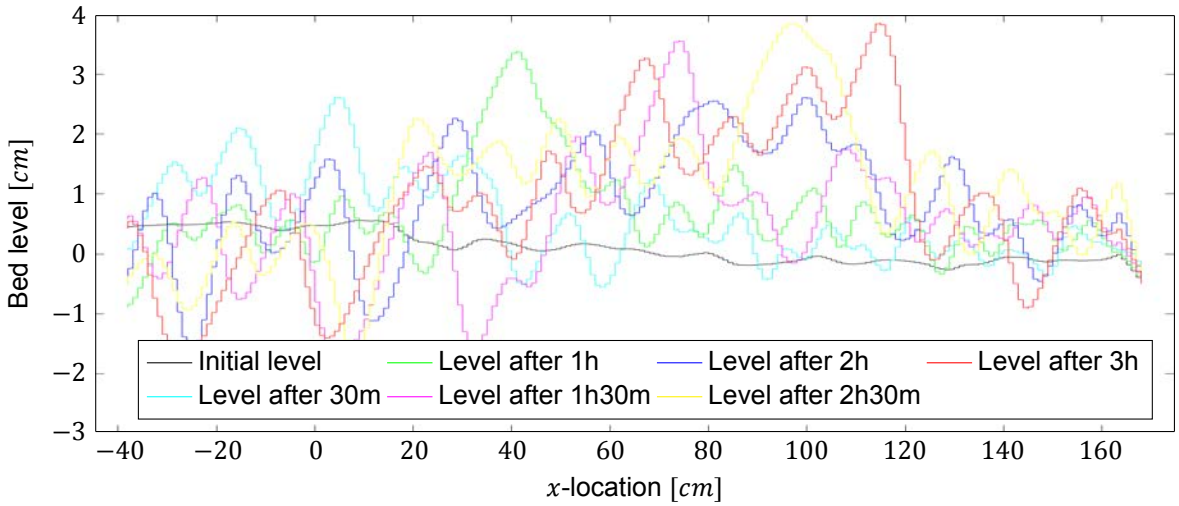

(b) Bed level measured by laser 1 at different times after starting the experiment.

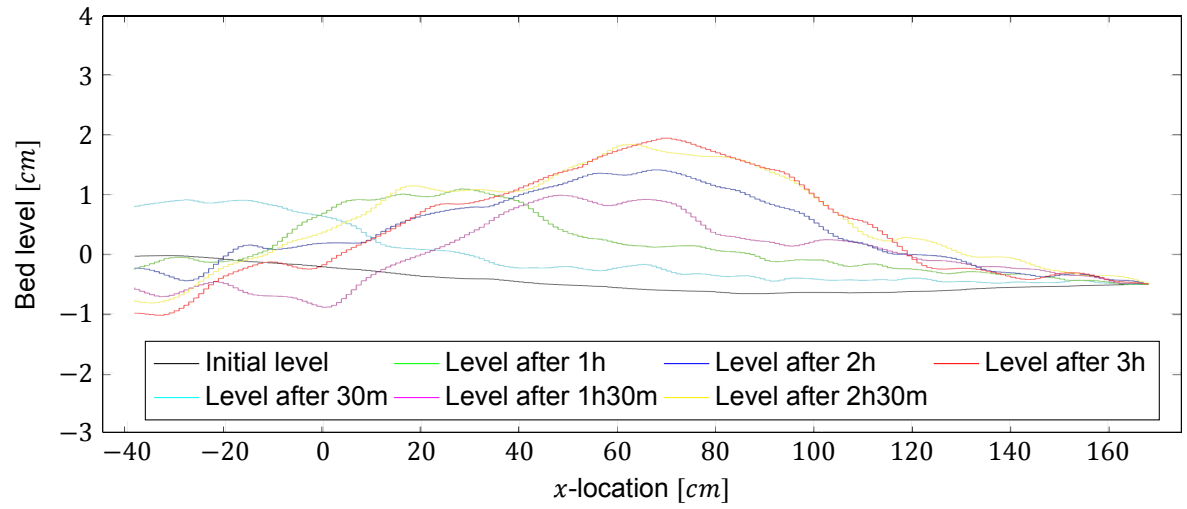

(c) Smoothed bed level measured by laser 1 at different times after starting the experiment. Results are smoothened to even out most of the bedforms.

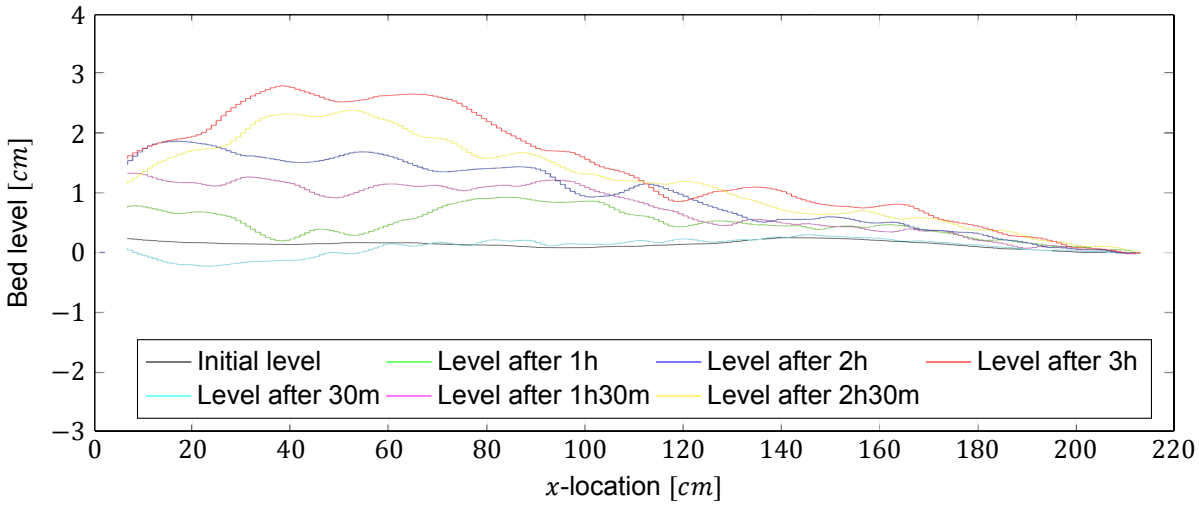

(d) Bed level measured by laser 2 at different times after starting the experiment.

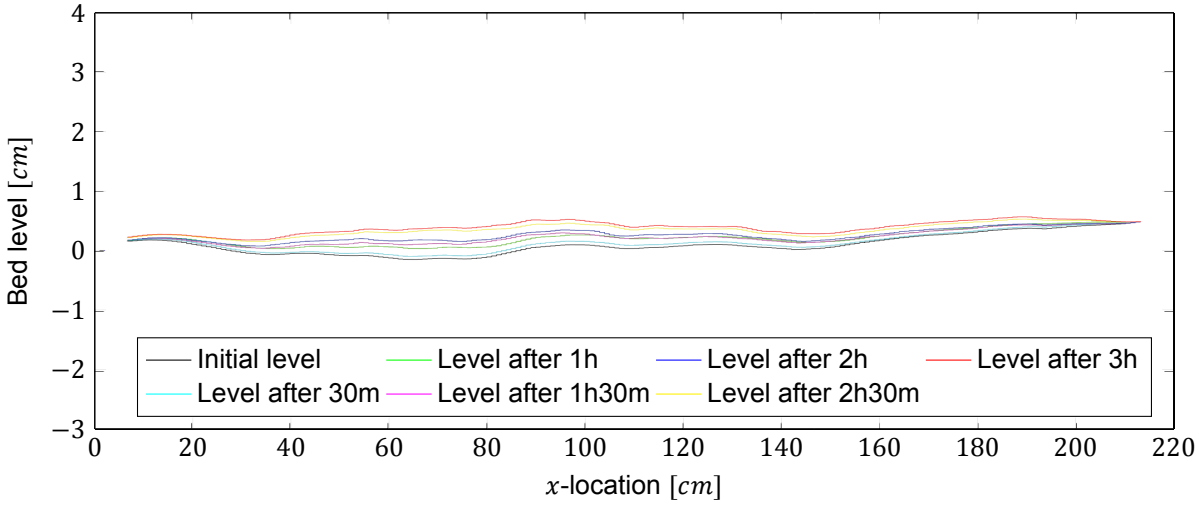

(e) Bed level measured by laser 3 at different times after starting the experiment.

Figure B.4: Bed level for experiment 4, measured by the different lasers. Laser 1 is located at y=38.7cm Laser 2 is located at y=27.4cm Laser 3 is located at y=8.4cm

Experiment 5

(a) Photograph of the final erosion and sedimentation pattern for experiment 5. The photograph is made at the just after the expansion, showing the bed until about one metre downstream of the expansion.

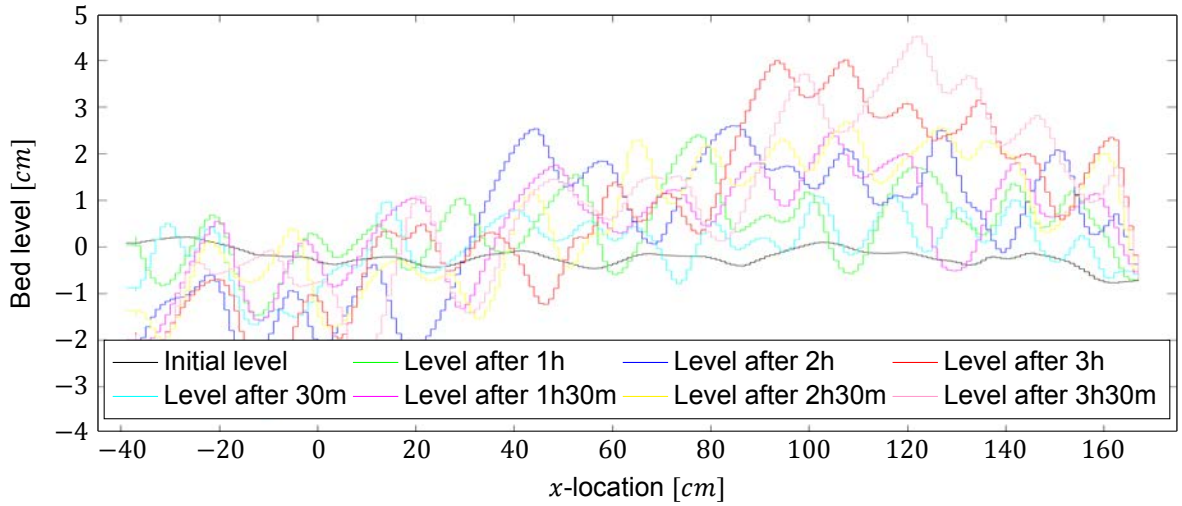

(b) Bed level measured by laser 1 at different times after starting the experiment.

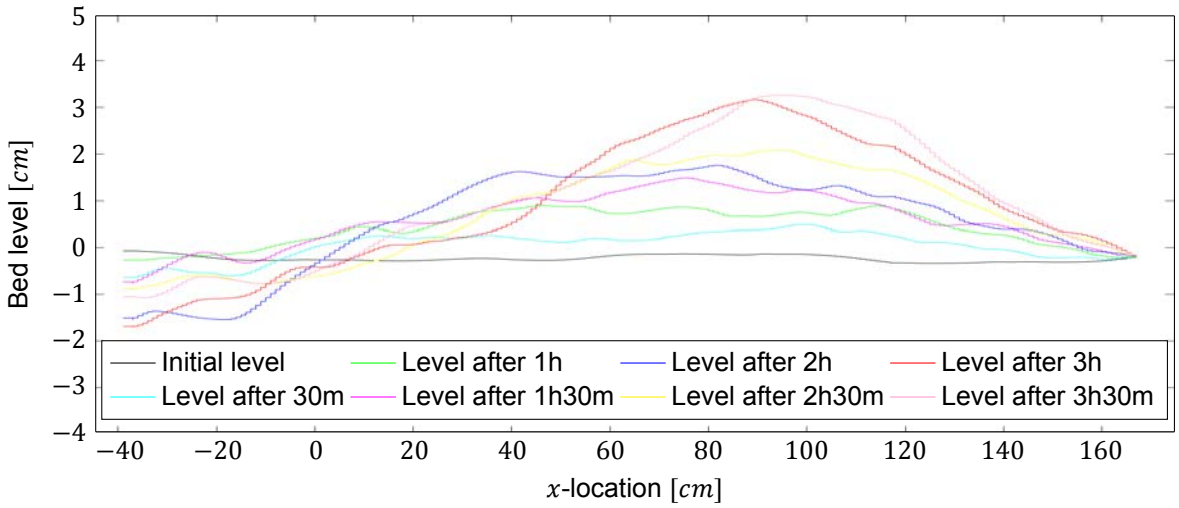

(c) Smoothed bed level measured by laser 1 at different times after starting the experiment. Results are smoothened to even out most of the bedforms.

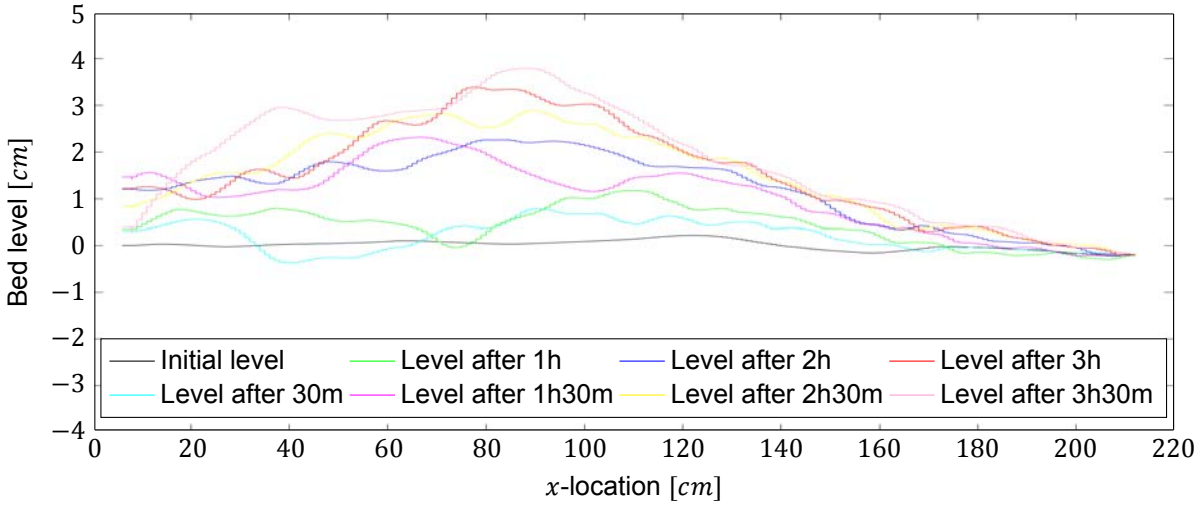

(d) Bed level measured by laser 2 at different times after starting the experiment.

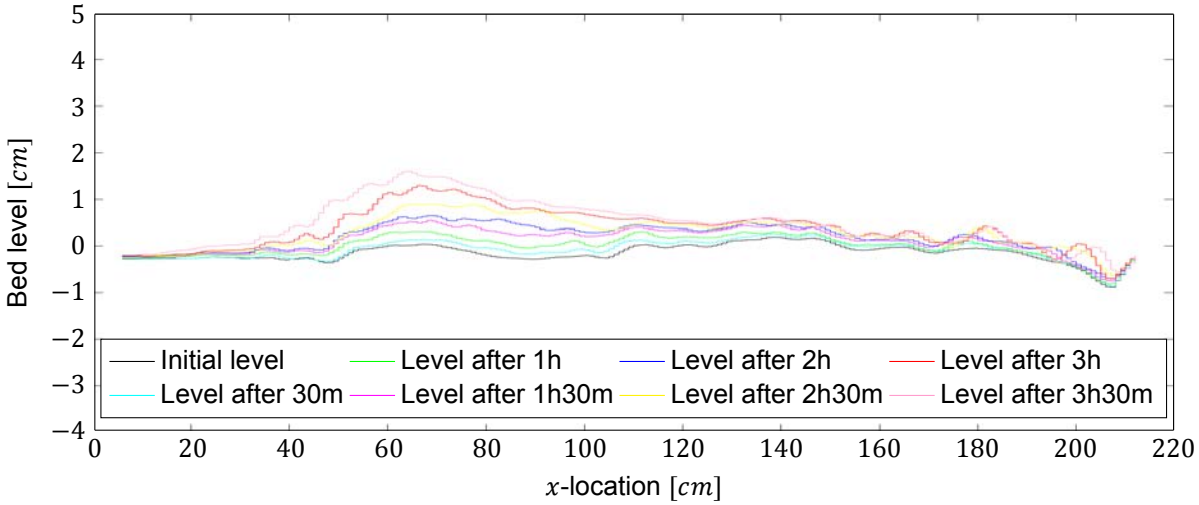

(e) Bed level measured by laser 3 at different times after starting the experiment.

Figure B.5: Bed level for experiment 5, measured by the different lasers. Laser 1 is located at y=38.7cm Laser 2 is located at y=27.4cm Laser 3 is located at y=8.4cm

Experiment 6

(a) Photograph of the final erosion and sedimentation pattern for experiment 6. The photograph is made at the just after the expansion, showing the bed until about one metre downstream of the expansion.

(b) Photograph of the final erosion and sedimentation pattern for experiment 6. The photograph is made at the end of the flume, showing the bed between 0.5 and 1.5 metres downstream of the expansion.

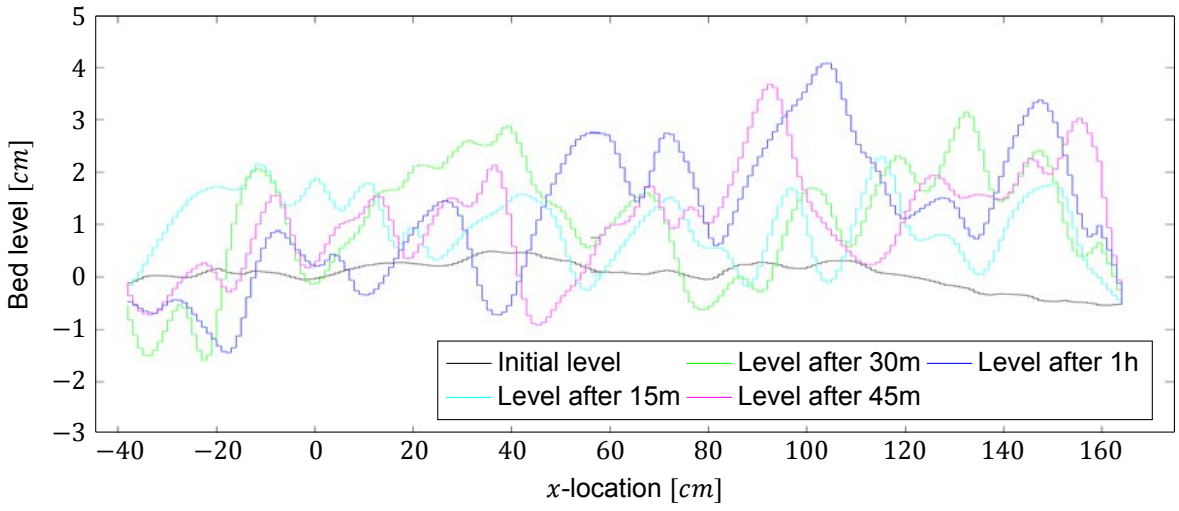

(c) Bed level measured by laser 1 at different times after starting the experiment.

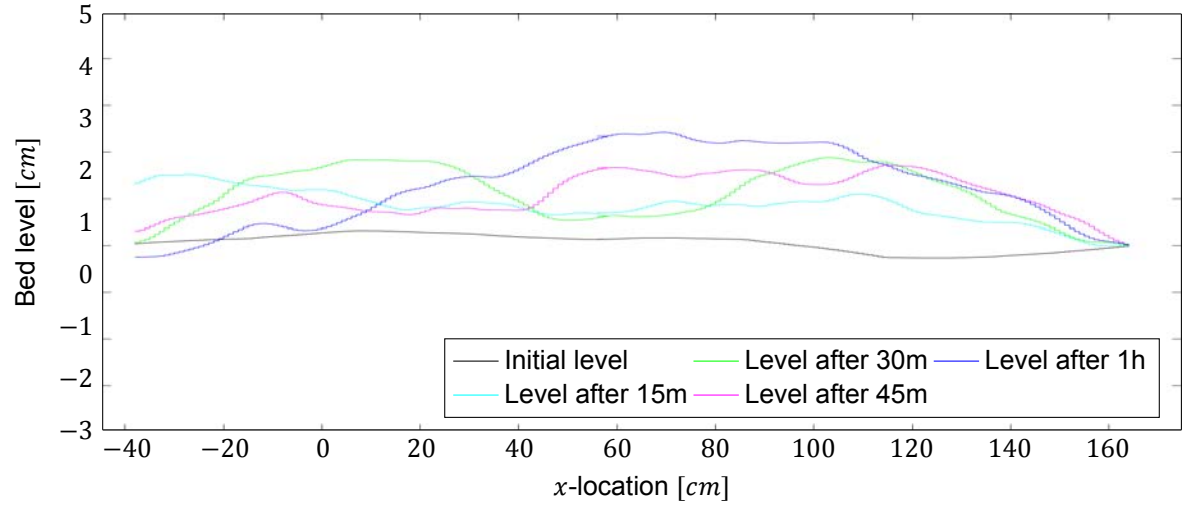

(d) Smoothed bed level measured by laser 1 at different times after starting the experiment. Results are smoothened to even out most of the bedforms.

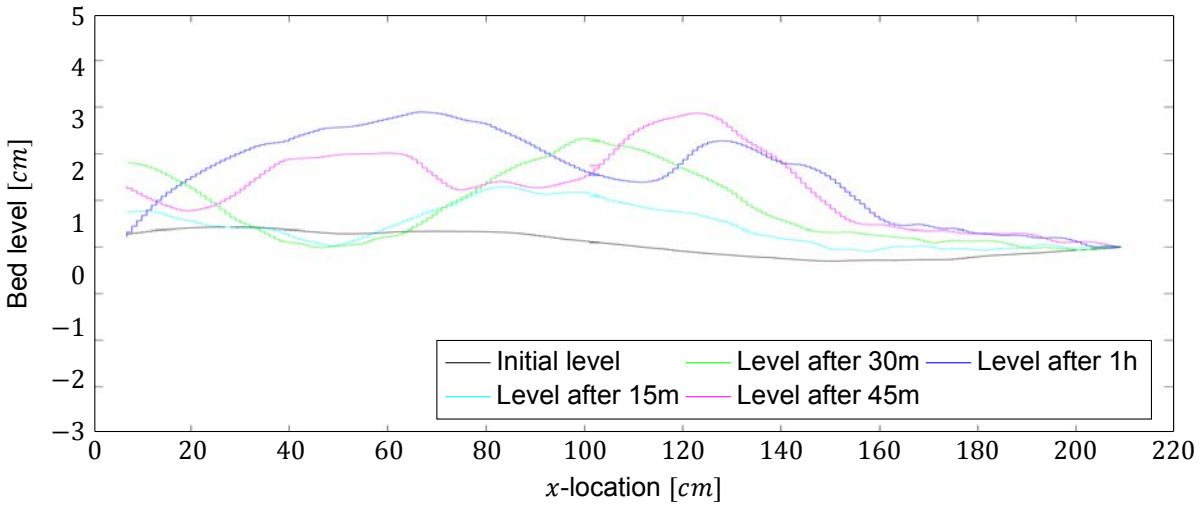

(e) Bed level measured by laser 2 at different times after starting the experiment.

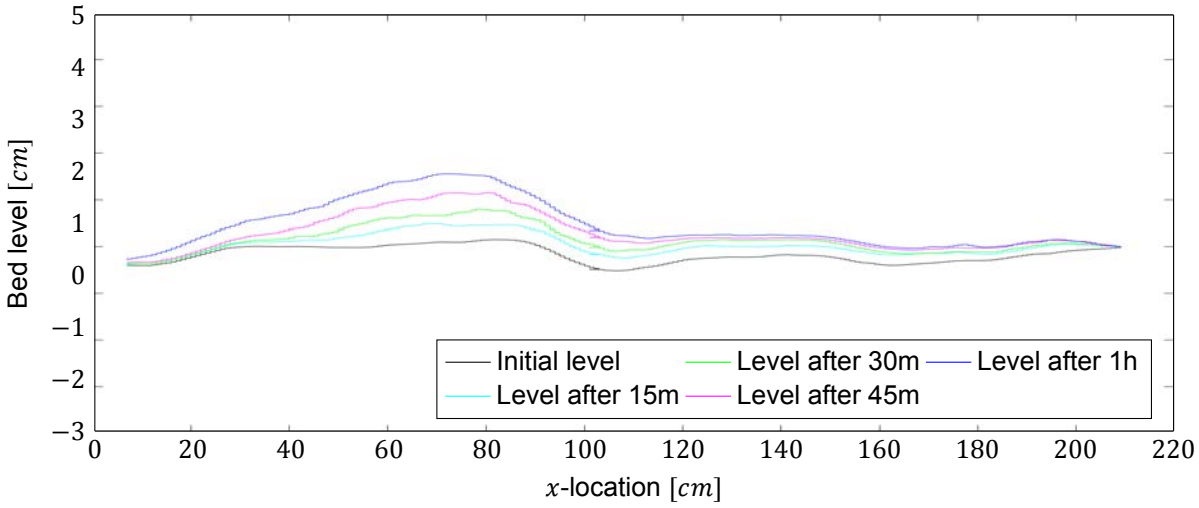

(f) Bed level measured by laser 3 at different times after starting the experiment.

Figure B.6: Bed level for experiment 6, measured by the different lasers. Laser 1 is located at y=38.7cm Laser 2 is located at y=27.4cm Laser 3 is located at y=8.4cm

Experiment 7

(a) Photograph of the final erosion and sedimentation pattern for experiment 7. The photograph is made at the just after the expansion, showing the bed until about one metre downstream of the expansion.

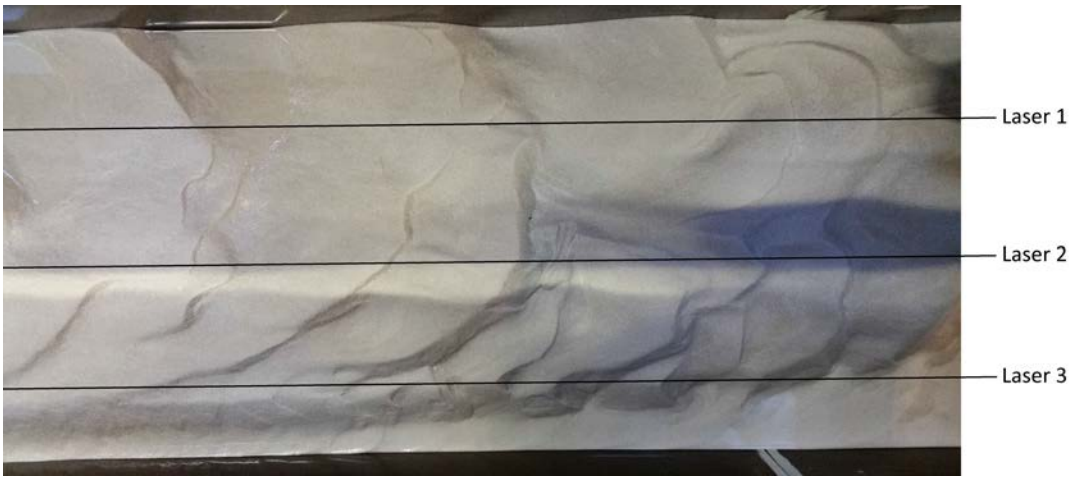

(b) Photograph of the final erosion and sedimentation pattern for experiment 7. The photograph is made at the end of the flume, showing the bed between 0.5 and 1.5 metres downstream of the expansion.

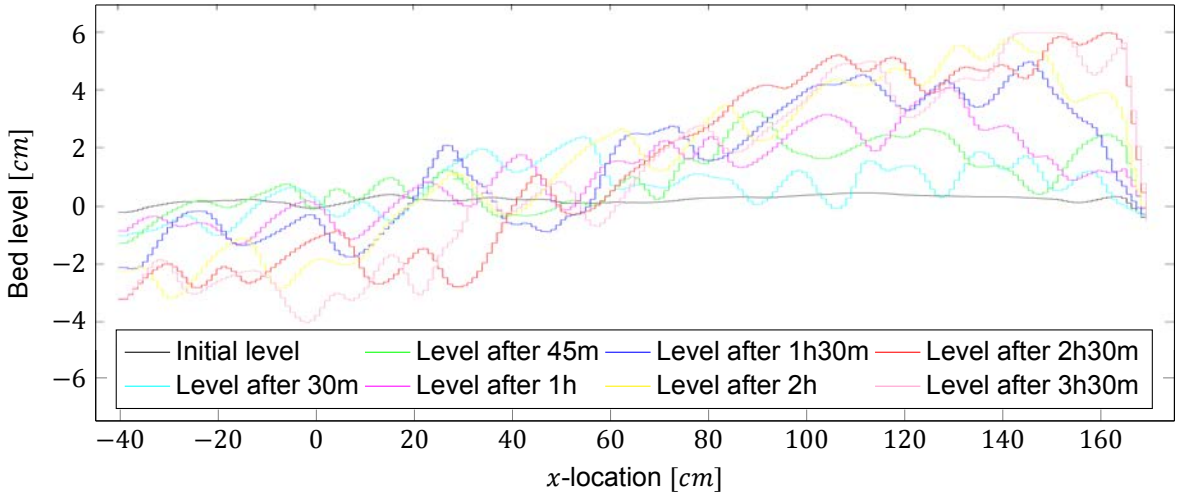

(c) Bed level measured by laser 1 at different times after starting the experiment.

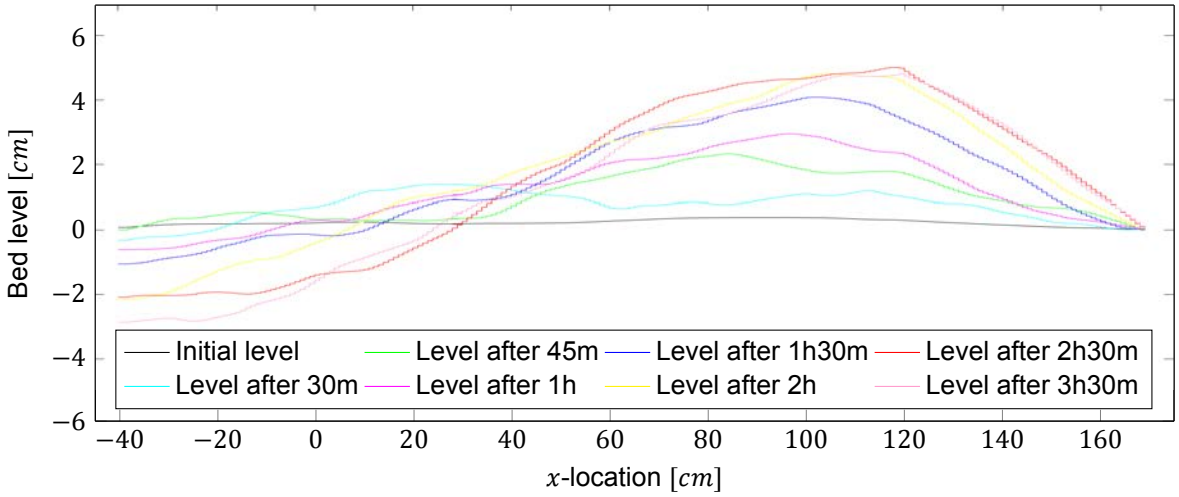

(d) Smoothed bed level measured by laser 1 at different times after starting the experiment. Results are smoothened to even out most of the bedforms.

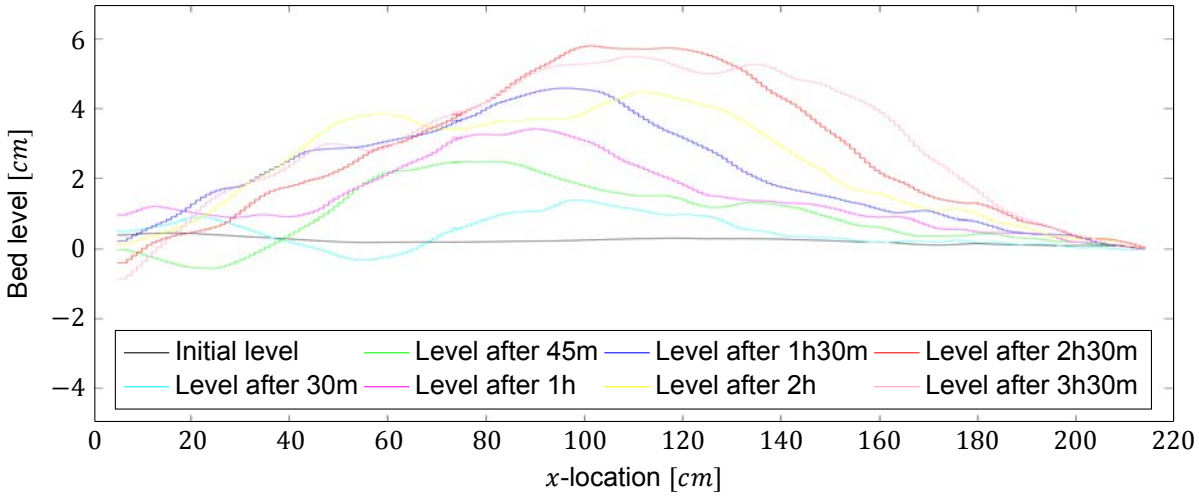

(e) Bed level measured by laser 2 at different times after starting the experiment.

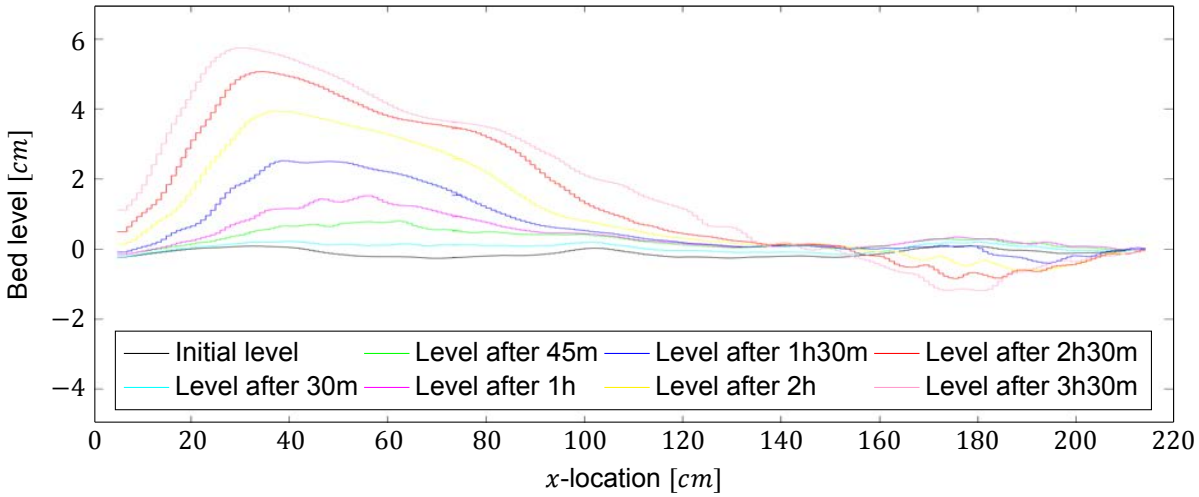

(f) Bed level measured by laser 3 at different times after starting the experiment.

Figure B.7: Bed level for experiment 7, measured by the different lasers. Laser 1 is located at y=38.7cm Laser 2 is located at y=27.4cm Laser 3 is located at y=8.4cm

Experiment 8

(a) Photograph of the final erosion and sedimentation pattern for experiment 8. The photograph is made at the end of the flume, facing in the direction of the expansion.

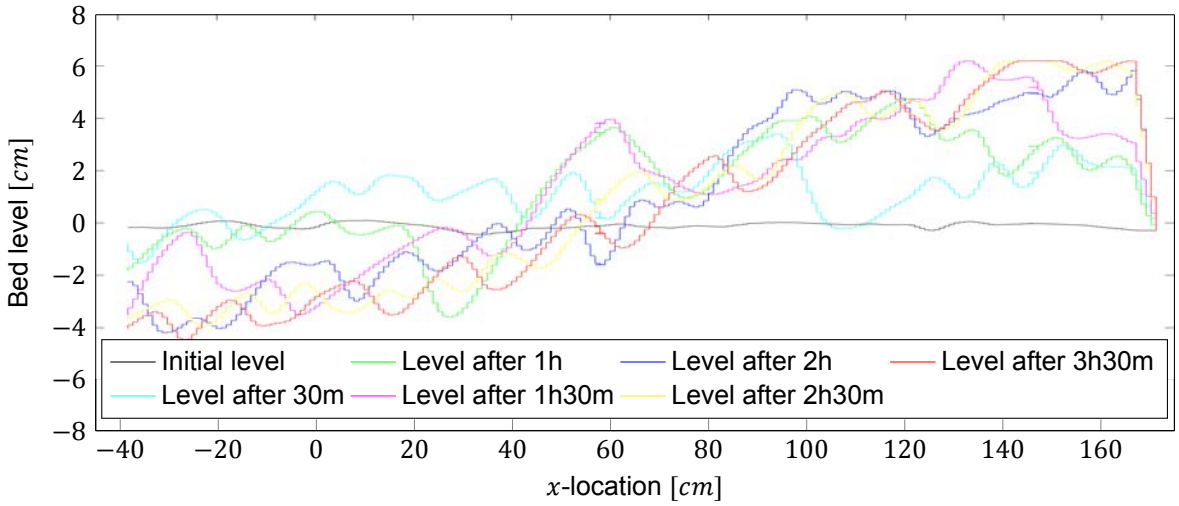

(b) Bed level measured by laser 1 at different times after starting the experiment.

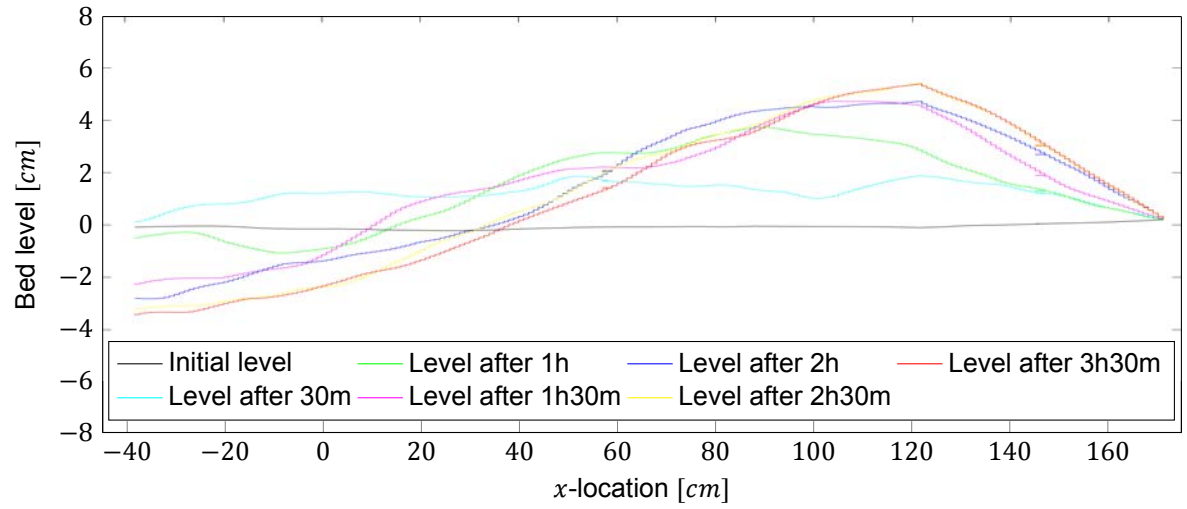

(c) Smoothed bed level measured by laser 1 at different times after starting the experiment. Results are smoothened to even out most of the bedforms.

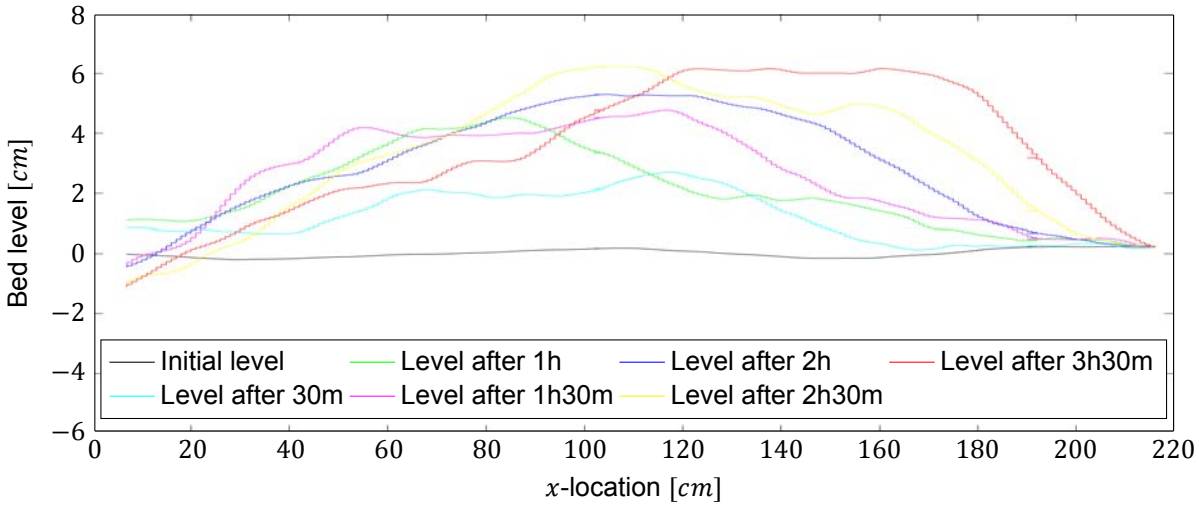

(d) Bed level measured by laser 2 at different times after starting the experiment.

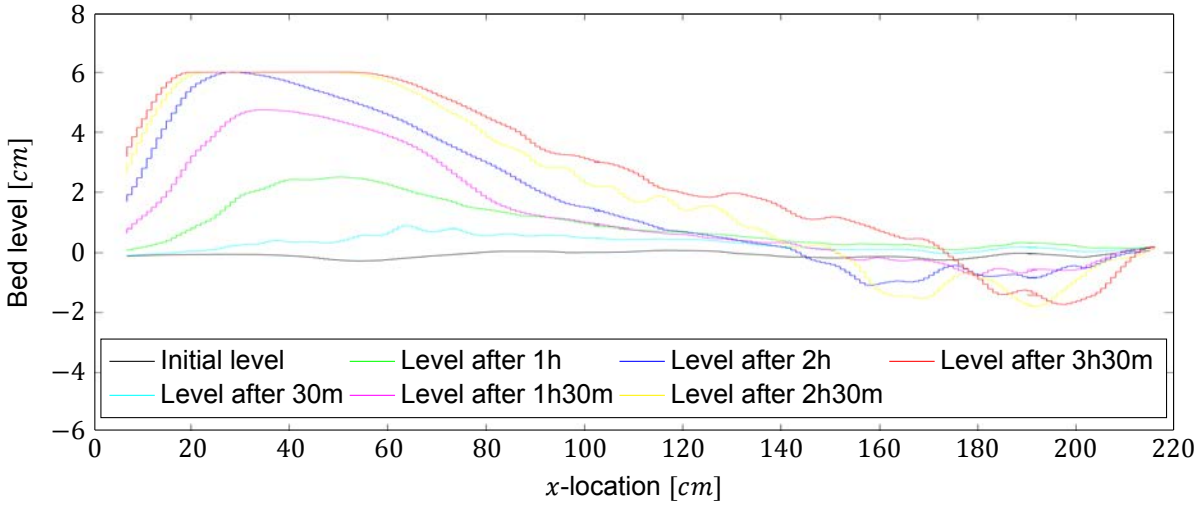

(e) Bed level measured by laser 3 at different times after starting the experiment.

Figure B.8: Bed level for experiment 8, measured by the different lasers. Laser 1 is located at y=38.7cm Laser 2 is located at y=27.4cm Laser 3 is located at y=8.4cm

Experiment 4 - repeat test 1

(a) Photograph of the final erosion and sedimentation pattern for experiment 4. The photograph is made at the just after the expansion, showing the bed until about one metre downstream of the expansion.

(b) Photograph of the final erosion and sedimentation pattern for experiment 4. The photograph is made at the end of the flume, showing the bed between 0.5 and 1.5 metres downstream of the expansion.

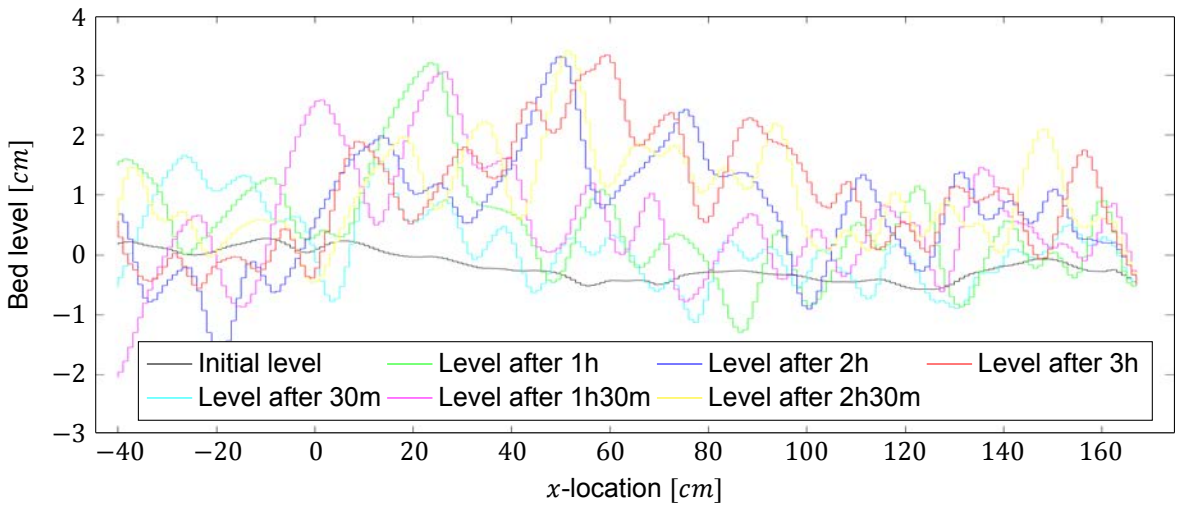

(c) Bed level measured by laser 1 at different times after starting the experiment.

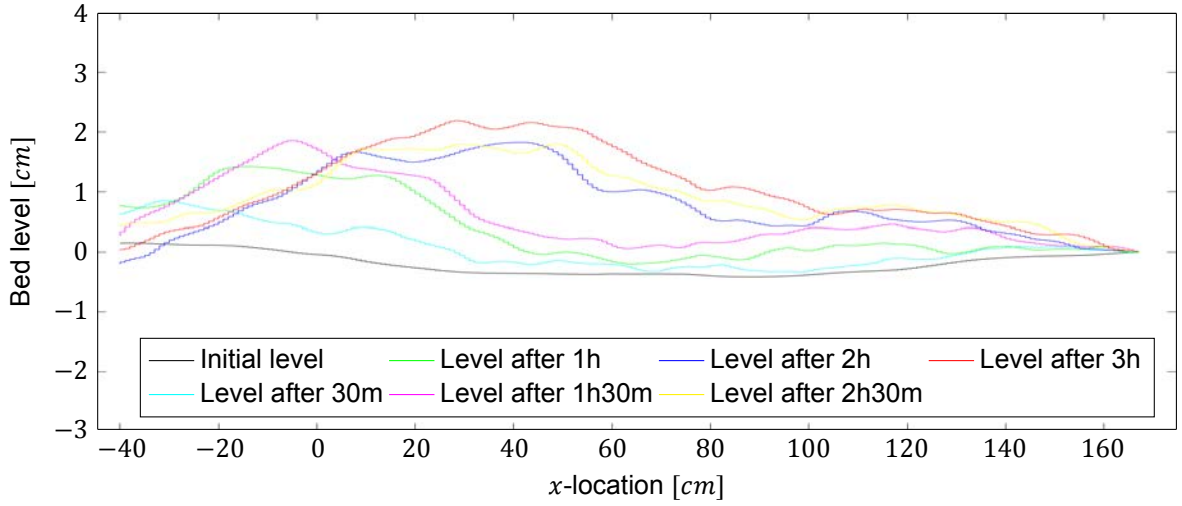

(d) Smoothed bed level measured by laser 1 at different times after starting the experiment. Results are smoothened to even out most of the bedforms.

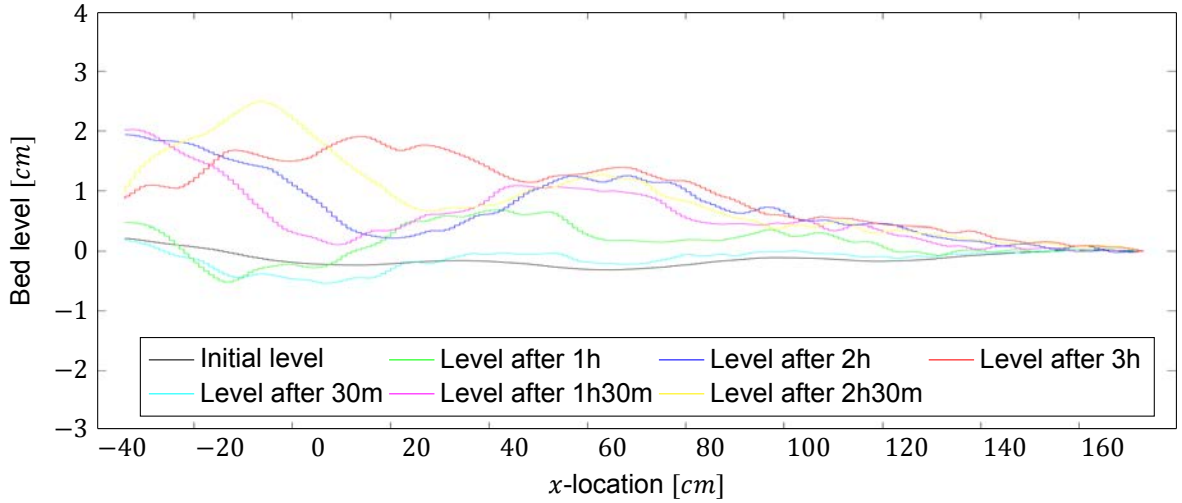

(e) Bed level measured by laser 2 at different times after starting the experiment.

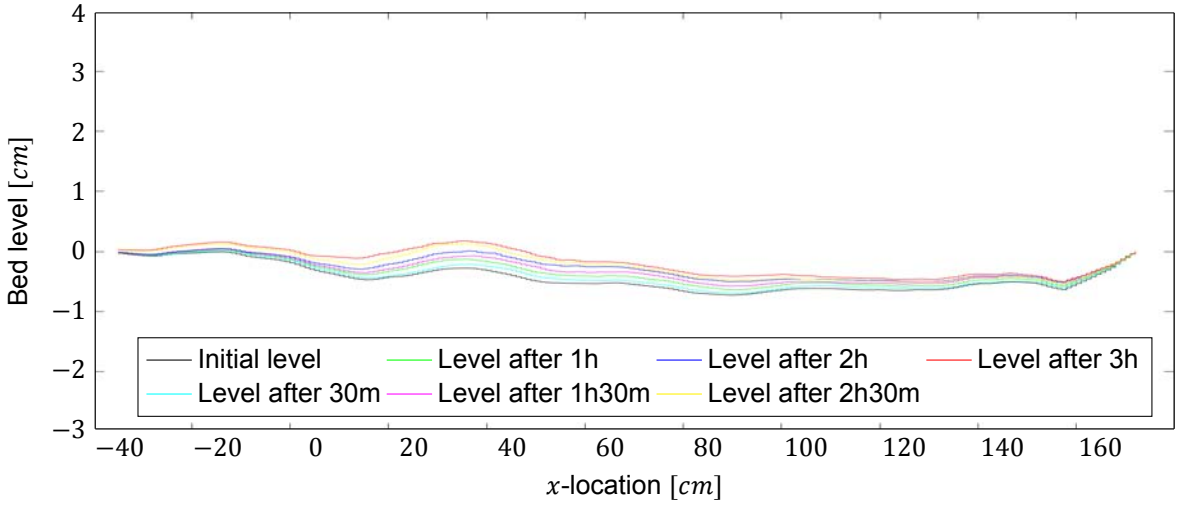

(f) Bed level measured by laser 3 at different times after starting the experiment.

Figure B.9: Repeat test 1. Bed level for experiment 4, measured by the different lasers. Laser 1 is located at y=38.7cm Laser 2 is located at y=27.4cm Laser 3 is located at y=8.4cm

Experiment 4 - repeat test 2

(a) Photograph of the final erosion and sedimentation pattern for experiment 4. The photograph is made at the just after the expansion, showing the bed until about one metre downstream of the expansion.

(b) Photograph of the final erosion and sedimentation pattern for experiment 4. The photograph is made at the end of the flume, showing the bed between 0.5 and 1.5 metres downstream of the expansion.

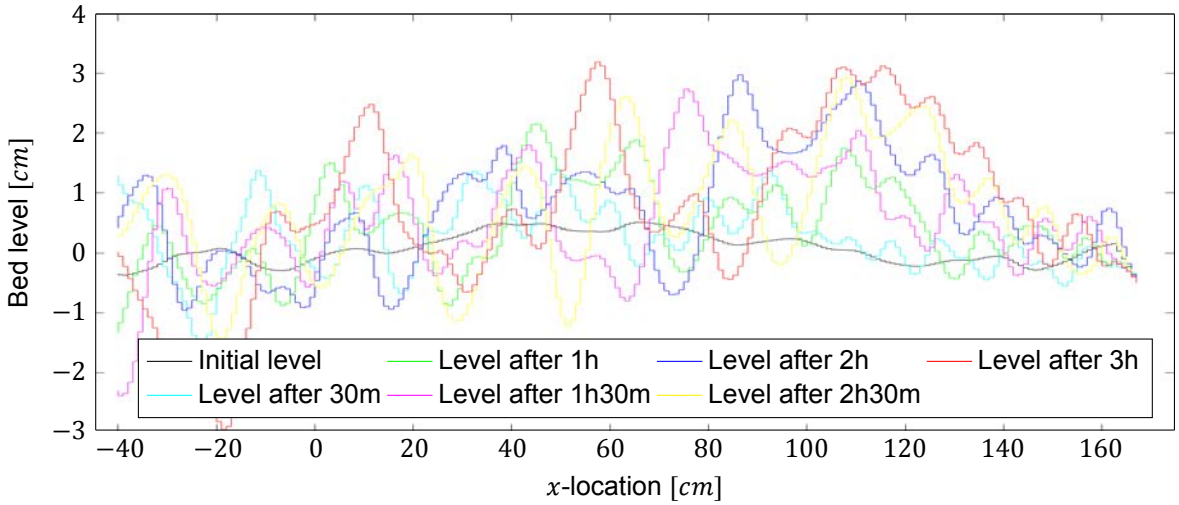

(c) Bed level measured by laser 1 at different times after starting the experiment.

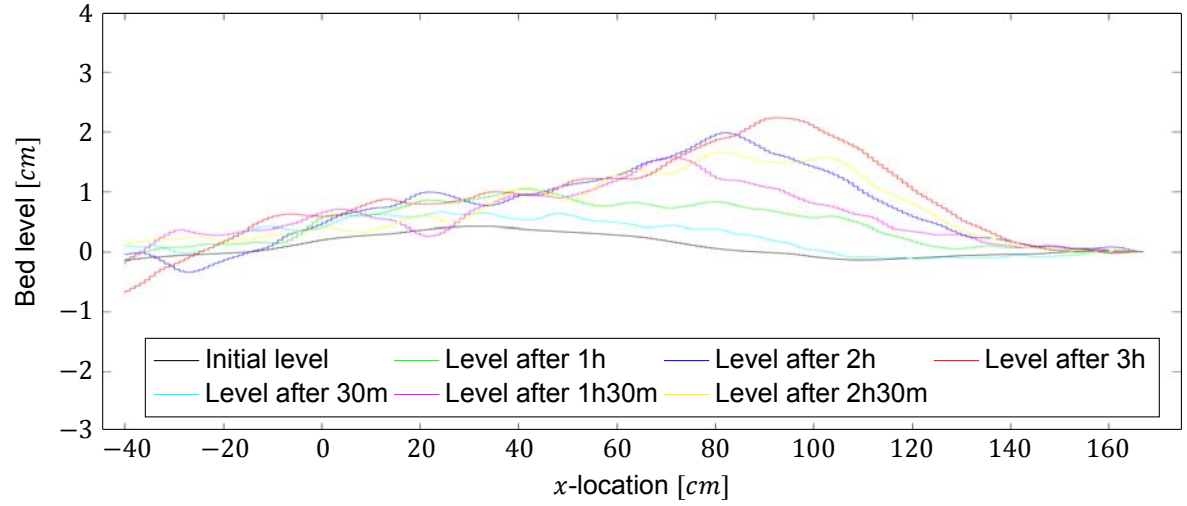

(d) Smoothed bed level measured by laser 1 at different times after starting the experiment. Results are smoothened to even out most of the bedforms.

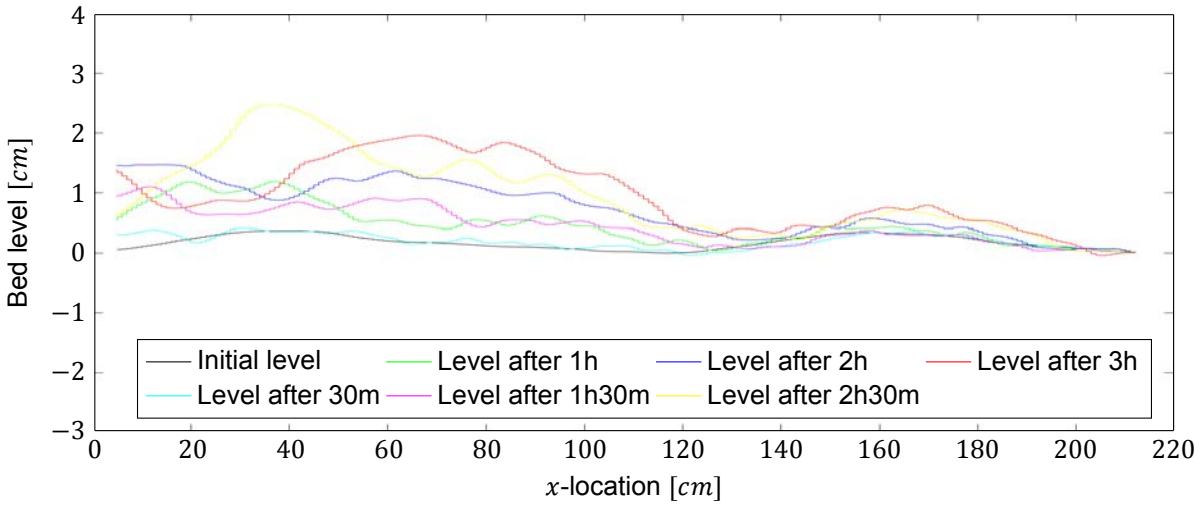

(e) Bed level measured by laser 2 at different times after starting the experiment.

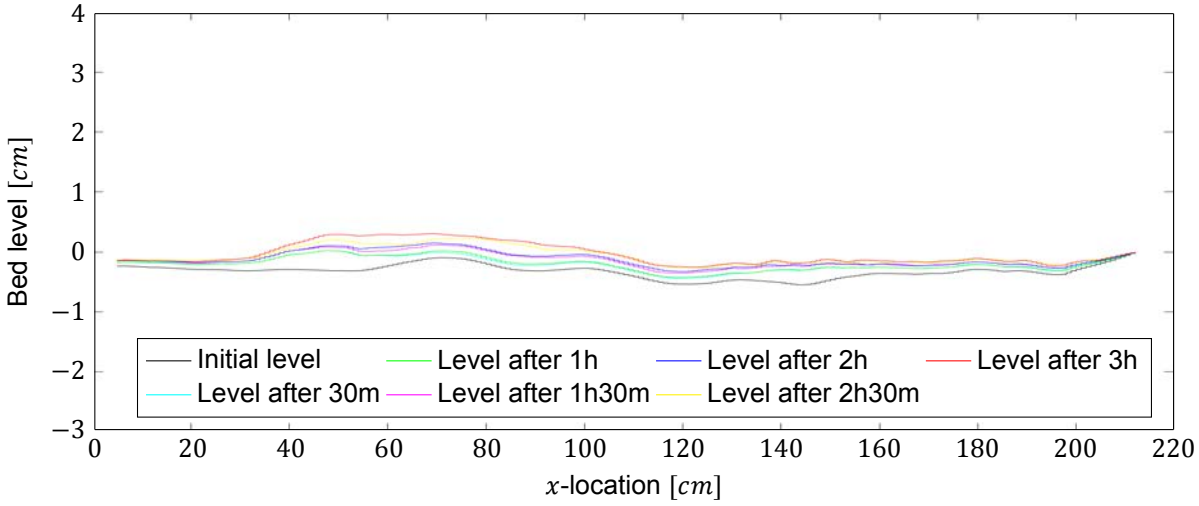

(f) Bed level measured by laser 3 at different times after starting the experiment.

Figure B.10: Repeat test 2. Bed level for experiment 4, measured by the different lasers. Laser 1 is located at y=38.7cm Laser 2 is located at y=27.4cm Laser 3 is located at y=8.4cm

C

Numerical results - flow patterns

This appendix provides the results from the hydrodynamic numerical simulations with TUDflow3d. The grid size in x- and y-direction is one centimetre for these simulations. The grid size in z-direction is 0.4 centimetre. The simulated time for the experiments was five minutes. Two resilience checks were executed: for the first check the simulated time was doubled, and for the second check a simulation was executed with a twice as small grid size in all directions. Table C.1 gives an overview of the executed simulations. For each simulation, three plots are depicted: one of the mean flow velocity, one showing the turbulence intensity, and the last plot depicts the secondary circulation downstream of the expansion.

Table C.1: Overview of the executed numerical simulations.

	U_1	U_2
	[m/s]	[m/s]
Experiment 1	0.2	0.1
Experiment 2	0.25	0.13
Experiment 3	0.3	0.15
Experiment 4	0.35	0.18
Experiment 5	0.4	0.2
Experiment 6	0.45	0.23
Experiment 7	0.5	0.25
Experiment 8	0.54	0.27
Experiment 4 - ten minutes simulated time	0.35	0.18
Experiment 4 - grid refinement	0.35	0.18

Experiment 1

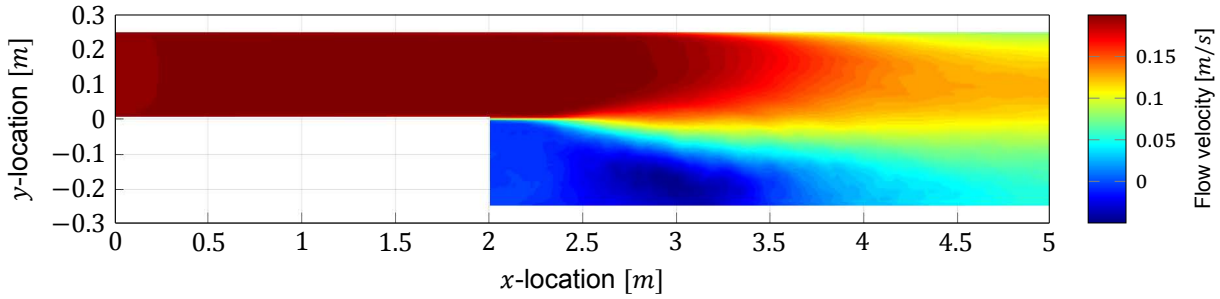

(a) Time-averaged flow velocity for experiment 1 at eight centimetres above the bed.

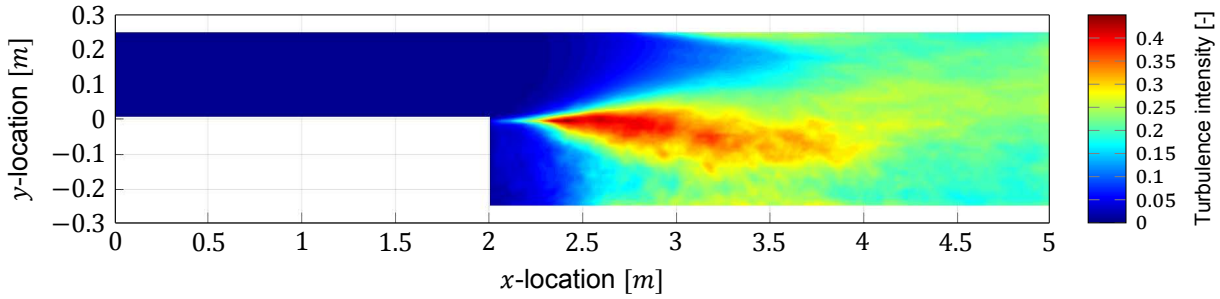

(b) Time-averaged turbulence intensity throughout the flume for experiment 1 at eight centimetres above the bed.

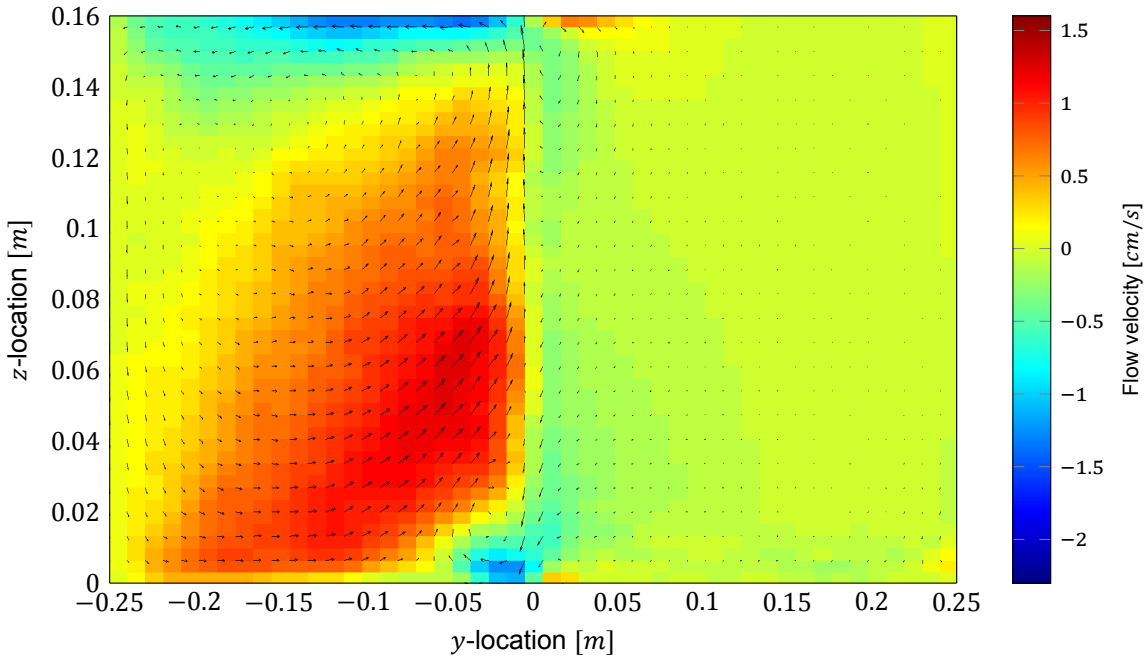

(c) Flow pattern of experiment 1 for a cross-section perpendicular to the flume 35 centimetres downstream of the expansion.

Figure C.1: Resulting flow patterns for the numerical simulation of experiment 1.

Experiment 2

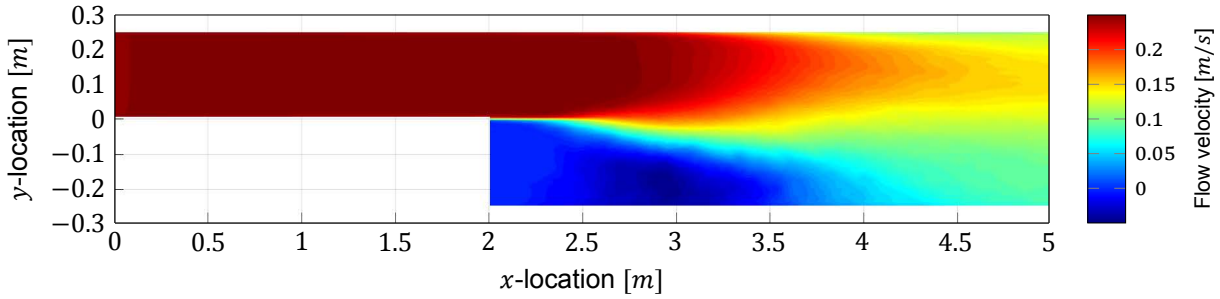

(a) Time-averaged flow velocity for experiment 2 at eight centimetres above the bed.

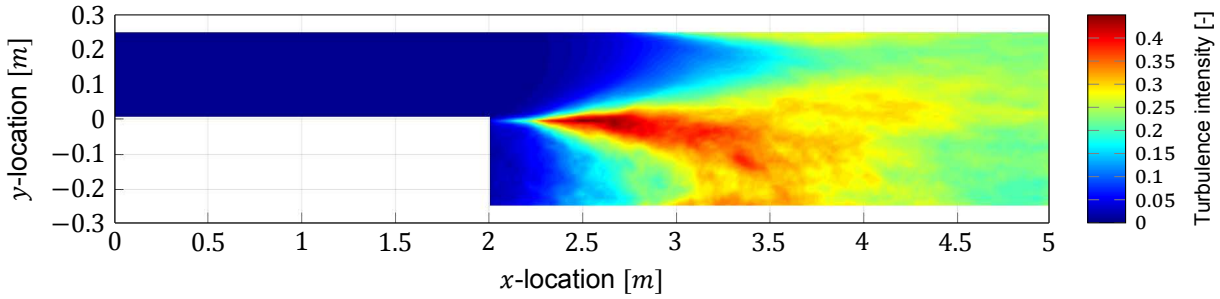

(b) Time-averaged turbulence intensity throughout the flume for experiment 2 at eight centimetres above the bed.

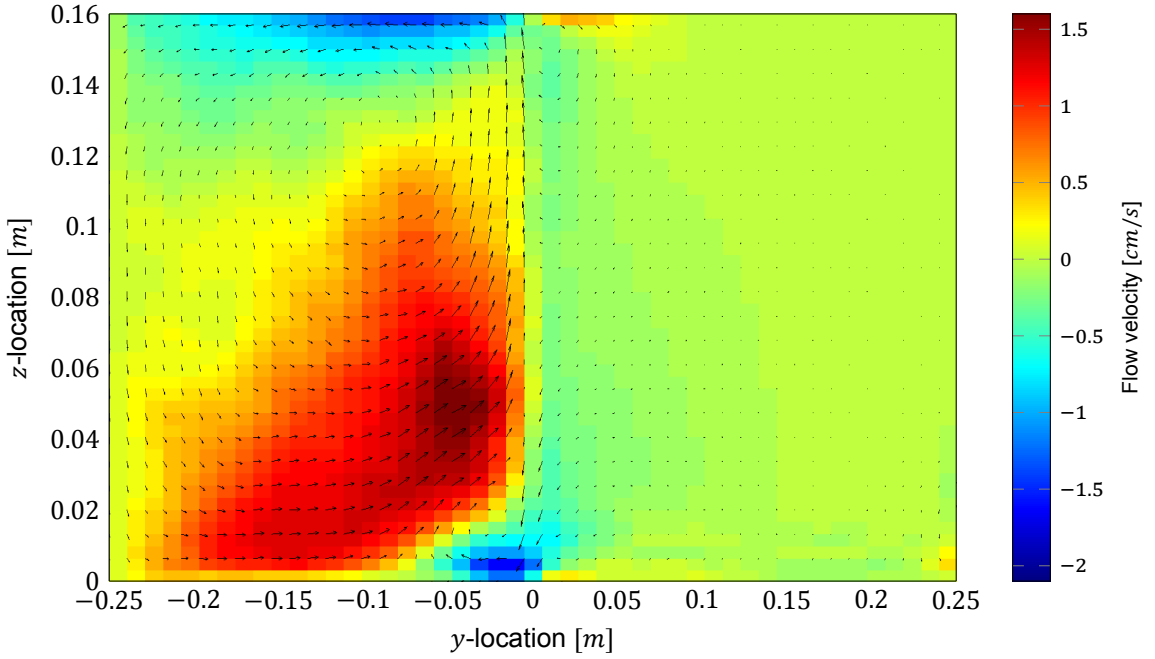

(c) Flow pattern of experiment 2 for a cross-section perpendicular to the flume 35 centimetres downstream of the expansion.

Figure C.2: Resulting flow patterns for the numerical simulation of experiment 2.

Experiment 3

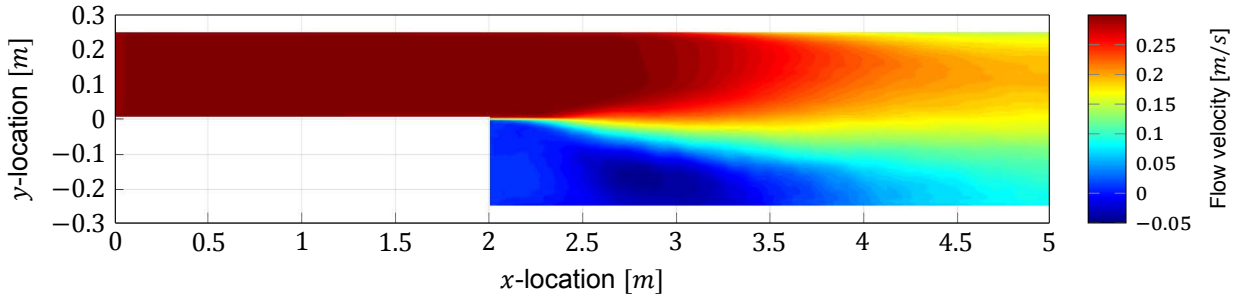

(a) Time-averaged flow velocity for experiment 3 at eight centimetres above the bed.

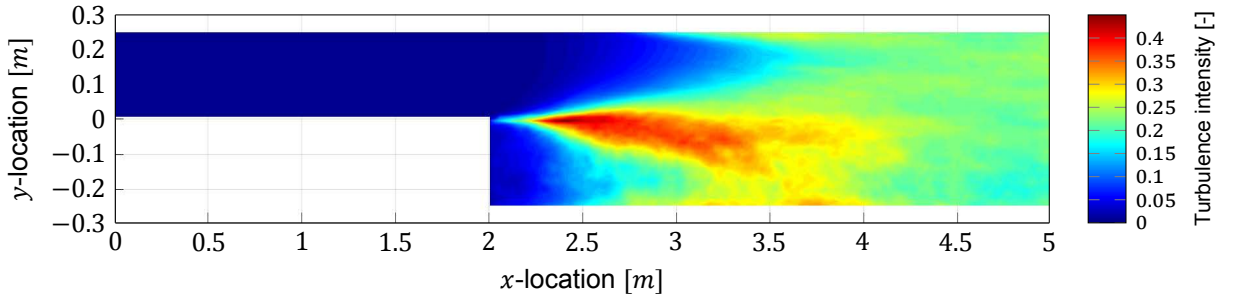

(b) Time-averaged turbulence intensity throughout the flume for experiment 3 at eight centimetres above the bed.

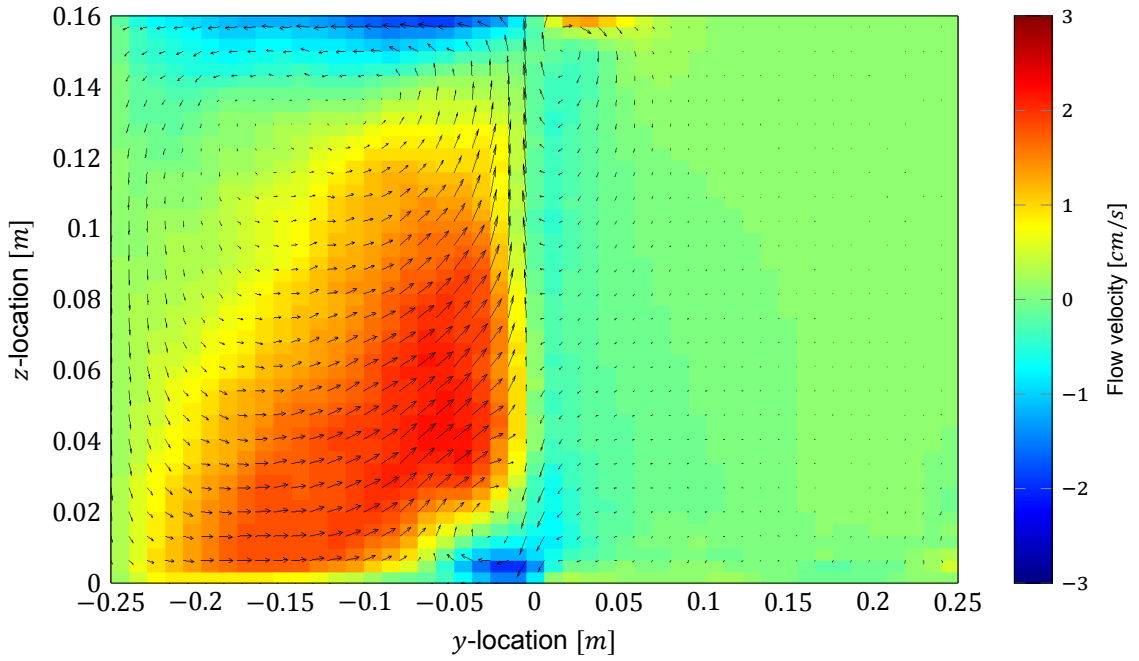

(c) Flow pattern of experiment 3 for a cross-section perpendicular to the flume 35 centimetres downstream of the expansion.

Figure C.3: Resulting flow patterns for the numerical simulation of experiment 3.

Experiment 4

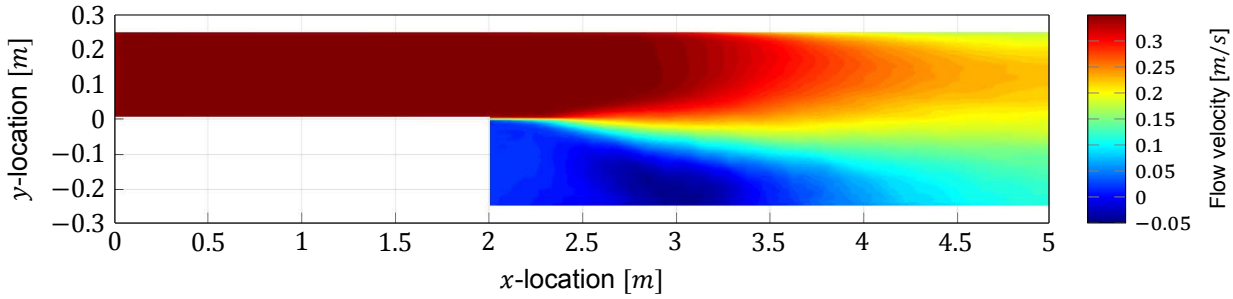

(a) Time-averaged flow velocity for experiment 4 at eight centimetres above the bed.

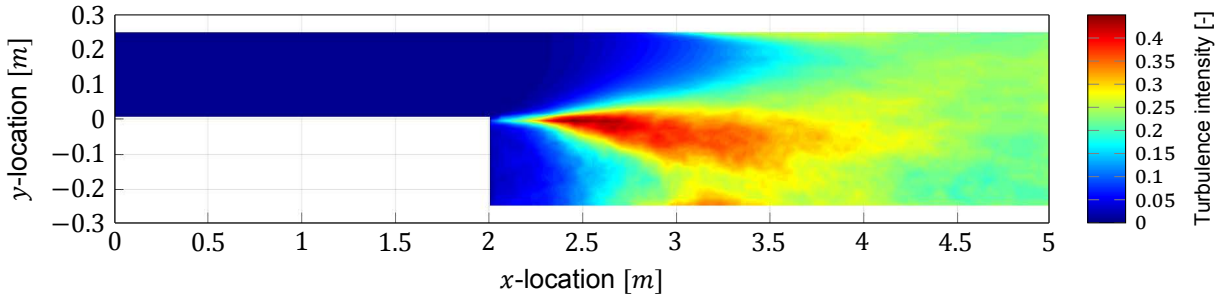

(b) Time-averaged turbulence intensity throughout the flume for experiment 4 at eight centimetres above the bed.

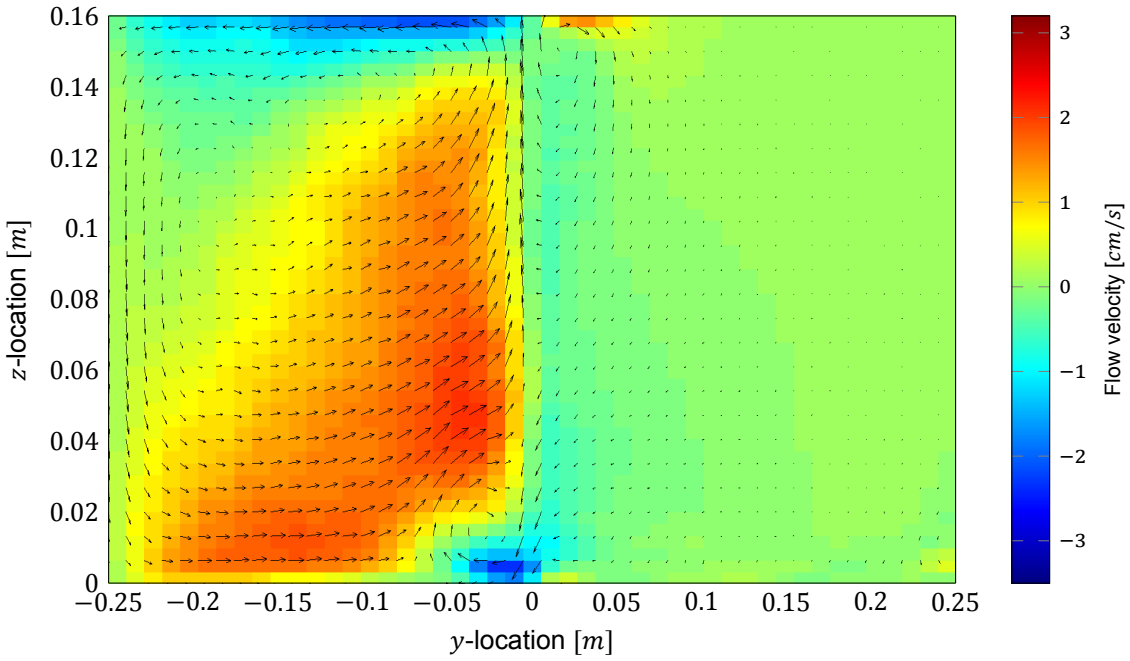

(c) Flow pattern of experiment 4 for a cross-section perpendicular to the flume 35 centimetres downstream of the expansion.

Figure C.4: Resulting flow patterns for the numerical simulation of experiment 4.

Experiment 5

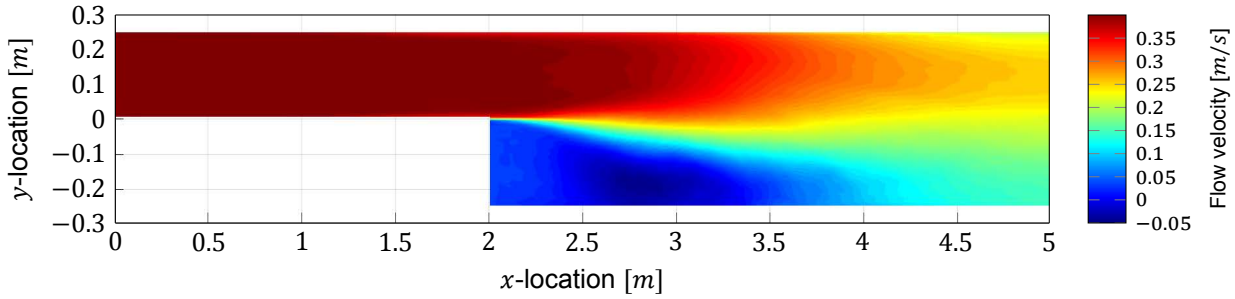

(a) Time-averaged flow velocity for experiment 5 at eight centimetres above the bed.

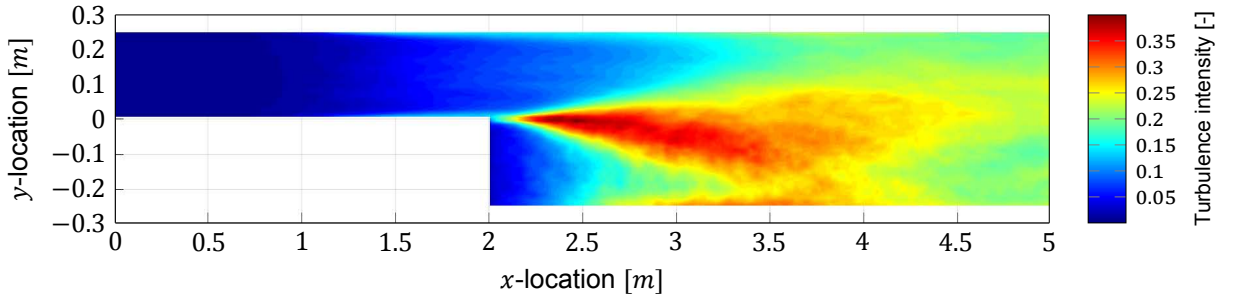

(b) Time-averaged turbulence intensity throughout the flume for experiment 5 at eight centimetres above the bed.

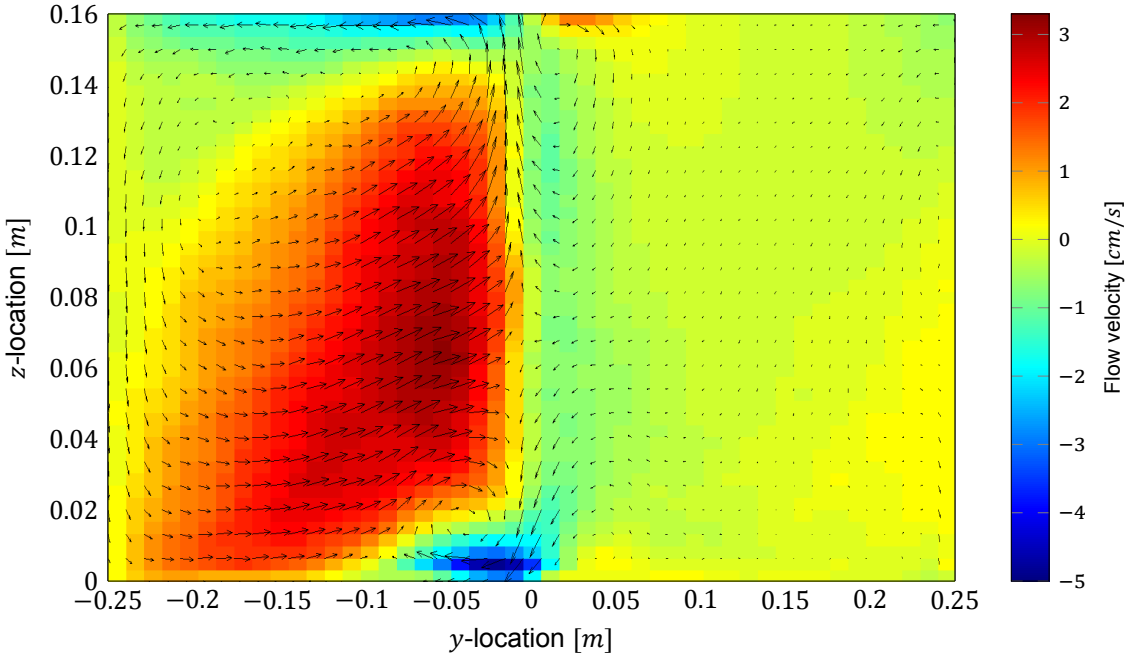

(c) Flow pattern of experiment 5 for a cross-section perpendicular to the flume 35 centimetres downstream of the expansion.

Figure C.5: Resulting flow patterns for the numerical simulation of experiment 5.

Experiment 6

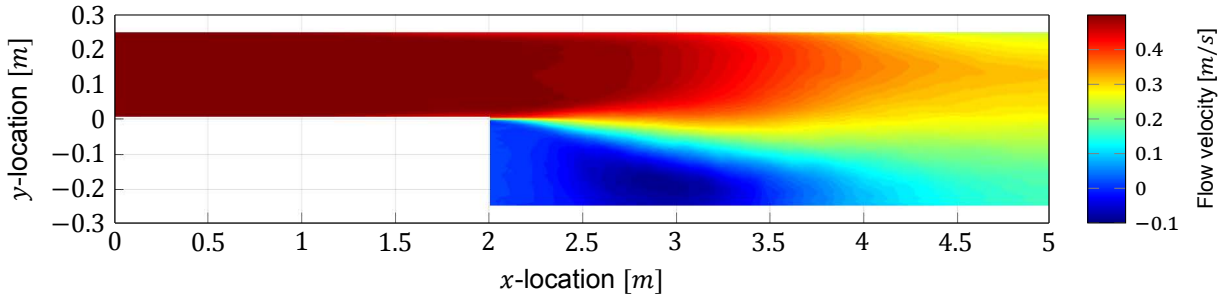

(a) Time-averaged flow velocity for experiment 6 at eight centimetres above the bed.

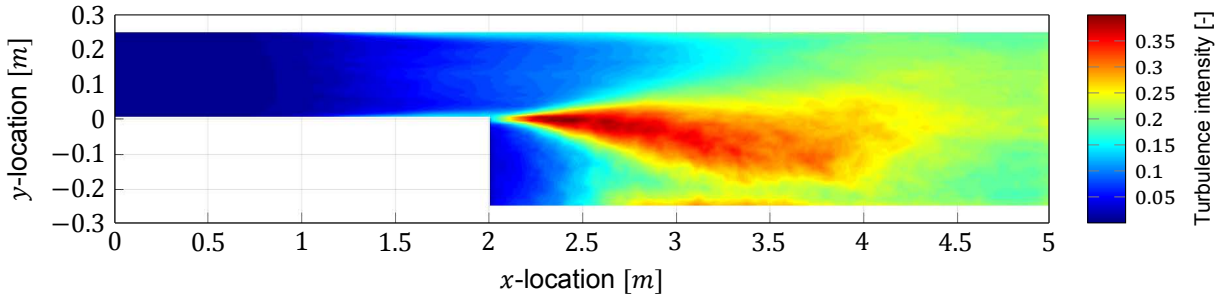

(b) Time-averaged turbulence intensity throughout the flume for experiment 6 at eight centimetres above the bed.

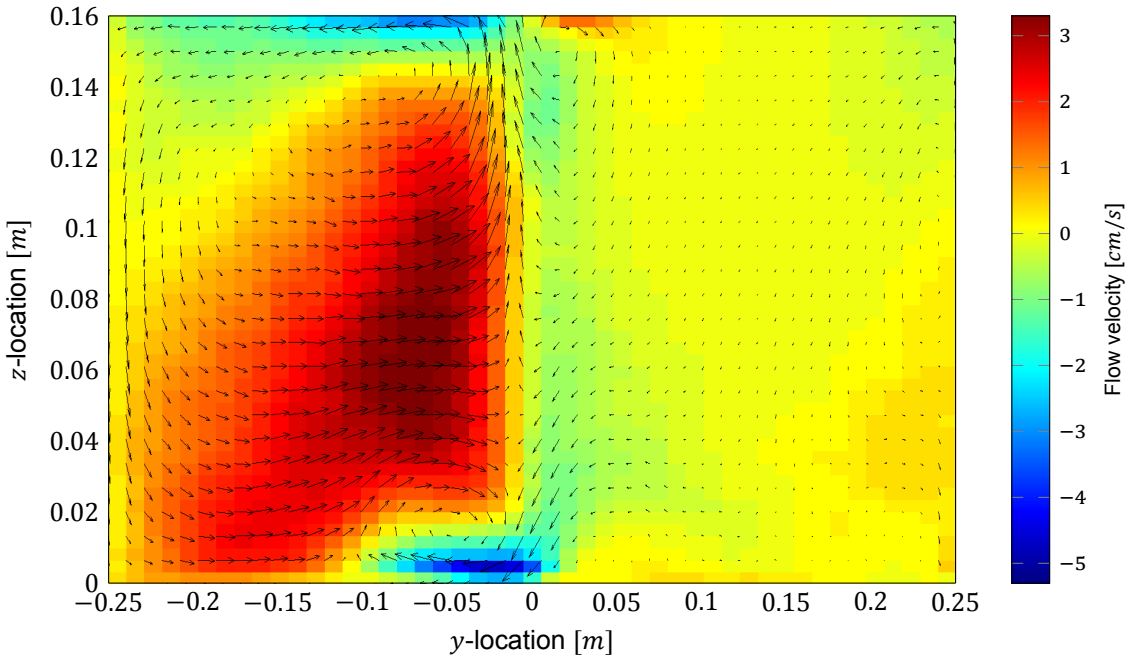

(c) Flow pattern of experiment 6 for a cross-section perpendicular to the flume 35 centimetres downstream of the expansion.

Figure C.6: Resulting flow patterns for the numerical simulation of experiment 6.

Experiment 7

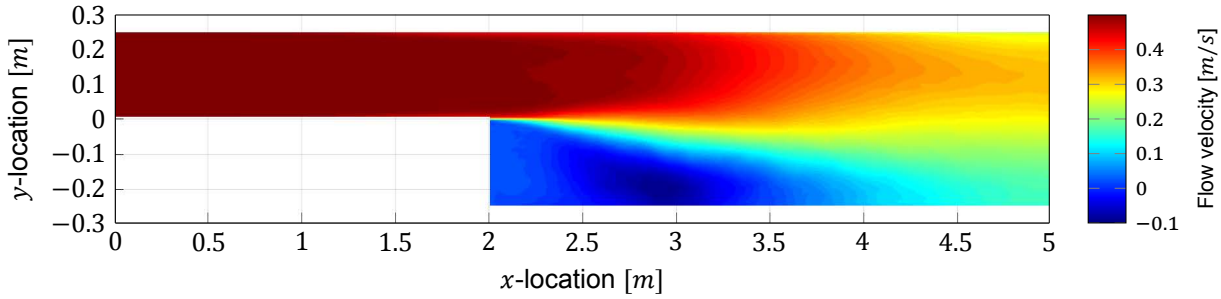

(a) Time-averaged flow velocity for experiment 7 at eight centimetres above the bed.

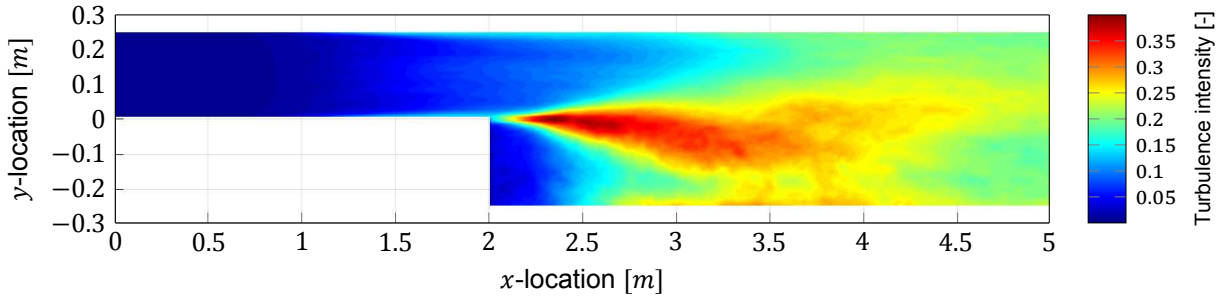

(b) Time-averaged turbulence intensity throughout the flume for experiment 7 at eight centimetres above the bed.

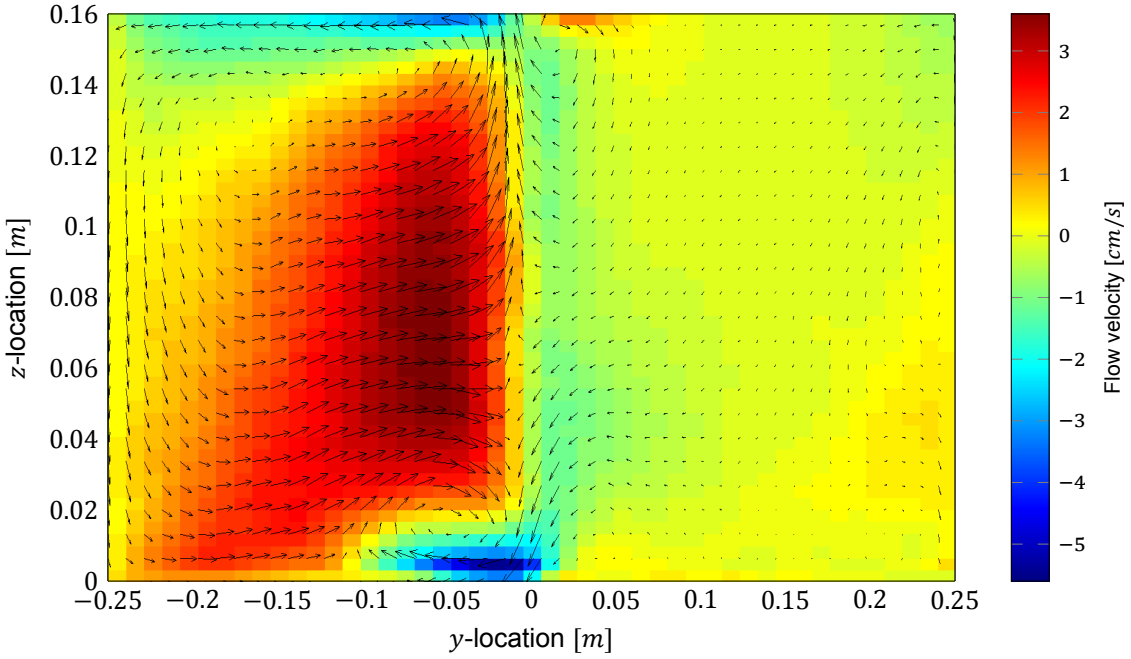

(c) Flow pattern of experiment 7 for a cross-section perpendicular to the flume 35 centimetres downstream of the expansion.

Figure C.7: Resulting flow patterns for the numerical simulation of experiment 7.

Experiment 8

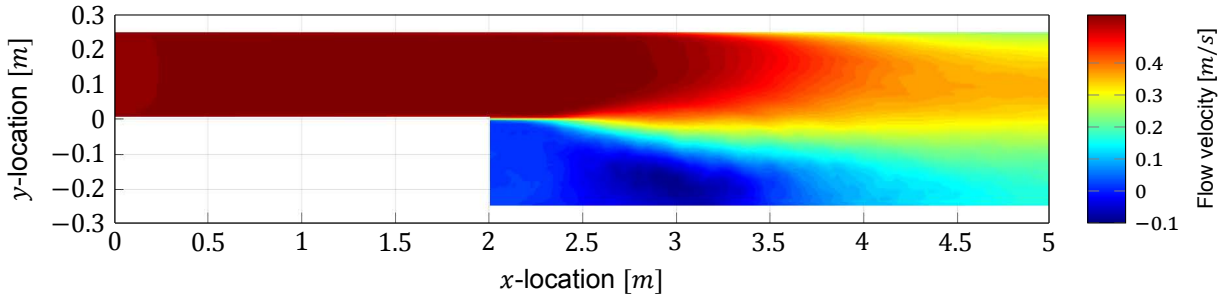

(a) Time-averaged flow velocity for experiment 8 at eight centimetres above the bed.

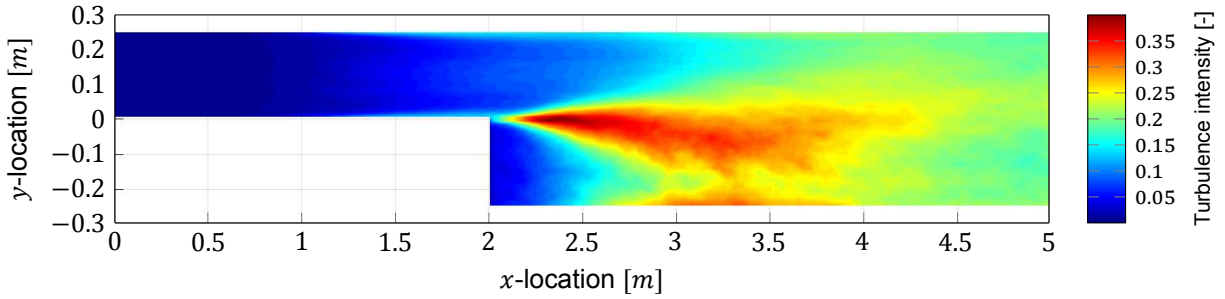

(b) Time-averaged turbulence intensity throughout the flume for experiment 8 at eight centimetres above the bed.

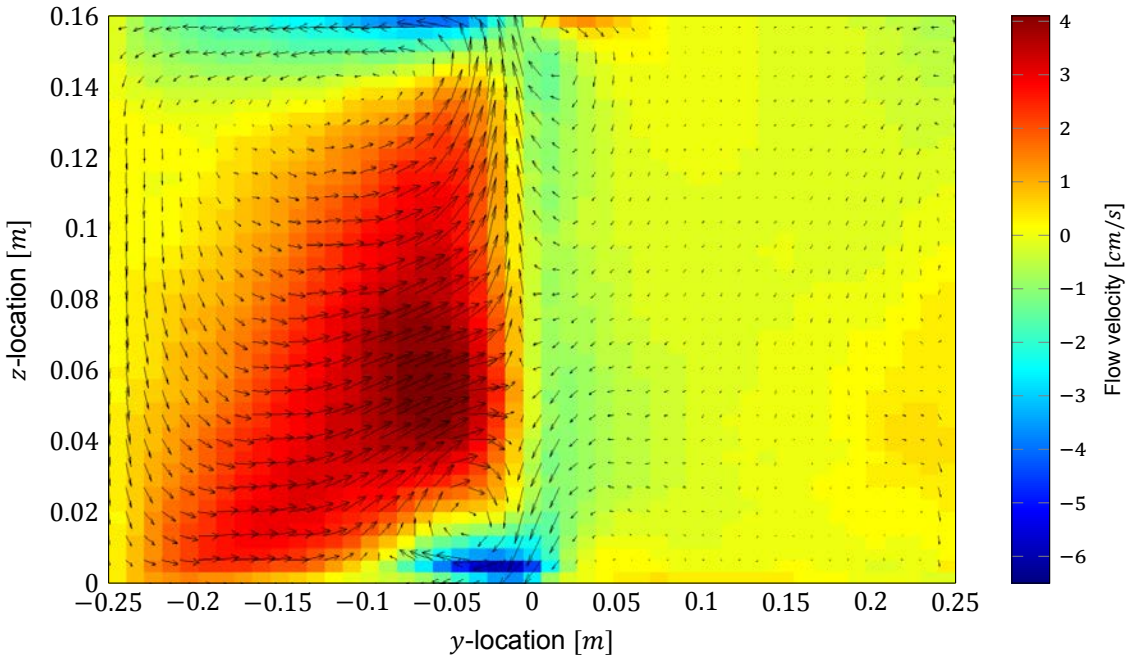

(c) Flow pattern of experiment 8 for a cross-section perpendicular to the flume 35 centimetres downstream of the expansion.

Figure C.8: Resulting flow patterns for the numerical simulation of experiment 8.

Model check: ten minutes simulated time

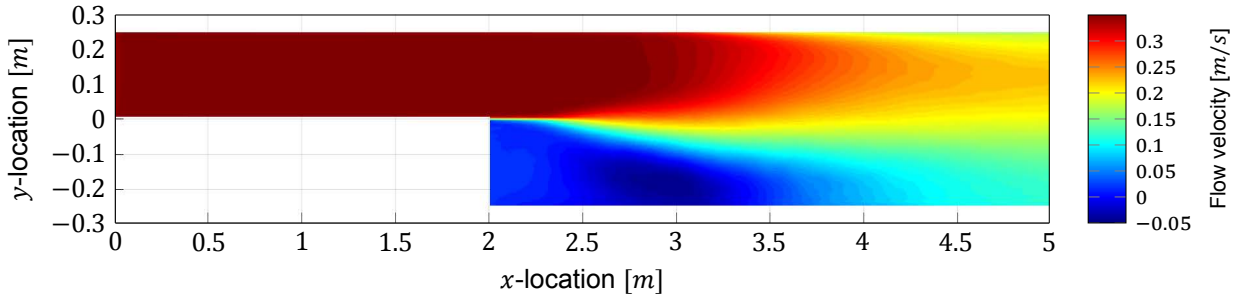

(a) Time-averaged flow velocity for experiment 4 at eight centimetres above the bed with 10 minutes simulated time.

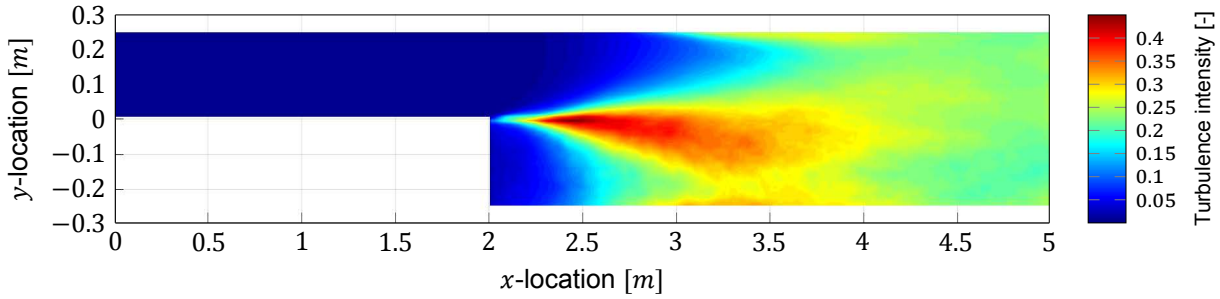

(b) Time-averaged turbulence intensity throughout the flume for experiment 4 at eight centimetres above the bed with 10 minutes simulated time.

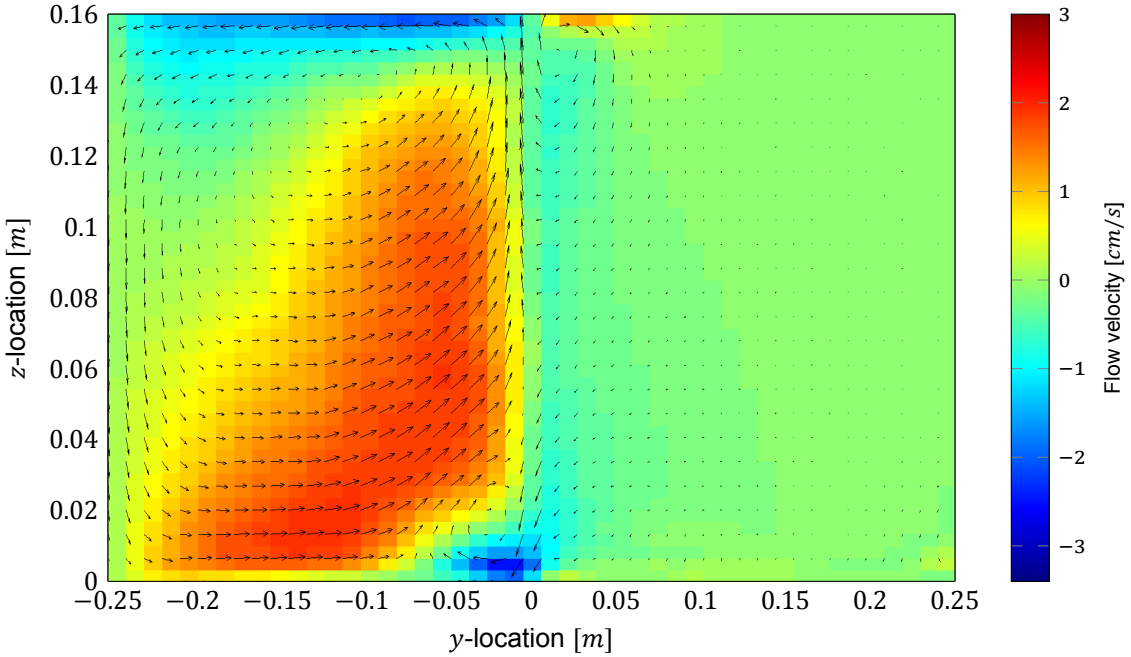

(c) Flow pattern of experiment 4 with 10 minutes simulated time for a cross-section perpendicular to the flume 35 centimetres downstream of the expansion.

Figure C.9: Resulting flow patterns for the numerical simulation of experiment 4 with a simulated time of ten minutes.

Model check: grid refinement

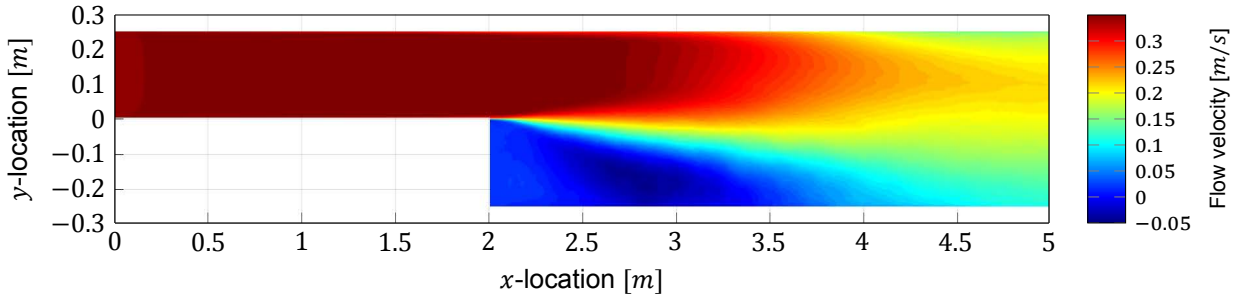

(a) Time-averaged flow velocity for experiment 4 at eight centimetres above the bed with a twice as small grid size.

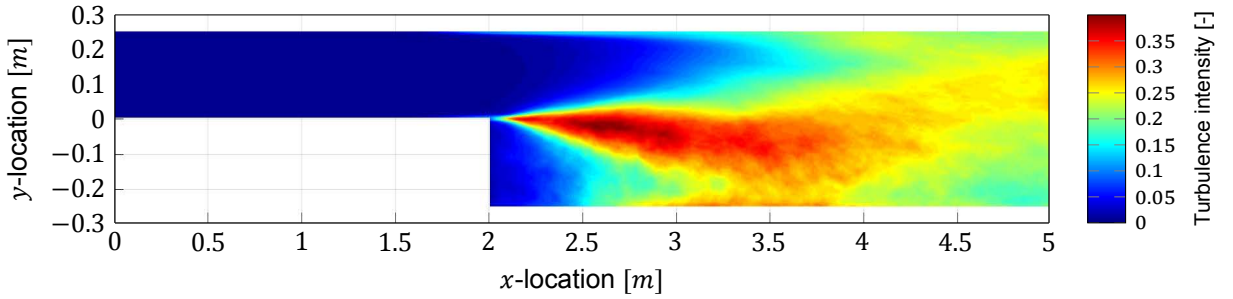

(b) Time-averaged turbulence intensity throughout the flume for experiment 4 at eight centimetres above the bed with a twice as small grid size.

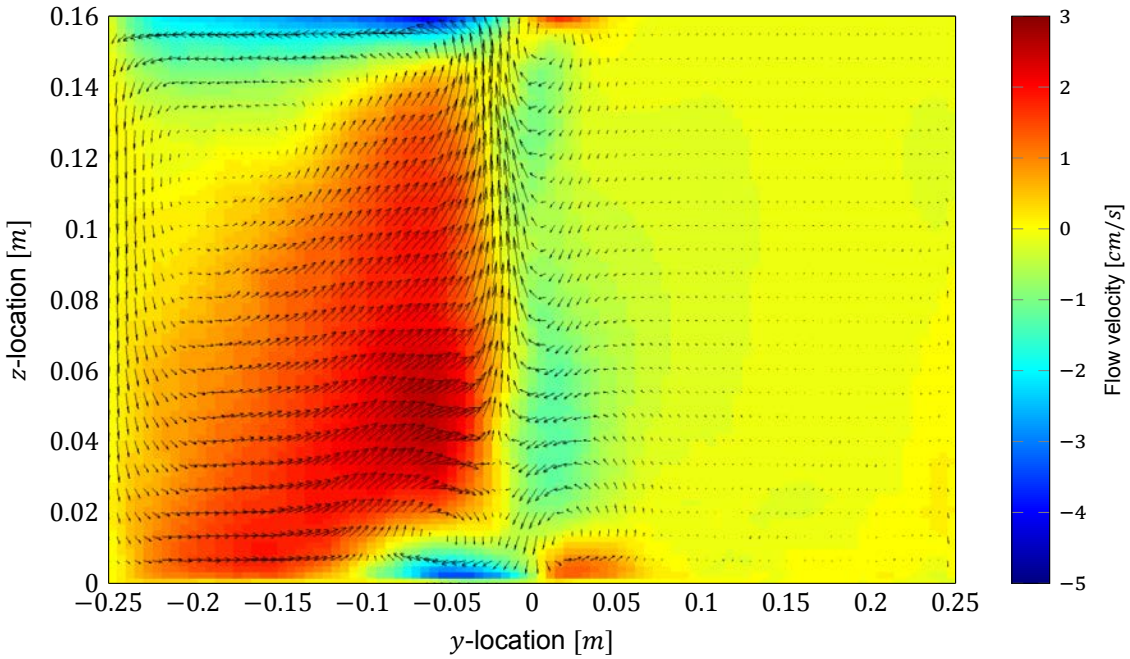

(c) Flow pattern of experiment 4 with a twice as small grid size for a cross-section perpendicular to the flume 35 centimetres downstream of the expansion.

Figure C.10: Resulting flow patterns for the numerical simulation of experiment 4 with a twice as small grid size.

D

Numerical results - morphology

This appendix gives the results of the morphodynamic numerical simulations. For three of the eight laboratory experiments morphodynamic simulations were executed. Furthermore, several simulations were performed as a sensitivity analysis, for which the elaboration can be found in Section 5.6. The grid size in x- and y-direction is one centimetre for these simulations. The grid size in z-direction is 0.4 centimetre. The simulated time of the experiments was one hour. An overview of the executed simulations is depicted in Table D.1. For each simulation, three plots are depicted: the first plot depicts the erosion and sedimentation pattern at the end of the simulation, one shows the mean flow velocity in the first cell above the bed, and the last plot depicts turbulence intensity in the first cell above the bed.

Table D.1: Overview of the executed numerical simulations.

	U_1	U_2
	[m/s]	[m/s]
Experiment 1	0.2	0.1
Experiment 4	0.35	0.18
Experiment 7	0.5	0.25
Experiment 4 - three hours simulated time	0.35	0.18
Experiment 4 - pick-up equation Van Rijn	0.35	0.18
Experiment 4 - grain diameter 100 micrometres	0.35	0.18
Experiment 4 - initial bed perturbation narrow part flume	0.35	0.18

Experiment 1

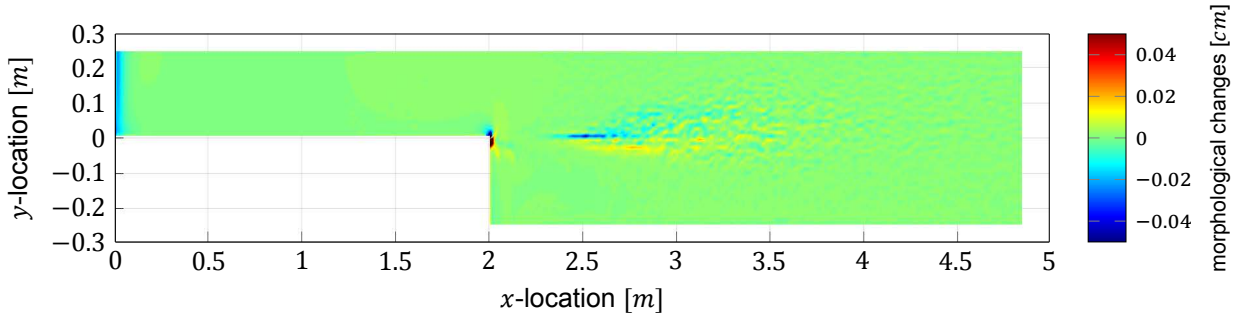

(a) Simulated bed level changes for experiment 1.

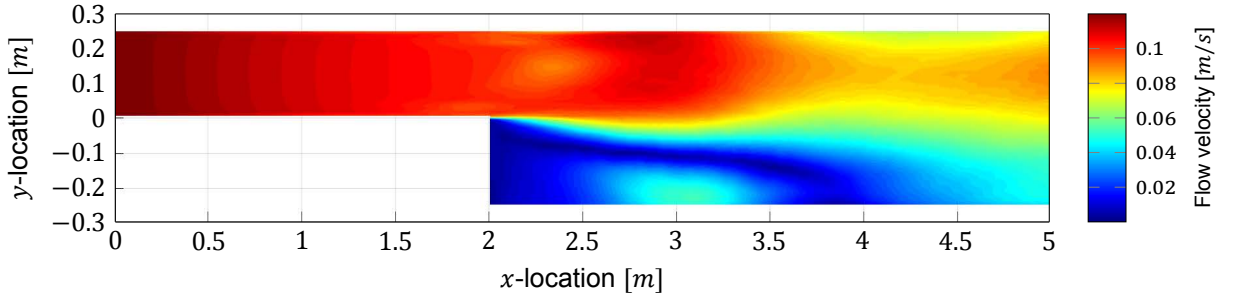

(b) Time-averaged flow velocity in the first cell above the bed for experiment 1.

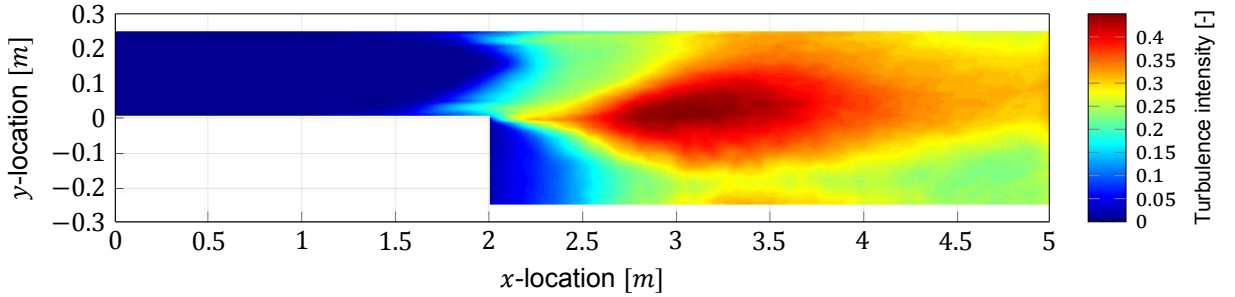

(c) Time-averaged turbulence intensity throughout the flume in the first cell above the bed for experiment 1.

Figure D.1: Results experiment 1

Experiment 4

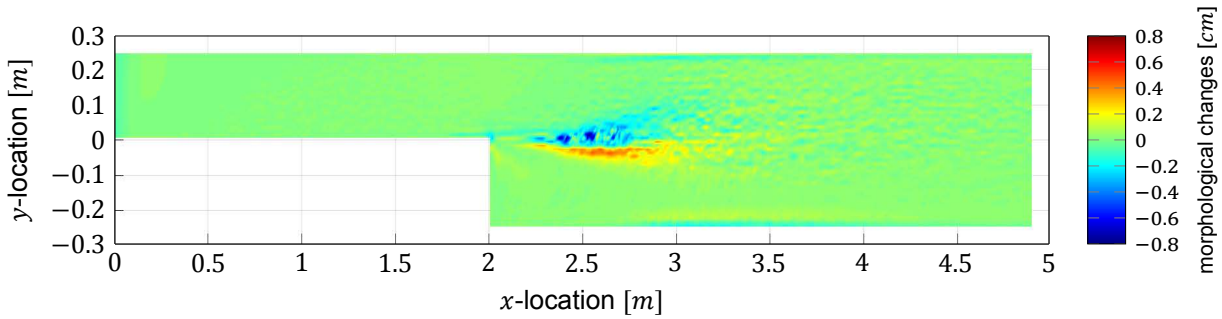

(a) Simulated bed level changes for experiment 4.

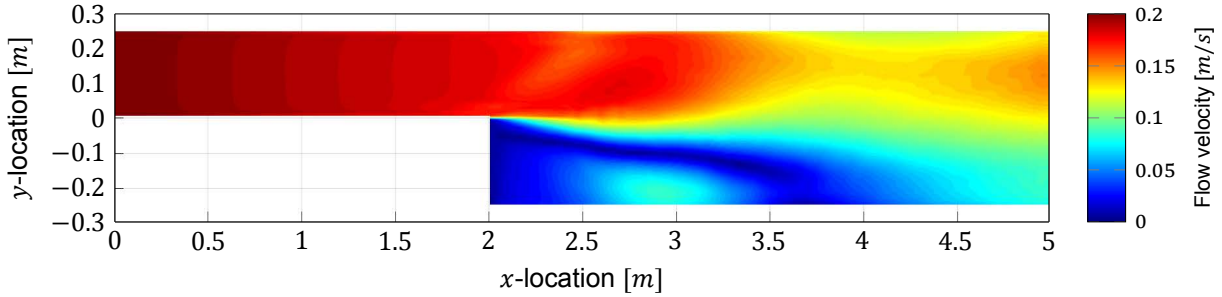

(b) Time-averaged flow velocity in the first cell above the bed for experiment 4.

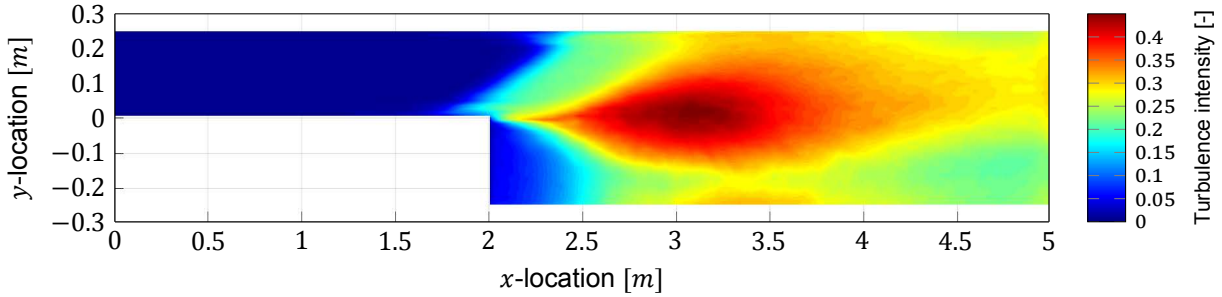

(c) Time-averaged turbulence intensity throughout the flume in the first cell above the bed for experiment 4.

Figure D.2: Results experiment 4

Experiment 7

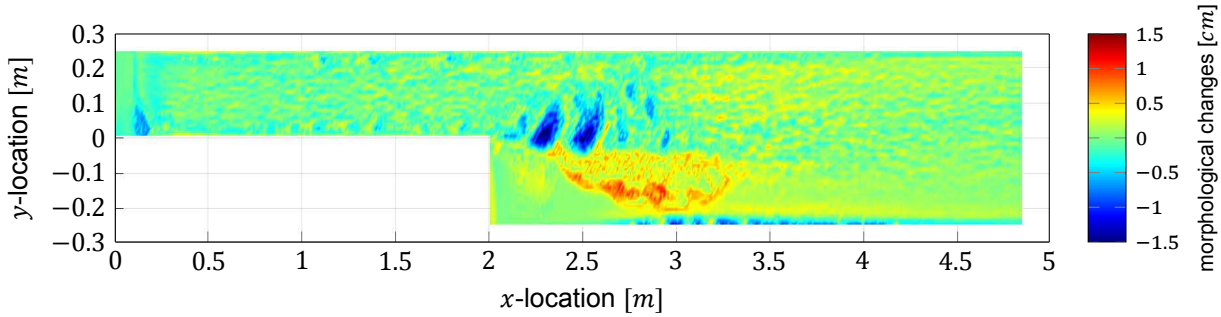

(a) Simulated bed level changes for experiment 7.

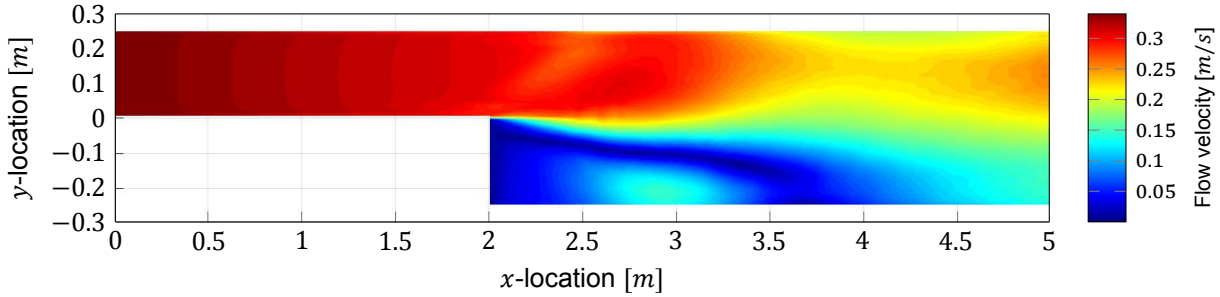

(b) Time-averaged flow velocity in the first cell above the bed for experiment 7.

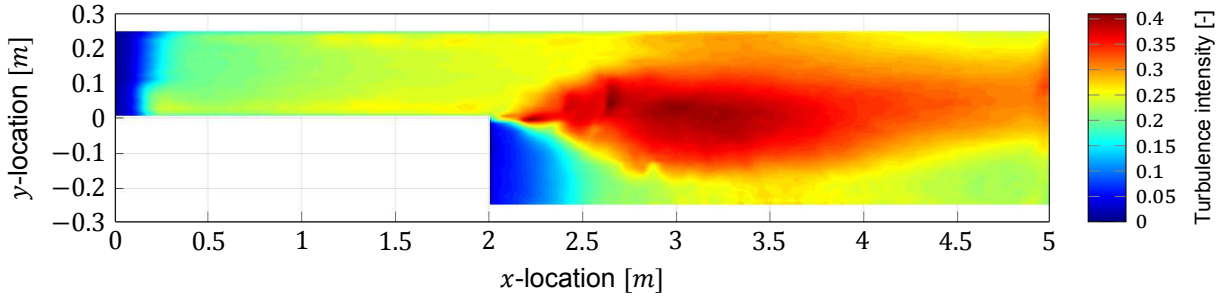

(c) Time-averaged turbulence intensity throughout the flume in the first cell above the bed for experiment 7.

Figure D.3: Results experiment 7

Experiment 4 - three hours simulated time

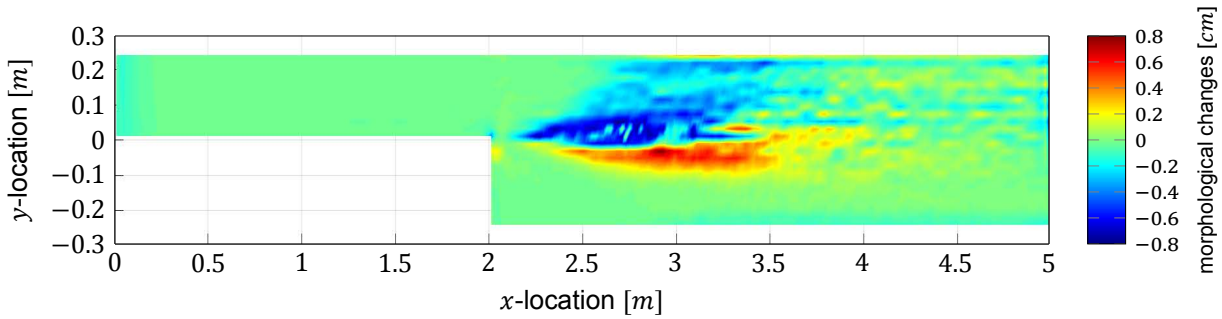

(a) Simulated bed level changes for experiment 4 with a simulated time of three hours.

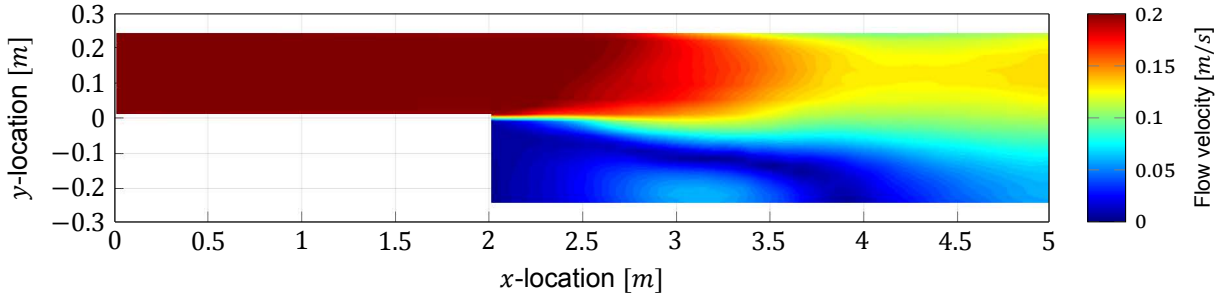

(b) Time-averaged flow velocity in the first cell above the bed for experiment 4 with a simulated time of three hours.

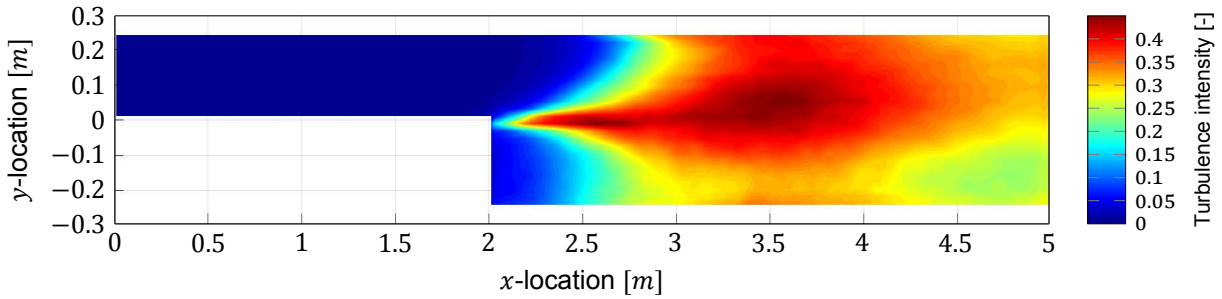

(c) Time-averaged turbulence intensity throughout the flume in the first cell above the bed for experiment 4 with a simulated time of three hours.

Figure D.4: Results experiment 4 with a simulated time of three hours.

Experiment 4 - pick-up equation Van Rijn

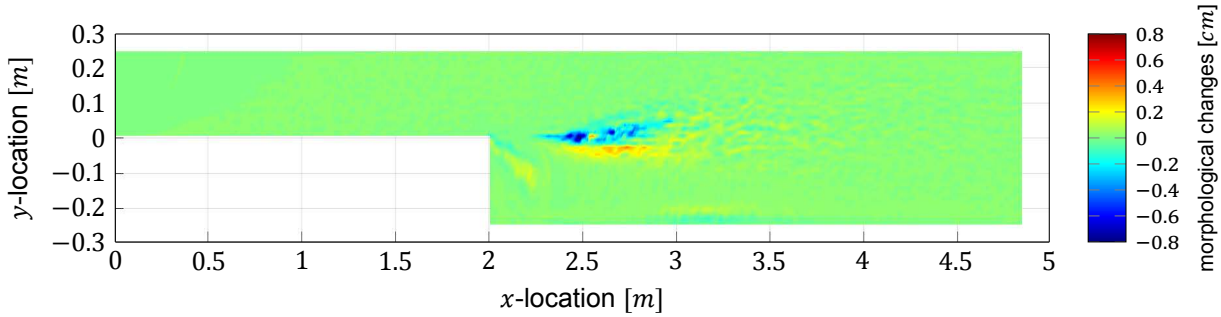

(a) Simulated bed level changes for experiment 4 using the pick-up equation of Van Rijn.

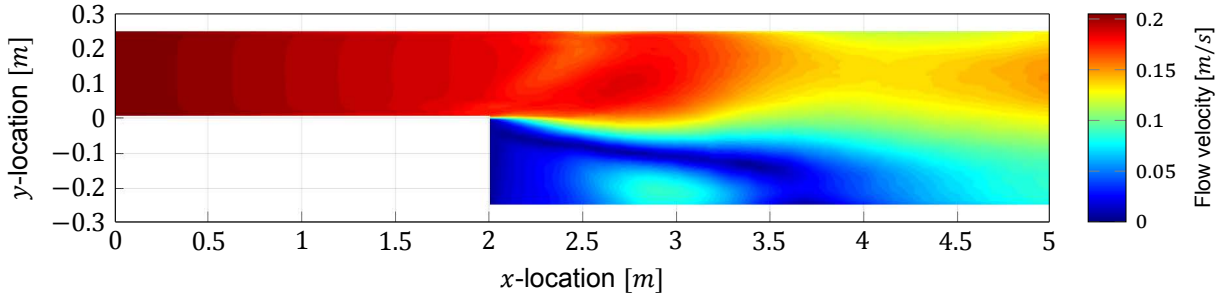

(b) Time-averaged flow velocity in the first cell above the bed for experiment 4 using the pick-up equation of Van Rijn.

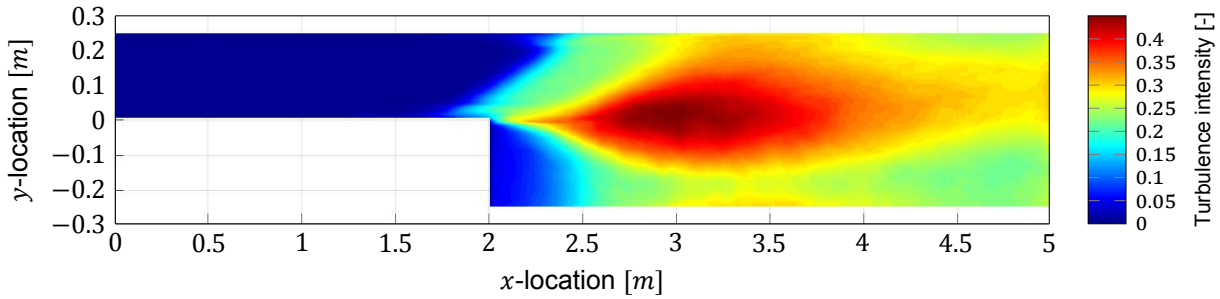

(c) Time-averaged turbulence intensity throughout the flume in the first cell above the bed for experiment 4 using the pick-up equation of Van Rijn.

Figure D.5: Results experiment 4 using the pick-up equation of Van Rijn

Experiment 4 - grain diameter 100 micrometres

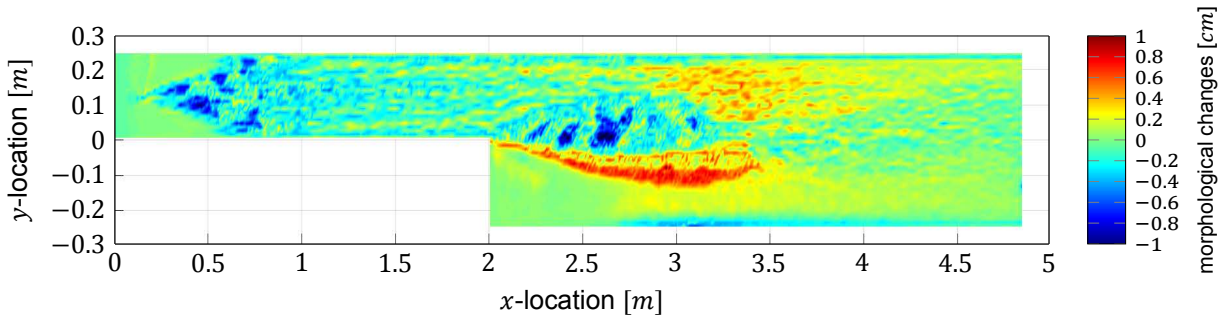

(a) Simulated bed level changes for experiment 4 with a grain diameter of 100 micrometres.

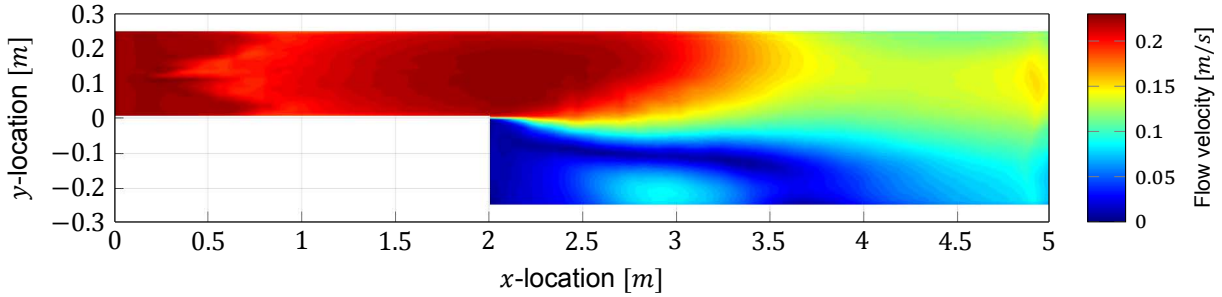

(b) Time-averaged flow velocity in the first cell above the bed for experiment 4 with a grain diameter of 100 micrometres.

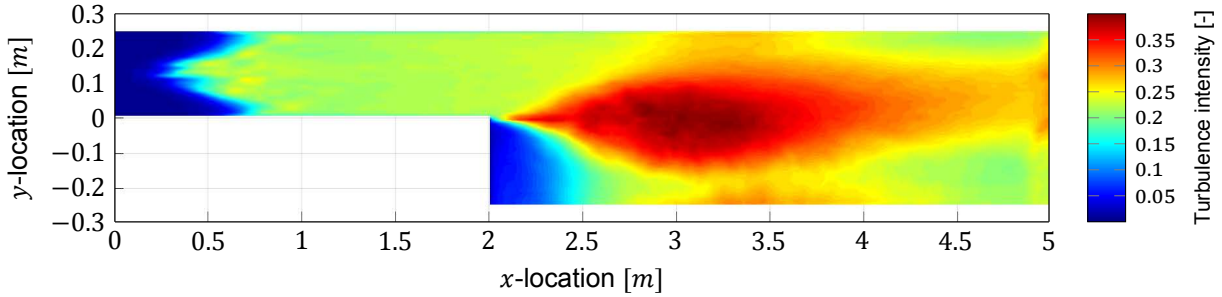

(c) Time-averaged turbulence intensity throughout the flume in the first cell above the bed for experiment 4 with a grain diameter of 100 micrometres.

Figure D.6: Results experiment 4 with a grain diameter of 100 micrometres.

Experiment 4 - initial bed perturbation narrow part flume

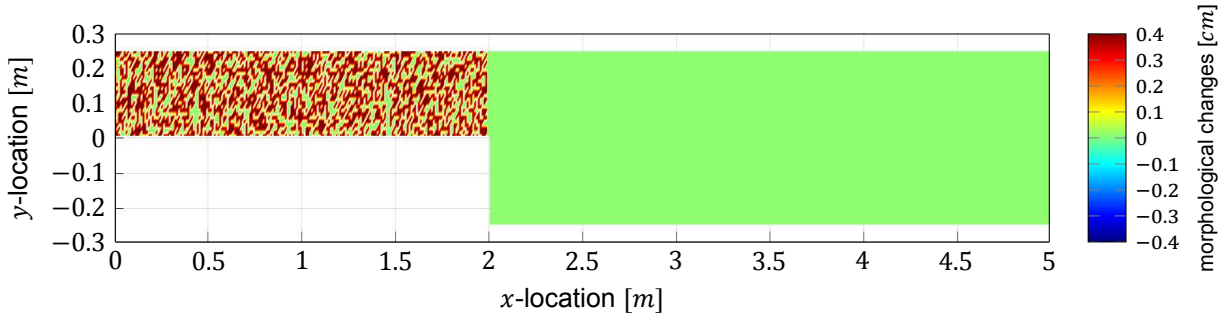

(a) Initial bed for experiment 4 with an initial random perturbation of the bed in the narrow part of the flume.

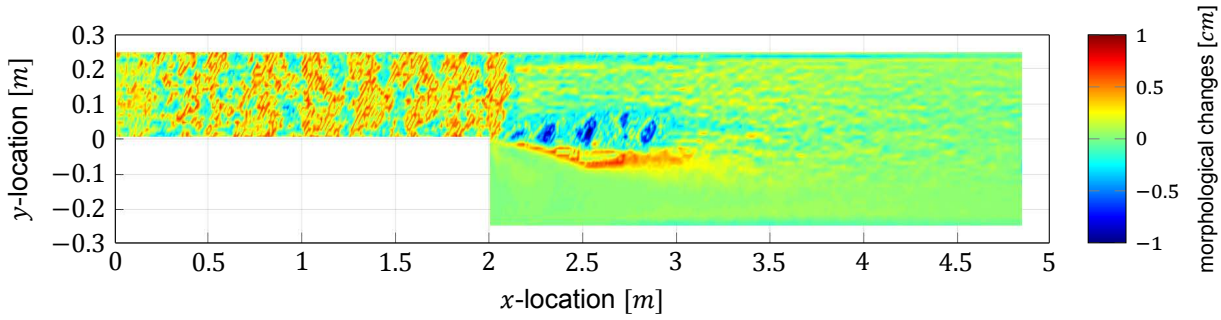

(b) Simulated bed level changes for experiment 4 with an initial random perturbation of the bed in the narrow part of the flume.

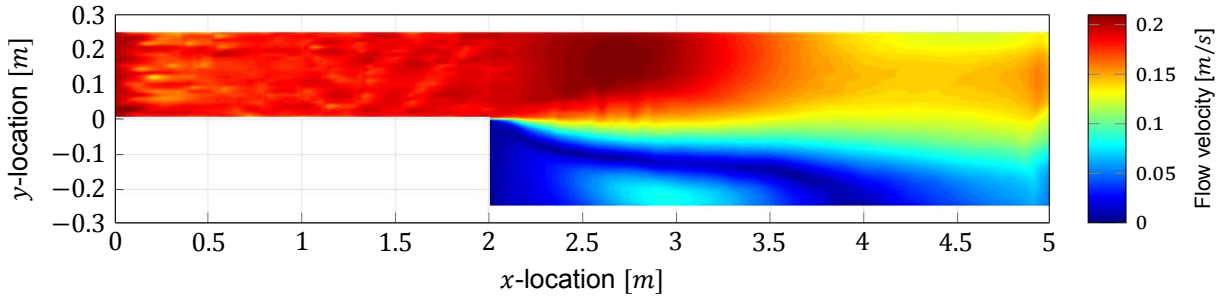

(c) Time-averaged flow velocity in the first cell above the bed for experiment 4 with an initial random perturbation of the bed in the narrow part of the flume.

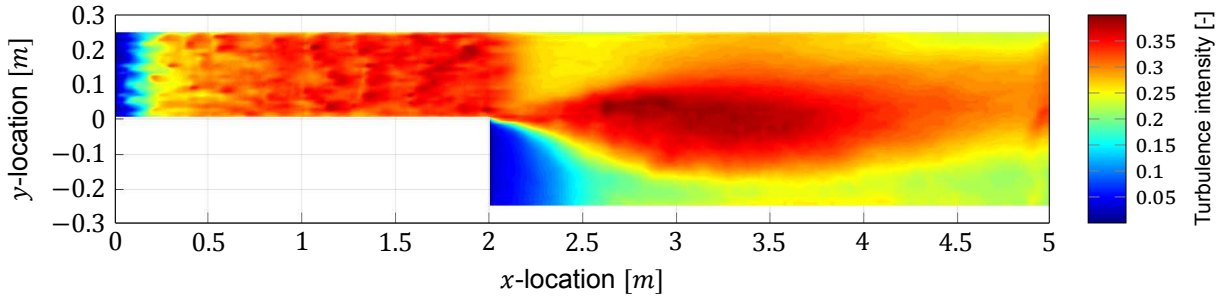

(d) Time-averaged turbulence intensity throughout the flume in the first cell above the bed for experiment 4 with an initial random perturbation of the bed in the narrow part of the flume.

Figure D.7: Results experiment 4 with an initial random perturbation to the bed in the narrow part of the flume.